HOKKAIDO UNIVERSITY

Title	Impact of multiple inter-tillage weeding on greenhouse gas emissions, carbon stock, and yield in organic rice farming paddy fields in Hokkaido
Author(s)	浪江, 日和
Degree Grantor	北海道大学
Degree Name	博士(農学)
Dissertation Number	甲第16530号
Issue Date	2025-06-30
DOI	https://doi.org/10.14943/doctoral.k16530
Doc URL	https://hdl.handle.net/2115/95730
Type	doctoral thesis
File Information	NAMIE_Hiyori.pdf

Hokkaido University Collection of Scholarly and Academic Papers : HUSCAP

2025 Doctoral Thesis

Impact of multiple inter-tillage weeding on greenhouse gas emissions, carbon stock, and yield in organic rice farming paddy fields in Hokkaido

北海道の有機栽培水田における多数回の中耕除草が

温室効果ガス・炭素貯留・収量に与える影響

Hokkaido University Graduate School of Agriculture
Division of Frontiers in Environmental Sciences,
Unit of Regional Environment, Laboratory of Soil Science
Doctor Course

Hiyori Namie

Acknowledgements (Japanese)

この博士論文を完成させるにあたり，多大なるご指導とご支援を賜りました当真要教授に心より感謝申し上げます。学会発表の準備や日々の研究活動において，的確で温かいご助言をいただいたおかげで，困難を乗り越え，自信を持って研究に取り組むことができました。特に，厳しくも的を射たご指摘と励ましの言葉が，私の成長と研究の質を高める大きな原動力となりました。また，研究に向き合う姿勢や問題解決のための思考方法についても，多くのことを学ばせていただきました。教授からいただいた教えは，今後の私の研究者としての道標となると確信しております。改めて，深い感謝の意を表します。

研究の初期段階での方向性の設定や課題に取り組むための視点を示していただいた波多野隆介名誉教授には，心より御礼申し上げます。教授のご指導があったからこそ，本研究を進めるうえでの重要な基盤を築くことができました。

本論文の審査にあたり，副査として適切なご指導・ご鞭撻を賜りました土壌保全学研究室の濱本昌一郎教授に心より感謝申し上げます。濱本先生には，ゼミを通じて貴重なご助言を賜り，研究を前進させることができました。また，作物栄養学研究室の信濃卓郎教授に深く感謝申し上げます。学会でご一緒させていただいた際には，研究内容だけではなく，私の立場や状況を気にかけてくださり，親身になって叱咤激励していただきました。そのお言葉やご助言に何度も元気づけられ，研究への意欲を新たにすることができました。

本研究の遂行にあたり，土壌保全学研究室前任の石黒宗秀教授には研究圃場のご提供だけではなく，学会発表や論文添削についてもご指導いただきました。心より御礼申し上げます。ゼミ活動を通じて貴重なご指導とご助言を賜りました土壌学研究室の倉持寛太講師，土壌保全学研究室の柏木淳一講師, 辰野宇大助教に心より感謝申し上げます。ゼミでの議論やアドバイスを通じて，研究の方向性を見出すことができました。

夏の猛暑や悪天候の中でも根気強く調査を続け，貴重なデータ収集をサポートしてくださった周之舵さん，坂口香帆さん，島田かさねさん，趙双双さん，井上拓海さん，内田研究室の皆さまに心から感謝申し上げます。測定方法の工夫や実験手順の改善を通じて，互いに知識を共有し，

高め合えたことは，私にとって大きな財産です。多くのフィールドワークも，同じ目標を持つ仲間がいたからこそ楽しく乗り越えることができました。

本研究を遂行するにあたり，圃場管理を通じて多大なるご支援を賜りました北海道大学北方生物圏フィールド科学センター付属農場の植物生産技術室の角田貴敬さん，市川伸次さん，橋本哲也さん，長野宏則さんに心より感謝申し上げます。日々の圃場の維持管理や，調査に必要な環境の整備にご尽力いただいたおかげで，研究を円滑に進めることができました。また，作業の合間にも貴重なご助言や励ましの言葉をいただき，現場での作業が一層充実したものとなりました。

本研究にご関心をお持ちいただき，貴重な書籍の提供や温かい励ましを通じてご支援をくださった長谷川周一先生，粕渕辰昭先生に心より感謝申し上げます。先生方からの的確なご助言と専門的な知識の共有は，研究の幅を広げ，課題に取り組む際の大きな助けとなりました。そのご厚意に深く感謝するとともに，研究活動を続ける中で常に励みになっておりました。

研究生活を共に過ごし，切磋琢磨しながら励まし合い，共に困難を乗り越えてきた先輩の三原州人さん，同期の楊椅麟さん，吉村元博さん，内林大志さんにも心より感謝いたします。皆さんとの議論は，私の研究を深める上で欠かせないものでした。ときには悩みを共有し，ときには互いを奮い立たせながら進んできた日々は，私にとってかけがえのない経験です。この場を借りて，皆さんに改めて感謝の意を表します。

本研究の遂行にあたり，学会などでお会いする度に温かいご助言や貴重なご意見をくださった土壌学研究室の先輩方に，心より感謝申し上げます。先輩方のアドバイスは，私の研究を進める上で重要な指針となりました。また，時折いただく励ましのお言葉や，親身に相談に乗っていただけるそのお姿に，大きな安心感をいただきました。また，時に真剣に，時に笑い合いながら議論を共にしてくれた土壌学研究室の後輩たちにも心より感謝いたします。皆さんとの交流を通じて，研究に対する意欲を新たにし，元気と自信を持って研究活動に取り組むことができました。その支えがあったからこそ，困難な場面にも前向きに挑むことができたと感じています。

本研究を進めるにあたり，事務手続きや研究の運営面で多大なるご支援をいただきました立川美奈さん，森滝奈緒子さんに心より感謝申し上げます。実験や調査の準備に伴う手続きや資料の

手配など，迅速かつ丁寧にご対応いただきましたおかげで，研究活動に集中することができました。また，日々の温かいお心遣いや励ましの言葉が，研究を続ける上で大きな支えとなりました。

本研究は，日本学術振興会(JSPS)，科学研究費助成事業(科研費)[JP18H03963]，JST SPRING[JPMJSP2119]，ヤンマー資源循環支援機構[KG0230009]の助成を受けて実施されました。この場をお借りして，関係者の皆様に感謝申し上げます。

最後に，これまで長きにわたり研究に専念できる環境を支えてくれた家族と愛犬，日々の励ましをくれた友人に心から感謝いたします。

2025 年 6 月 30 日

浪江　日和

List of Tables

Table 3.1. Initial soil characteristics in conventional rice farming (CF) and organic rice farming (OF) site. 30

Table 3.2 Schedule of field management in 2019. 33

Table 3.3. Schedule of field management in 2020. 34

Table 3.4. Schedule of field management in 2021. 35

Table 3.5. Schedule of field management in 2022. 36

Table 3.6. Schedule of field management in 2023. 37

Table 3.7. The amount of chemical fertilizer applied in CF in each year. 38

Table 3.8. Water management for each year. 38

Table 4.1. Comparison of each pathways of CH_4 during multiple inter-tillage weeding (MIW) period. 59

Table 4.2. Peason correlation coefficient between CH_4 flux from each pathways and environmental factors during MIW period. 60

Table 4.3. Cumulative CH_4 emissions (mean ± SD) during the cultivation period and contribution ratio of multiple inter-tillage weeding (MIW). 61

Table 4.4. Comparison of each pathways of N_2O during multiple inter-tillage weeding (MIW) period. 64

Table 4.5. Peason correlation coefficient between N_2O flux from each pathways and environmental factors during MIW period. 66

Table 4.6. Cumulative N_2O emissions (mean ± SD) during the cultivation period and contribution ratio of multiple inter-tillage weeding (MIW). 67

Table 4.7. Concentration of gaseous and dissolved CH_4 in soil during multiple inter-tillage weeding (MIW) period in 2022. 69

Table 5.1.Cumulative period and number of days from 2019 to 2023. 83

Table 5.2. Soil physicality at 0-5 cm depth (average of MIW period). 93

Table 5.3. Rice growth indicators for each rice-growing stage. 94

Table 5.4. Net primary production (NPP) of rice plants from 2019 to 2023. 95

Table 5.5. Characteristics of yield components and brown rice yields. 97

Table 5.6. Pearson correlation coefficients for greenhouse gas (GHG) fluxes against soil environmental factors from 2019 to 2023. 103

Table 5.7. Seasonal cumulative greenhouse gas (GHG) emissions and global warming potential (GWP_{total}) at each treatment from 2019 to 2023. 104

Table 5.8. RH (heterotrophic respiration) or CH_4 emissions per carbon input from 2019 to 2023. 105

Table 5.9. Greenhouse gas balance (GHGB) from 2019 to 2023. 110

Table 5.10. Greenhouse gas intensity (GHGI) from 2019 to 2023. 111

Table 5.11. Net ecosystem carbon balance (NECB) from 2019 to 2023. 112

List of Figures

Figure 2.1. Global monthly means CO_2 concentration since 1980 (NOAA, 2024). The dashed red line with diamond symbols represents the monthly mean values, centered on the middle of each month. The black line with the square symbols represents the same, after correction for the average seasonal cycle. 15

Figure 2.2. Global monthly means CH_4 concentration since 1980 (NOAA, 2024). The red lines and circles are globally averaged monthly mean values centered on the middle of each month. The black line and squares show the long-term trend (in principle, similar to a 12-month running mean) where the average seasonal cycle has been removed. 16

Figure 2.3. Global monthly means N_2O concentration since 1980 (NOAA, 2024). The red lines and circles are globally averaged monthly mean values centered on the middle of each month. The black line and squares show the long-term trend (in principle, similar to a 12-month running mean) where the average seasonal cycle has been removed. 17

Figure 2.4. Current Greenhouse gas (GHG) emissions (MAFF, 2024 improve). 18

Figure 2.5. Global cropland greenhouse gas emissions (a) and intensities of the top ten emitting food crops and regions (b) (Carlson et al., 2017). 19

Figure 2.6. Carbon and nitrogen dynamics in a rice paddy field : Pathways of CH_4 and N_2O emissions (Qian et al., 2023). AMO, ammonia monooxygenase; HAO, hydroxylamine oxidoreductase; *mcrA*, methyl coenzyme M reductase; *narG*, nitrate reductase; *nirK*, copper-containing nitrite reductase; *nirS,* haem-containing nitrite reductase; *norB*, nitric oxide reductase; *nosZ*, nitrous oxide reductase. 23

Figure 2.7. Manual weeding machines called "taguruma" 29

Figure 3.1. Location of the study site in Sapporo, Hokkaido, Japan. 31

Figure 3.2. Layout of the paddy field with organic rice farming without fertilizer and agricultural chemicals which divided 3 plots by inter-tillage weeding times (a) and conventional rice farming (CF) plots (b). The lowercase alphabet means repetition. 32

Figure 3.3. The devices of multiple inter-tillage weeding (MIW) for weeding between the rows in 2019-2021 (a), 2022-2023 (b) and for weeding between rice plants (c). 39

Figure 3.4. The devices of CO_2 (GPP (sum of gross primary production) + RE (ecosystem respiration)), CH_4, and N_2O fluxes sampling during the rice-growing season (a), RH (heterotrophic respiration) flux sampling during flooding period (b) and CH_4, N_2O and RH fluxes sampling during the fallow season (c). 40

Figure 3.5. The equipment for measuring soil air gas. Scheme of existing equipment (a), improved equipment (b), and state of sampling (c). 44

Figure 4.1. Scheme of bubble traps. 52

Figure 4.2. The device of multiple inter-tillage weeding (MIW)-mediated CH_4 and N_2O flux sampling. 54

Figure 4.3. Seasonal variation in total methane (CH_4) flux in 2022 (a), 2023 (b), diffusive CH_4 flux in 2022 (c), 2023 (d), ebullitive CH_4 flux in 2022 (e), 2023 (f), rice-mediated CH_4 flux in 2022 (g), 2023 (h). Black and white arrows denote the timing of irrigation and drainage. Md indicates mid-season drainage, Id indicates intermittent drainage and Cd indicates complete drainage. Dotted arrows indicated inter-tillage weeding. Gray scale denotes the MIW period (June 10 to July 13 in 2022 and June 9 to July in 2023). 58
Figure 4.4. Seasonal variation in total nitrous oxide (N_2O) flux in 2022 (a), 2023 (b), diffusive N_2O flux in 2022 (c), 2023 (d), ebullitive N_2O flux in 2022 (e), 2023 (f), rice-mediated N_2O flux in 2022 (g), 2023 (h). Black and white arrows denote the timing of irrigation and drainage. Md indicates mid-season drainage, Id indicates intermittent drainage and Cd indicates complete drainage. Dotted arrows indicated inter-tillage weeding. Gray scale denotes the MIW period (June 10 to July 13 in 2022 and June 9 to July in 2023). 63
Figure 4.5. Seasonal variation in dissolved methane (CH_4) concentration in paddy field water in 2022 (a), 2023 (b), CH_4 concentration in soil air gas at 5 cm depth in 2022 (c), 2023 (d), CH_4 concentration in soil air gas at 10 cm depth in 2022 (e), 2023 (f). Black and white arrows denote the timing of irrigation and drainage. Md indicates mid-season drainage, Id indicates intermittent drainage and Cd indicates complete drainage. Gray scale denotes the MIW period (June 10 to July 13 in 2022 and June 9 to July in 2023). 68
Figure 4.6. Pearson correlation between gaseous CH_4 concentrations, which was calculated from the CH_4 concentrations in the trapped bubbles and the air-phase ratio, and CH_4 concentrations in soil air gas at 10 cm depth. 70
Figure 4.7. Seasonal variation in dissolved nitrous oxide (N_2O) concentration in 2022 (a), 2023 (b), N_2O concentration in soil air gas at 5 cm depth in 2022 (c), 2023 (d), N_2O concentration in soil air gas at 10 cm depth in 2022 (e), 2023 (f). Black and white arrows denote the timing of irrigation and drainage. Md indicates mid-season drainage, Id indicates intermittent drainage and Cd indicates complete drainage. Gray scale denotes the MIW period (June 10 to July 13 in 2022 and June 9 to July in 2023). 71
Figure 4.8. Seasonal variation in precipitation, air temperature and atmospheric pressure in 2022 (a), 2023 (b), water temperature in paddy field water in 2022 (c), 2023 (d), soil temperature at 3 cm depth in 2022 (e), 2023 (f), water depth in 2022 (g), 2023 (h), plant height in 2022 (i), 2023 (j), tiller number in 2022 (k), 2023 (l), soil Eh at 5 cm depth in 2022 (m), 2023 (n). Black and white arrows denote the timing of irrigation and drainage. Md indicates mid-season drainage, Id indicates intermittent drainage and Cd indicates complete drainage. Gray scale denotes the MIW period (June 10 to July 13 in 2022 and June 9 to July in 2023). 72
Figure 5.1. Seasonal variation of air temperature and precipitation (a), soil temperature (b), soil pH (c), NH_4^+ content (d), NO_3^- content (e), Fe^{2+} content (f) and SO_4^{2-} content (g) from 2019 to 2023. The black arrow at the top of the figure indicates irrigation and the white arrow indicates drainage. The dotted arrows indicate the timing of inter-tillage weeding. The gray scale indicates the rice-

growing season; the other scales indicate the fallow season. Error bars indicate standard deviation. 91
Figure 5.2. Seasonal variation of soil redux condition (Eh) (a) and water extract organic carbon content (b) from 2022 to 2023. The black arrow at the top of the figure indicates irrigation and the white arrow indicates drainage. The dotted arrows indicate the timing of inter-tillage weeding. The gray scale indicates the rice-growing season; the other scales indicate the fallow season. Error bars indicate standard deviation..... 92
Figure 5.3. Cumulative of brown rice yields each year from 2019 to 2023. Error bars indicate standard deviation. The same letters show no significant difference in cumulative values among the treatments (p <0.05)..... 96
Figure 5.4. Seasonal variation of RH (heterotrophic respiration) flux (a), CH_4 flux (b) and N_2O flux (c) from 2019 to 2023. The black arrow at the top of the figure indicates irrigation and the white arrow indicates drainage. The dotted arrows indicate the timing of inter-tillage weeding. The gray scale indicates the rice-growing season; the other scales indicate the fallow season. Error bars indicate standard deviation. 101
Figure 5.5. Carbon input total (a), from weeds (b), from residues (c). Error bars indicate standard deviation. The same letters are not significantly different among treatments (p <0.05). 102
Figure 5.6. Peason correlation coefficient for GHG emissions against soil environmental factors. * <0.05, **<0.01, ***<0.001.....108
Figure 5.7. The relationship between each factor (correlation coefficient ≥ 0.6). 109
Figure 5.8. Relationship between greenhouse gas balance (GHGB) and GWP_{RH} (a) and GWP_{CH4} (b). Treatments of T0, T2 and T5 are organic rice farming paddy fields without fertilizers and agrochemicals and 0-, 2-, and 5-times inter-tillage weeding respectively. 113
Figure 5.9. Relationship between net ecosystem carbon balance (NECB) and RH emission. Treatments of T0, T2 and T5 are organic rice farming paddy fields without fertilizers and agrochemicals and 0-, 2-, and 5-times inter-tillage weeding, respectively. 113
Figure 5.10. The appearance of weeds before the last multiple inter-tillage weeding (MIW). Treatments of T0, T2 and T5 are organic rice farming paddy fields without fertilizers and agrochemicals and 0-, 2-, and 5-times inter-tillage weeding, respectively. 115
Figure 5.11. Relationship between sulfuric acid reduction, iron reduction, methane and carbon dioxide formation over organic acids (Hori et al. 1990 improve) 123

Contents

Acknowledgements (Japanese) 1
List of Tables 4
List of Figures 5
Contents 8
1. General Introduction 11
1.1. Greenhouse Gas Emissions from Rice Paddy Field 11
1.2. Importance of Transitioning to Organic Rice Farming and Enhancing Yield 11
1.3. Potential and Concern of Multiple Inter-tillage Weeding Practice 12
1.4. Objectives and Structure 14
2. Literature Review 15
2.1. Trend of Greenhouse Gas Emissions 15
2.1.1. Dynamics of Greenhouse Gas in Rice Paddy Field 20
2.1.2. Existing Greenhouse Gas Mitigation Measures 25
2.2. Decline and Revival of Organic Rice Farming 26
2.3. History and Potential of Multiple Inter-tillage Weeding Practice 28
3. Common Material and Methods 30
3.1. Study Site 30
3.2. Experimental Design and Field Management 31
3.3. Multiple Inter-tillage Weeding (MIW) Practice 38
3.4. Measuring Greenhouse Gas Fluxes by Static Closed Chamber Method 39
3.4.1. Gas sampling 39
3.4.2. Analysis of Gas concentrations 41
3.4.3. Calculation for Gas Fluxes 41
3.4.4. Calculation for Cumulative Gas Emissions 42
3.5. Measuring Gas Concentrations in Paddy Field Water and Soil Air 43
3.5.1. Sampling for Soil Air and Dissolved Gas in Paddy Field Water 43
3.5.2. Calculation for Dissolved Gas Concentration in Paddy Field Water 44
3.6. Environmental Factors 45
3.6.1. Ancillary measurements 45
3.6.2. Soil Sampling and Soil Solution Extraction 45
3.6.3. Analysis of Soil Physicochemical Properties 46
3.6.4. Analysis of Soil Physical Properties 46
3.6.5. Measurement of Soil Environmental Conditions 47
3.6.6. Plant Measurement 47
4. Multiple Inter-tillage Weeding Effect on Methane and Nitrous Oxide Emissions Pathways from Rice Paddy Fields 48
4.1. Introduction 48

4.2. Materials and methods 50
4.2.1. Investigating periods 50
4.2.2. Total and diffusive gas flux 50
4.2.3. Ebullitive gas flux 51
4.2.4. Rice-mediated gas flux 53
4.2.5. Calculation for cumulative gas emission 53
4.2.6. MIW-mediated gas flux 53
4.2.7. Measurement of environmental factors 55
4.2.8. Statistical analysis 55
4.3. Results 56
4.3.1. Each CH_4 flux during the MIW period 56
4.3.2. Relationship between each CH_4 flux and environmental factors during the MIW period 57
4.3.3. Comparison of CH_4 emission pathways during the MIW period 61
4.3.4. Each N_2O flux during the MIW period 61
4.3.5. Relationship between each N_2O flux and environmental factors during the MIW period 65
4.3.6. Comparison of N_2O emission pathways during the MIW period 65
4.3.7. Gas concentration during the MIW period 67
4.4. Discussion 73
4.4.1. CH_4 emission during the MIW period 73
4.4.2. MIW effects on CH_4 emission pathways 74
4.4.3. N_2O emission during the MIW period 76
4.4.4. MIW effects on N_2O emission pathways 77
4.4.5. Validation of quantitative methods 78
4.5. Conclusion 79
5.Five-year Assessment of Multiple Inter-tillage Weeding on Greenhouse Gas Emissions, Rice Yield, and Carbon Balance in Organic Rice Farming 81
5.1. Introduction 81
5.2. Materials and methods 83
5.2.1. Study site 83
5.2.2. Experimental design and field management 84
5.2.3. Environmental factors 84
5.2.4. Plant production and grain yield 84
5.2.5. Greenhouse gas fluxes 86
5.2.6. Calculation of GWP, GHGB, GHGI and NECB 87
5.2.7. Statistical analysis 89
5.3. Results 89

5.3.1. Environmental factors 89
5.3.2. Rice plants characteristics 93
5.3.3. RH emissions 98
5.3.4. CH_4 emissions 99
5.3.5. N_2O emissions 100
5.3.6. Interactions among environmental factors for RH and CH_4 fluxes 106
5.3.7. GWP, GHGB, GHGI and NECB 106
5.4. Discussion 114
5.4.1. Effect of MIW on GHGB 114
5.4.2. Effects of MIW on rice yield and GHGI 118
5.4.3. Effects of MIW on NECB 119
5.4.4. Mechanisms of MIW Involvement in RH and CH_4 Emissions 120
5.4.5. Limitation and future research 124
5.5. Conclusion 124
6. General Discussion 126
7. Conclusion 129
Summary (Japanese) 130
Funding 133
Reference 134

1. General Introduction

1.1. Greenhouse Gas Emissions from Rice Paddy Field

Rice paddy fields supply staple food for half of the world's population but account for about 48% of greenhouse gas (GHG) emissions from agricultural land (Qian et al., 2023). Methane (CH_4) emissions from rice paddy fields are particularly high in irrigated areas, which comprise 60% of the global rice harvested area and are responsible for 78% of total rice CH_4 emissions (Carlson et al., 2017). Rice paddy fields function as a major source of CH_4, but nitrous oxide (N_2O) emissions are generally lower than those from upland fields (Akiyama, 2024). On the other hand, rice paddy fields have been shown to have a high capacity for soil carbon stock, which helps stabilize carbon dioxide (CO_2) in the soil (Chen et al., 2021; Lal, 2004; Pan et al., 2004). In recent years, increasing attention has been given to negative emissions, which aim to remove atmospheric CO_2 by capturing it and sequestering carbon in the soil, due to the long residence time of CO_2 in the atmosphere. Additionally, the atmospheric lifetime of CH_4 is estimated to be about 9.1 years, whereas that of N_2O is 116 years and that of CO_2 is 1 to several thousand years (IPCC, 2023). Therefore, CH_4 emission reductions in particular are likely to reflect the effectiveness of global warming countermeasures.

1.2. Importance of Transitioning to Organic Rice Farming and Enhancing Yield

Furthermore, a major issue in the future is that global rice demand is projected to increase by approximately 28% by 2050, mainly due to population growth in developing countries (Alexandratos and Bruinsma, 2012). The application of large amounts of chemical fertilizers can significantly increase rice yields, it also comes at the cost of increased environmental burdens. Avoiding excessive fertilization is fundamentally tied to the principles of organic farming. In Japan, organic agriculture is defined as organic agriculture as agriculture that uses methods that basically do not, in principle, use chemically synthesized fertilizers, pesticides or genetic modification technology and which aims to minimize the burden of agricultural

production on the environment (MAFF, 2024). Therefore, the overapplication of fertilizers, one of the major sources of environmental pressure, is considered inconsistent with organic agriculture. In fact, according to the planetary boundary assessments, nitrogen and phosphorus have already accumulated beyond safe environmental thresholds (Rockström et al., 2009), and further dependence on fertilizers poses a serious risk to sustainability. Particularly in rice cultivation, it has been shown that the majority of essential nutrients required by rice plants such as nitrogen, phosphorus, potassium, and silica are supplied from the soil (Mitsueda and Kimura, 2010), making it possible to enhance productivity by harnessing the soil's natural fertility. Thus, organic cultivation emphasizes strategies that avoid over-fertilization while drawing on inherent soil fertility, making it a highly important approach in the pursuit of sustainable agriculture. Furthermore, in order to address the increasing rice demand due to global population growth and mitigate global warming, it is urgent to establish sustainable organic rice farming that can enhance soil carbon stock and reduce GHG emissions from rice paddy fields while maintaining high yields under low-input conditions.

1.3. Potential and Concern of Multiple Inter-tillage Weeding Practice

There is an organic rice farming practice known as Multiple Inter-tillage Weeding (MIW) that has been passed down since Japan's Edo period. It has been reported that combining more than four times of MIW in rice paddy fields without fertilizer and agrochemicals results in high-quality rice with high yields sustained over a long term (five years) (Kasubuchi et al., 2019). Additionally, according to reports by Zhou et al. (2023), MIW have been shown to increase the nitrogen concentration in both paddy field water and soil, promoting rice growth and yield. MIW are conducted in a flooded state during the rice-growing season, which facilitates oxygen supply to paddy field water and soil due to the disturbances caused by MIW (Kasubuchi et al., 2019). The oxygen supply associated with MIW is expected to improve the anaerobic conditions of soil, significantly reducing CH_4 emissions. Additionally, MIW plows weeds into

the soil while maintaining a flooded state. Some classical literature explains that the decomposition of organic matter in flooded soil is slower than in well-drained soil (Song et al., 2024; Witt et al., 2000). Therefore, the incorporation of weeds associated with MIW may contribute to the enhancement of soil carbon stock. Soil carbon stock is considered one of the most cost-effective methods for mitigating global warming (Lal, 2004).

On the other hand, there are several concerns. In paddy soils that are clearly saturated with water, gas bubbles account for more than 60% of the CH_4 balance in the soil, with the remainder existing in dissolved form (Tokida et al., 2013). This suggests that the disturbance of MIW may induce bubble release, leading to the release of high concentrations of CH_4. According to Booth et al. (2021), the intermediate disturbance frequency (every 7 days) resulted in the highest total GHG emission rate. In contrast, the most frequent disturbance (every 3 days) and no disturbance (0 days) reduced total GHG emissions by 24% and 15%, respectively, compared to the 7-day interval. These patterns mainly depended on differences in ebullitive CH_4 emissions released during the disturbances. Therefore, the frequency of MIW may strongly influence ebullitive CH_4 release, potentially affecting overall GHG emissions and carbon stock. It is important to quantify gaseous CH_4 emissions during MIW and incorporate them into evaluation of GHG emissions and carbon stock balance.

The oxygen associated with MIW is supplied to areas in soil under flooded conditions. This may accelerate oxygen consumption by microorganisms, increase CO_2 (heterotrophic respiration, RH) emissions, and could also accelerate the mineralization of organic matter in both aerobic and anaerobic environments. Since CH_4 production is strongly influenced by the availability of carbon substrates, the addition of organic matter may strongly stimulate CH_4 production (Le Mer and Roger, 2001; Song et al., 2024). N_2O emissions from rice paddy fields occur as a result of nitrification and denitrification processes, both of which have different optimal soil moisture levels (Chen et al., 2021; Wang et al., 2020). Conditions that alternate between wet and dry, such as intermittent irrigation, have been observed to produce high N_2O

concentration. Therefore, the oxygen supply resulting from the regular disturbance of MIW may fluctuate the soil redox condition, promoting N_2O production and increasing emissions.

While there are several previous studies that found MIW to be effective in increasing yield (Kasubuchi et al., 2019; Zhou et al., 2023), few studies have assessed the impact of MIW on GHG emissions and carbon stock. Furthermore, providing incentives such as carbon credits or increased yields to farmers can be a shortcut to social implementation, making it important to evaluate MIW farming practice in terms of environmental impact perspective.

1.4. Objectives and Structure

The objective of this study is to clarify the effects of MIW on GHG emissions, carbon stock, and rice yield, and to evaluate its applicability to sustainable organic rice farming. To achieve this, CH_4 and N_2O emissions from rice-mediated, ebullition, diffusion, and MIW-mediated pathways are quantified. Furthermore, GHG emissions, including MIW-mediated CH_4 and N_2O emissions, rice growth and yield, soil environmental factors, and carbon budget, are monitored to assess the long-term impacts of MIW on the GHG balance, rice yield, and carbon balance.

This thesis is composed of seven sections. **Section 1** presents a general introduction to the study and its objectives. **Section 2** provides a review of the relevant literature related to the research theme. **Section 3** describes the study site, materials, and the general methodologies used in the study. **Section 4** discusses the development of methods to quantify gas emissions through four major pathways, rice-mediated, diffusive, ebullitive, and MIW-mediated, as well as how MIW affects each of these pathways. **Section 5** evaluates the effects of MIW on rice growth, yield, soil environmental factors, GHG balance, and carbon balance based on the results obtained from a five-year monitoring study. **Section 6** is a general discussion of this study. **Section 7** is a general conclusion. Through these sections we verify the feasibility of adaptation.

2. Literature Review

2.1. Trend of Greenhouse Gas Emissions

Since the Industrial Revolution, the rapid increase in GHG in the atmosphere has been mainly due to human activities, becoming a major driver of global warming. GHG with strong forcing includes CO_2, CH_4, and N_2O, among others.

Figure 2.1 shows the trend in global monthly average atmospheric CO_2 concentrations since 1980. Atmospheric CO_2 concentrations have increased an average of 1.90 ppm $year^{-1}$ over the past 45 years (1979-2023), with the rate of increase accelerating to an average of 2.5 ppm $year^{-1}$ in the most resent decade (2014-2023), compared to an average of 1.6 ppm $year^{-1}$ over the past decade (1980-1990) (NOAA, 2024).

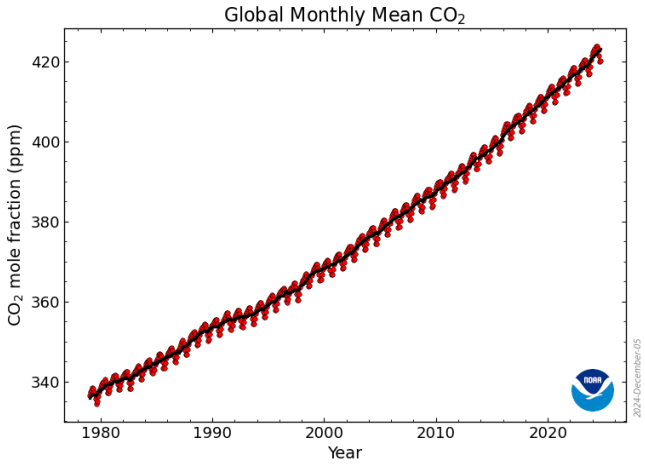


Figure 2.1. Global monthly means CO_2 concentration since 1980 (NOAA, 2024). The dashed red line with diamond symbols represents the monthly mean values, centered on the middle of each month. The black line with the square symbols represents the same, after correction for the average seasonal cycle.

Figure 2.2 shows the trend in global monthly average atmospheric CH_4 concentrations since 1980. Atmospheric CH_4 concentrations tended to increase from 1983 to 1999. This rapid CH_4 growth followed the green revolution with increased crop production and a fast rate of industrialization that caused rapid increases in CH_4 emissions from ruminant animals, rice

cultivation, landfills, oil and gas industry and coal mining (IPCC, 2023). But it remained almost constant during the period 1999-2006. The temporary pause in CH_4 growth rates can be attributed to several factors: a decline in gas flaring due to the surge in oil prices in the 1980s, reduced CH_4 emissions from wetlands caused by lower surface temperatures following the 1991 Mt Pinatubo eruption, and, from the late 1990s to 2006, emission reductions in the oil and gas sector as well as enhanced atmospheric CH_4 oxidation (IPCC, 2023). However, over the past few years (2019-2023), it has again shown a rapid increasing trend with an average of 13.2 ppb $year^{-1}$. The cause of the recent increase is not fully understood, but it has been attributed to warmer temperatures in the Arctic in 2007 and increased precipitation in the tropics in 2007 and 2008, and isotopic measurements indicate that microbial emissions (i.e., from wetlands or agriculture) have continued to increase since 2008 (NOAA, 2024).

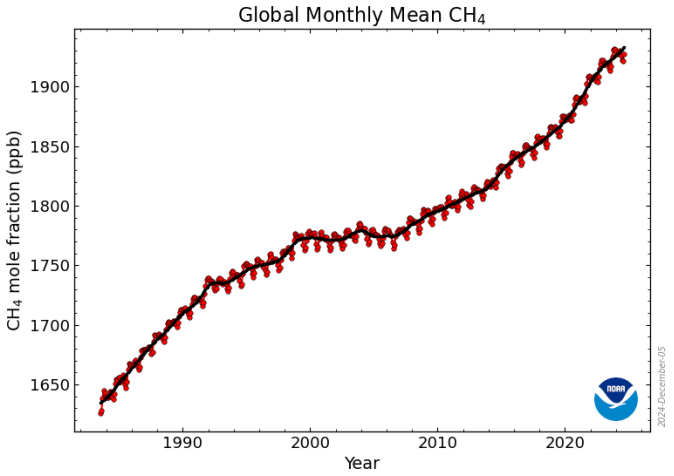


Figure 2.2. Global monthly means CH_4 concentration since 1980 (NOAA, 2024). The red lines and circles are globally averaged monthly mean values centered on the middle of each month. The black line and squares show the long-term trend (in principle, similar to a 12-month running mean) where the average seasonal cycle has been removed.

Figure 2.3 shows the trend in global monthly average atmospheric N_2O concentrations since 1980. The atmospheric load of N_2O has continued to increase over time. In addition, its annual rate of increase, which averaged 1.1 ppb $year^{-1}$ over the past decade, has also increased; the

annual increases measured in N_2O in 2020, 2021, and 2022 are the fastest recorded since measurements began (1.3 ppb $year^{-1}$), while the 2023 increase was 1.03 ppb $year^{-1}$.

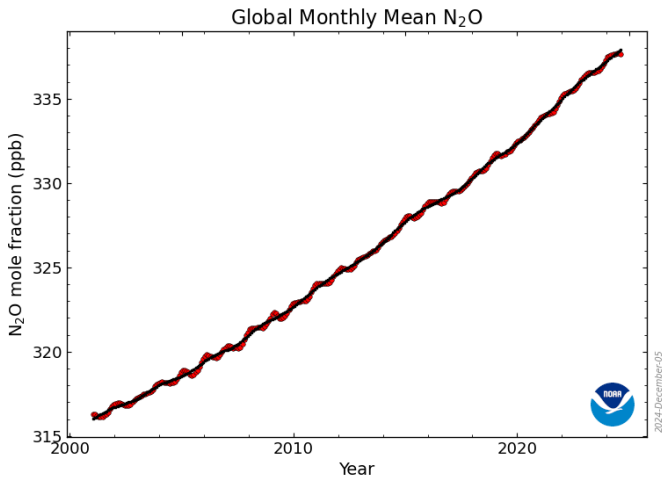


Figure 2.3. Global monthly means N_2O concentration since 1980 (NOAA, 2024). The red lines and circles are globally averaged monthly mean values centered on the middle of each month. The black line and squares show the long-term trend (in principle, similar to a 12-month running mean) where the average seasonal cycle has been removed.

Thus, we can see that atmospheric CO_2, CH_4, and N_2O concentrations have increased rapidly over the past several years. According to IPCC (2023) there is no doubt that human activities have caused global warming mainly through GHG emissions, it's also reporting that the global average temperature based on the 1850-1900 baseline increased by 1.1°C from 2011 to 2020. Therefore, the reduction of these GHG emissions is an urgent issue to mitigate global warming.

Amidst the demand for GHG reductions, the agricultural sector is receiving particular attention. It is reported that emissions from agriculture will account for 11% of the world's total GHG emissions (59 Gt-CO_2) in 2019 (MAFF, 2024, Figure 2.4). Furthermore, GHG emissions from agriculture, forestry, and fisheries in Japan in 2022 accounted for 4.2% of total emissions, of which CH_4 emissions accounted for the majority at 51.1% (MAFF, 2024, Figure 2.4). The

main cause of these CH_4 emissions is rice farming, as the flooded cultivation characteristic of rice paddy fields promotes anaerobic decomposition and increases CH_4 emissions.

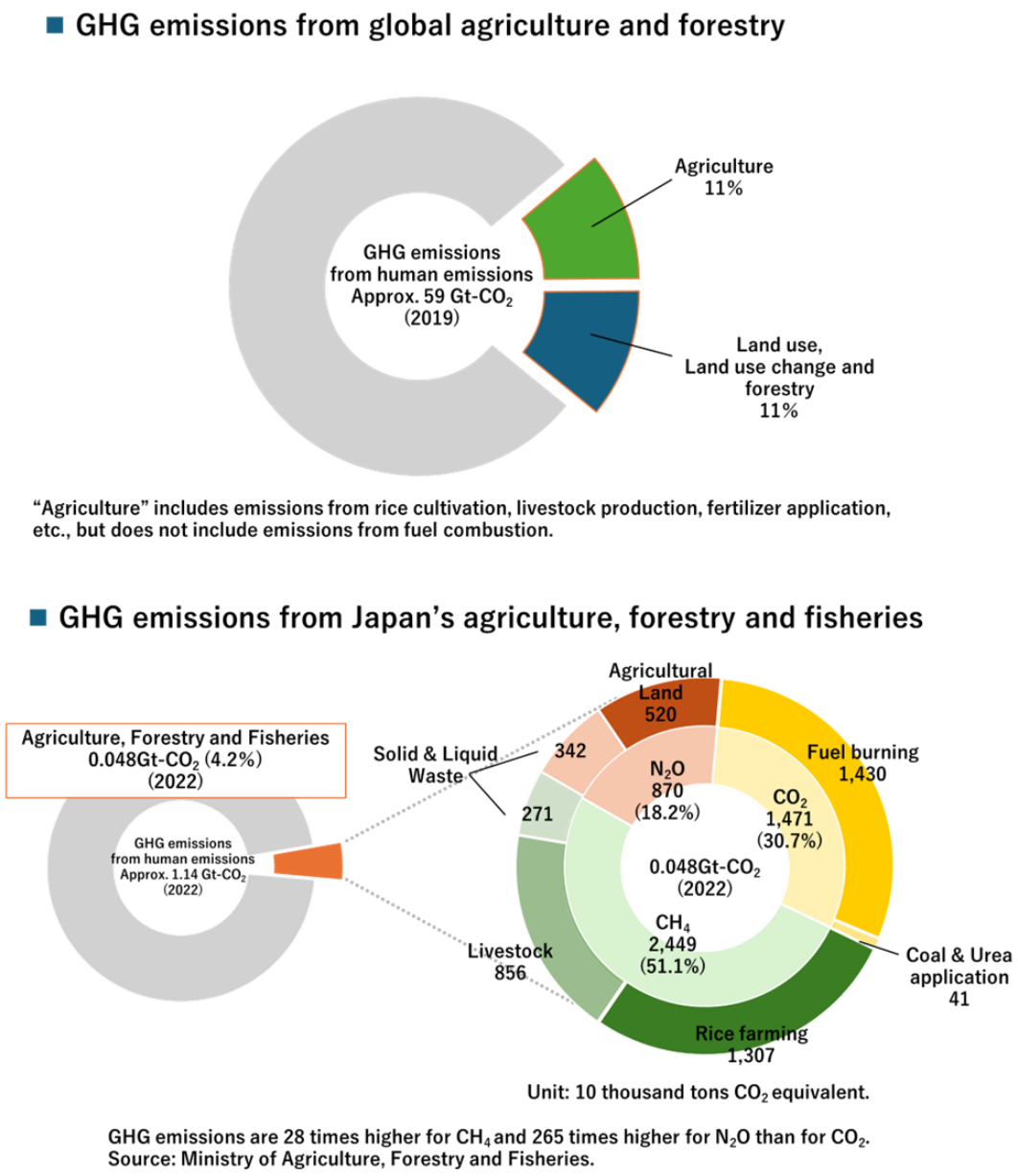


Figure 2.4. Current Greenhouse gas (GHG) emissions (MAFF, 2024 improve).

Rice (*Oryza sativa* L.) is a staple food for almost half of the world's population and is an important crop accounting for 15% of the total calorie supply of the entire crop (Carlson et al., 2017). However, rice production has a significant impact on GHG emissions, particularly CH_4 emissions. For example, according to estimates by Carlson et al. (2017) utilizing spatially

detailed irrigation data, organic material inputs, and cropping calendars, CH_4 emissions from flooded rice paddy fields amounted to 962 Tg CO_2-eq $year^{-1}$, accounting for 92% of total GHG emissions from rice paddy field (Figure 2.5a). Notably, CH_4 emissions from rice paddy fields are concentrated in irrigation areas, which represent 60% of the total harvested rice area but contributed 78% of total rice CH_4 emissions (Figure 2.5b). The results of the regional distribution of GHG emissions suggest that CH_4 emissions from paddy fields in monsoon Asia play an important role in the global GHG budget (Figure 2.5b).

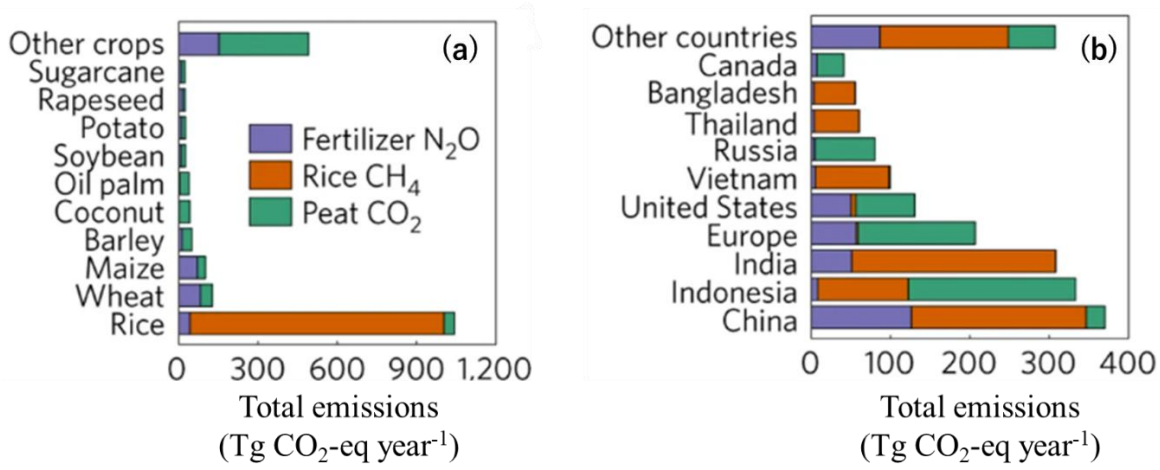


Figure 2.5. Global cropland greenhouse gas emissions (a) and intensities of the top ten emitting food crops and regions (b) (Carlson et al., 2017).

In recent years, international efforts to curb CO_2 emissions have been progressing, with the "4/1000 Initiative" and other initiatives attracting attention. This initiative promotes activities to increase soil carbon based on the concept that "if the amount of carbon in the world's soils could be increased by 4/1000 each year, the increase in atmospheric CO_2 concentration could be controlled" (Kon Kam King et al., 2018). Rice paddy fields, in particular, have the highest carbon concentrations of all terrestrial ecosystems, and the high productivity of rice, regular waterlogging in rice cultivation, and low anaerobic decomposition rates of organic matter associated with rice paddies are favorable for soil carbon storage (Song et al., 2024). Thus, the

management practices of rice paddy fields could make a significant contribution in terms of carbon stock.

2.1.1. Dynamics of Greenhouse Gas in Rice Paddy Field

The dynamics of CH_4 and N_2O in rice paddy fields are shown in Figure 2.6. CH_4 is the end product of anaerobic decomposition of organic matter under anaerobic conditions with a redox potential (Eh) below -150 mV. This process proceeds after inorganic electron acceptors such as nitrate (NO_3^-), ferric (Fe^{3+}) and sulfate ion (SO_4^{2-}) are depleted (Takai, 1969). CH_4 is produced primarily by methanogenic bacteria belonging to the archaeal domain, which includes acetotrophic and hydrogenotrophic methanogens (Qian et al., 2023). Substrate sources for methanogenesis include soil organic carbon (SOC), root leachate, residues from previous crops, and externally added organic matter (Qian et al., 2023, Figure 2.6.).

On the other hand, CH_4 produced in rice paddy fields may be consumed by aerobic methanotroph microorganisms in the topsoil and rhizosphere, where the concentration gradients of O_2 and CH_4 overlap (Qian et al., 2023, Figure 2.6). It has been reported that about 80% of the CH_4 produced in rice paddy field soils is oxidized during its passage through the soil surface layer (Conrad and Rothfuss, 1991). Since the production and oxidation of CH_4 is dependent on microbial activity, the rate of CH_4 production and oxidation is expected to be highly variable depending on environmental conditions. Furthermore, anaerobic oxidation of methane (AOM) has been reported to consume 10-20% of the CH_4 produced in the process where alternative electron acceptors such as NO_3^-, Fe^{3+}, SO_4^{2-} are utilized (Qian et al., 2023, Figure. 2.6). In recent years, this AOM has attracted attention as a mitigation strategy for greenhouse gas emissions, especially the possible important role of electron acceptors including NO_3^-, Fe^{3+}, SO_4^{2-}, and humic acid in AOM (Fan et al., 2020; 2021).

CH_4 accumulated in rice paddy field soils is transported to the atmosphere by three main pathways: through the rice-mediated (about 90%), by ebullition (about 10%), and by liquid-

phase diffusion (<1%) (Schütz et al., 1989). Kajiura et al. (2024) reported that CH_4 emission by the ebullition pathway was particularly pronounced in rice paddy fields planted with "Koshihikari," indicating that the rice variety may affect the CH_4 emission pathway.

Furthermore, because of its low solubility, CH_4 is often trapped as bubbles in rice paddy field soils saturated with water and may account for more than 60% of the CH_4 inventory in the soil (Tokida et al., 2013). Traditionally, CH_4 emissions through the ebullition pathway have been estimated by placing an upside-down funnel on the soil surface to supplement the bubbles generated (Holzapfel-Pschorn et al., 1986) or by chamber measurements in the absence of rice (Komiya et al., 2015). However, with the former method, the shape of the inverted funnel may be affected by environmental variations in rice paddy fields, especially changes in water depth. For example, at shallow water depths, the funnel may not capture enough bubbles, and some emissions may be underestimated. Furthermore, if the surface area of the bubble trap is small, there is a high risk that bubbles will spill out of the funnel and the emissions will not be accurately measured. Therefore, it is important to increase the surface area of the bubble trap to improve the capture efficiency. On the other hand, the latter method is problematic because it assumes that CH_4 emissions from the diffusion pathway are a very small fraction of total emissions. Based on this assumption, there is a risk that the contribution of diffusion pathways will be estimated lower than it actually is, which may hinder an accurate understanding of the overall CH_4 emission dynamics in rice paddy fields. These challenges are major limitations in accurately quantifying CH_4 emission pathways in rice paddy field soils, indicating that it is difficult to adequately capture the dynamics of CH_4 emission pathways using conventional methods alone. In particular, it is important to measure CH_4 emissions in each pathway simultaneously using separate methods to assess the interactions between pathways. This allows for a comprehensive understanding of the impact of each pathway on the others. Recently, Tokida, (2021) demonstrated that by attaching a GasScouter^{TM} G4301 (Picarro Inc., CA, USA) to a chamber, it is possible to continuously and automatically measure gas fluxes from the

ebullition pathway, which are released randomly. However, this method is costly and lacks versatility, indicating the need for the development of inexpensive, accurate, and simple measurement techniques. Therefore, overcoming these challenges requires not only improvements to existing methods, but also the development of new measurement techniques and models capable of simultaneously measuring multiple pathways.

N_2O is produced in two processes: nitrification (under aerobic conditions) and denitrification (under anaerobic conditions). Specifically, N_2O is generated during NH_3 oxidation in nitrification, when NH_4^+ and NO_2^- or NH_2OH are formed as intermediate products (Figure 2.6). On the other hand, denitrification is the reduction process of NO_3^- to N_2 under anaerobic conditions, and N_2O is also generated in this intermediate step. These processes are accelerated by soil management influences, such as the application of synthetic and organic nitrogen fertilizers, crop residue inputs, and the promotion of mineralization of nitrogen of soil organic matter through continuous land cultivation and land use, resulting in N_2O emissions (Akiyama, 2024).

In rice paddy field soils, N_2O is reduced to N_2 by N_2O reductase (complete denitrification), and the activity of this enzyme is very sensitive to soil pH and O_2 concentration. Low soil pH decreases the activity of N_2O reductase and increases the N_2O and (N_2O+N_2) ratio (N_2O/(N_2O+N_2)). Also, when the pore space filled with water exceeds 80%, N_2, rather than N_2O, becomes the main product of denitrification (Qian et al., 2023, Figure 2.6).Therefore, N_2O emissions are generally lower in rice paddy fields under waterlogged conditions due to limited oxygen supply and nitrification rate limitation. However, if soil pH is too low, N_2O reductase activity is inhibited, which can lead to increased N_2O accumulation even under flooded conditions.

In flooded rice paddy soils, N_2O release is reported to be mainly via rice, accounting for 87.3% of the total, whereas in the absence of flooding, N_2O is mainly released via diffusion to the soil surface (Yan et al., 2000). Studies in wetlands have confirmed that aquatic plants absorb

N_2O from the atmosphere to the soil and vice versa based on the N_2O concentration gradient between the atmosphere and the rhizosphere (Li et al., 2018). Therefore, it is possible that a rice-mediated uptake or emission trend could be observed in rice paddy fields, depending on the N_2O concentration in the soil. However, because N_2O emissions in rice paddy fields are lower compared to CH_4 emissions, studies detailing N_2O emission pathways are still limited; for accurate quantification of N_2O emissions, it is important to quantify N_2O emissions in each pathway and to determine the interrelationships among pathways, as was done for CH_4. Such an approach will enable a more comprehensive understanding of the mechanisms of N_2O emissions and the development of effective strategies for emission reductions.

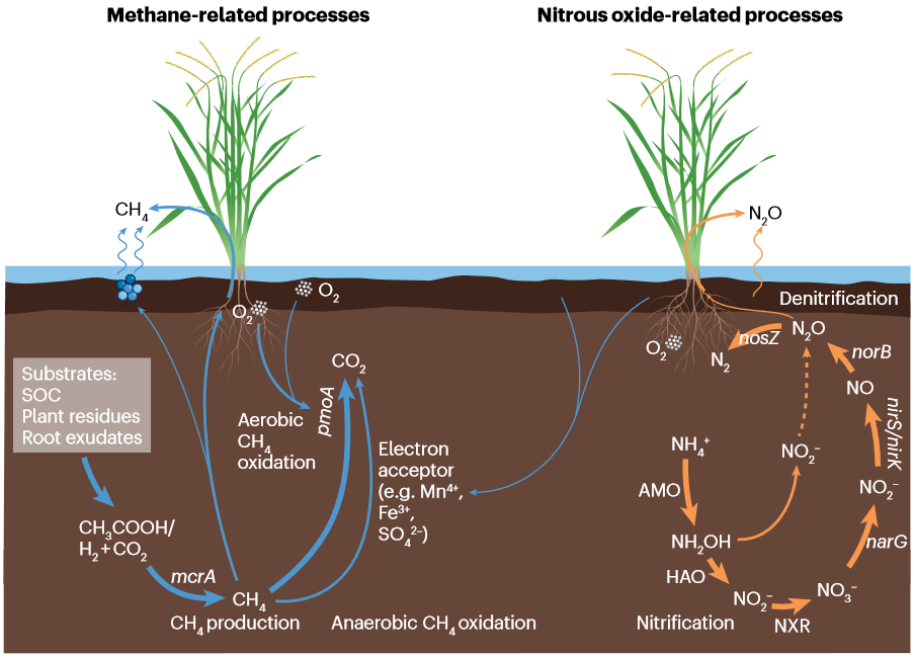


Figure 2.6. Carbon and nitrogen dynamics in a rice paddy field : Pathways of CH_4 and N_2O emissions (Qian et al., 2023). AMO, ammonia monooxygenase; HAO, hydroxylamine oxidoreductase; *mcrA*, methyl coenzyme M reductase; *narG*, nitrate reductase; *nirK*, copper-containing nitrite reductase; *nirS,* haem-containing nitrite reductase; *norB*, nitric oxide reductase; *nosZ*, nitrous oxide reductase.

CO_2 exchange in rice paddy fields results from photosynthesis by plants and respiration activities by autotrophs (plants) and heterotrophs (mainly microorganisms) (Minamikawa et al.,

2005). Plant photosynthesis contributes to CO_2 removal by absorbing not only atmospheric CO_2, but also respiration-derived CO_2 released from the soil.

Previous studies have indicated that both respiration and photosynthesis can offset the CO_2 concentration in the chamber, and it has been common practice to calculate the Global Warming Potential (GWP) mainly considering CH_4 and N_2O and excluding CO_2 (Yu et al., 2004). GWP is defined as the cumulative radiative forcing due to the emission of a unit mass of a GHG relative to a reference gas (CO_2) integrated over a period of time (Miller, 2005).

In recent years, the importance of soil carbon stock has gained attention from the "4/1000 Initiative" and carbon credit initiatives. In particular, it has been reported that under waterlogged conditions in rice paddy fields, the rate of carbon decomposition is reduced and the turnover time of soil carbon is longer as a result of the reduction environment in the soil (Song et al., 2024). This has drawn attention to the effects on carbon cycling and carbon storage in rice paddy fields. Since CH_4 and RH share the same substrate, soil carbon, a quantitative relationship may exist between CH_4 emissions, RH emissions, and soil carbon storage (Minamikawa et al., 2005, Figure 2.6). Naser et al. (2019) evaluated RH, CH_4, and N_2O emissions simultaneously and reported GWP_{RH}, GWP_{CH4}, and GWP_{N2O} contributions to total GWP of 13.8-26.5%, 71.9-86.1%, and 0.13-1.61%, respectively. The results indicate that CH_4 emissions during the rice-growing season contribute significantly to the GWP of rice paddy fields. On the other hand, Wang et al. (2019) reported that RH is the largest contributor to total GWP in early and late rice paddy fields in China. These studies suggest the need to evaluate the three GHG emission fluxes of RH, CH_4, and N_2O not only during the rice-growing season, but also during the fallow season, in order to gain a comprehensive understanding of the carbon cycle in the paddy field.

In particular, carbon stock and GHG emission processes are closely linked, and understanding the impact of one process on the other is essential for developing rice paddy field management strategies. For example, waterlogging management that promotes carbon stock

may increase CH_4 emissions, so assessing carbon stock and GHG emissions simultaneously can provide a more accurate determination of the carbon budget of rice paddy fields. It is also difficult to develop appropriate soil management strategies to control GHG emissions without a comprehensive assessment of the major GHG (especially RH, CH_4, and N_2O) that make up the total GWP. Comprehensive and simultaneous measurement of GHG emissions is important to minimize GHG emissions while maximizing carbon stock potential. In recent years, such comprehensive assessment methods have been revisited, and it is hoped that combining the assessment of GHG emissions by GWP with the assessment of carbon stock will lead to sustainable rice paddy field management.

2.1.2. Existing Greenhouse Gas Mitigation Measures

Field management and agricultural practices play an important role in reducing greenhouse gas emissions from rice paddy fields, including rice variety selection, water management, organic and inorganic fertilizer application, and tillage (Qian et al., 2023).

The effect of non-continuous flooding (NCF) is correlated with the total number of non-flooded days, with one and multiple dry periods expected to reduce CH_4 emissions by 33% and 64% on average, respectively, and other estimates by 29% and 45%, respectively (Qian et al., 2023). On the other hand, compared to continuous flooding, NCF practices effectively increase the activity of most nitrogen-converting microorganisms because they increase the supply of O_2, thus increasing the potential for increased N_2O emissions and the risk of increased RH emissions and carbon loss due to increased decomposition of organic matter in the soil. The practice of NCF increases soil carbon loss and N_2O emissions. However, it is generally reported that the reduction in CH_4 emissions outweighs these effects in terms of GWP. Nonetheless, exceptionally high N_2O emissions (33 kg ha^{-1} $season^{-1}$) have been observed, leading to an overall increase in GWP compared to continuous flooding (Qian et al., 2023). Therefore, further research tailored to different soil types and climatic conditions is necessary.

Long-term organic matter management practices, such as the application or removal of straw, green manure, cover crops, and crop residues, similarly have potential implications for net GHG emissions. In straw management, adding straw generally increases CH_4 emissions compared to its removal. However, promoting decomposition during fallow season (non-flooded) is expected to reduce CH_4 emissions. For instance, returning straw during fallow season could potentially reduce global CH_4 emissions by 5.4 Tg annually (Qian et al., 2023). Therefore, utilizing biochar has shown an average reduction of 13% in CH_4 emissions and 22% in N_2O emissions from rice paddies. Converting rice straw into biochar and applying it back to fields during fallow season could further reduce CH_4 emissions by 4.6 Tg annually (Qian et al., 2023). Nevertheless, these strategies come with challenges. While organic matter application enhances SOC storage and is expected to improve crop yields, the yield-increasing effects may saturate as SOC content increases. Balancing CH_4 mitigation with SOC storage requires optimizing the timing and method of application. Additionally, the high costs of biochar and the lack of production facilities hinder its widespread adoption (Qian et al., 2023). Against this background, it is crucial to comprehensively evaluate GHG mitigation measures and carbon stock effects through the application of organic fertilizers to promote sustainable agriculture while maintaining soil health.

2.2. Decline and Revival of Organic Rice Farming

The development of chemical nitrogen fertilizers using the Haber-Bosch process and phosphorus fertilizers using superphosphate lime marked the beginning of chemical fertilizer use, especially in Europe and the Americas. Stewart et al. (2005) estimated that the number of dependable people per hectare of cultivated land increased from 1.9 in 1908 to 4.3 in 2008, mainly due to the widespread use of chemical nitrogen fertilizers by the Haber-Bosch process. The birth of these chemical fertilizers can be considered a precursor to the “Green Revolution” that followed the agricultural revolution of the 18th century and occurred in the 1940 and 1960.

The Green Revolution encouraged increased production of certain staple foods (rice, wheat, corn, etc.) in developing countries, leading to significant economic growth (Ray, 2022). Against this background, intensive agriculture that relied on chemical fertilizers and synthetic pesticides developed, and there was a shift from conventional organic farming, which utilized the soil's natural resources, to conventional farming, which relied on chemical fertilizers and pesticides.

However, while the spread of conventional farming practices has led to a rapid increase in food production, it has also caused the emission of extra nitrogen into the atmosphere, soil, and hydrosphere. This has then led to various environmental problems such as soil acidification, eutrophication, adverse effects on microorganisms, soil pollution, loss of biodiversity, and reduction of soil organic matter (Wang et al., 2024). The impact of increased N_2O emissions from agricultural lands on global warming is also serious. Recent estimates indicate that about 24 billion tons of fertile soil are lost each year through the practice of conventional farming, with warnings that more than 90% of the Earth's arable land area could be degraded by 2050 (Gomiero, 2016). To deal with these challenges, there is a need to maintain and improve soil health and achieve sustainable and environmentally conscious agriculture, even while ensuring sufficient food production.

In terms of environmental conservation, low-input organic farming is once again attracting attention, with an emphasis on the reuse of unused food residues and the composting of livestock manure. In Japan, based on the “MIDORI Strategy,” the government has set a goal of increasing in organic farming to 1 million hectares (equivalent to 25% of farmland) by 2050 (MAFF, 2024). In fact, the land area for organic agriculture has increased by 37% in 10 years from 2011 to 2021. However, the current situation is far from the goal of 30%, with the organic agriculture land area accounting for only 0.6% of the total arable land in Japan in 2021. In contrast, in European countries such as Italy, Spain, Germany, and France, organic agriculture land area accounts for 9.6 to 16.7% of the total arable land. indicating that organic farming is making progress (MAFF, 2024).

The development of technology to stabilize yields and the clarification of economic benefits through subsidy programs and improved market value are essential to the spread of organic farming. In addition, organic farming is expected to maintain soil health, conserve biodiversity, and reduce environmental impact by controlling the use of chemical fertilizers and pesticides. Furthermore, the potential for GHG reduction and carbon stock is attracting attention, but the risk of increased GHG emissions from compost use must also be assessed. It is important to support the transition to sustainable agriculture through the verification of these short- and long-term effects.

2.3. History and Potential of Multiple Inter-tillage Weeding Practice

Weeding, the process of removing weeds that hinder the growth of rice, is an essential task in rice paddy fields management. The weeding process conducted during the growth period of rice is generally referred to as "inter-tillage weeding". Inter-tillage weeding involves tilling the flooded soil of the rice paddy field during the rice-growing season, burying the weeds in the soil to eliminate them.

According to study by Kasubuchi et al. (2016), in Japan, inter-tillage weeding was carried out using hand weeding or manual weeding machines called "taguruma" until the 1960s (Figure 2.7). Historical records have shown that performing inter-tillage weeding five or more times resulted in high-quality and high-yield rice even in rice paddy fields without the use of fertilizers or pesticides. This method, known as "multiple inter-tillage weeding (MIW)," had the advantage of producing high-quality rice at high yields. As a result, it spread throughout Japan and continued for about 150 years, from the Edo period until its decline at the end of the Edo era. However, with the introduction of Western agricultural practices focused on increasing productivity through the use of fertilizers and pesticides during the Meiji period, the practice of MIW gradually faded (Kasubuchi et al., 2016).



Figure 2.7. Manual weeding machines called "taguruma"

In modern conventional agriculture, the use of fertilizers, pesticides, and herbicides is common. However, due to growing concerns about global environmental issues, there is increasing pressure to reconsider these practices. Sustainable farming that minimizes input while ensuring nutrient self-sufficiency, provides safe and reliable food, and is in harmony with the environment, is becoming more urgent. In light of this, there is a renewed interest in reintegrating MIW into rice farming. (Kasubuchi et al., 2019) demonstrated that combining four or more inter-tillage weeding practices (at intervals of 4, 8, 12, and 16 times) with paddy fields that do not use fertilizers or pesticides resulted in approximately 5000 kg ha^{-1} of high-quality rice over multiple years (five years). This result confirmed the effectiveness of the traditional MIW practice, suggesting not only its weed control benefits but also the potential multifunctionality associated with soil disturbance.

However, few studies have evaluated the multifunctionality of soil disturbance caused by MIW. Among these, the "mineralization of nitrogen due to soil disturbance" is critical for assessing nutrient sustainability. Additionally, "oxygen supply from soil disturbance" could influence greenhouse gas emissions from rice paddy fields. Moreover, "the supply of residues and weeds due to disturbance" is an important factor affecting GHG emissions and could also contribute to improved carbon stock. Therefore, scientifically evaluating the effects of disturbance caused by MIW is crucial for addressing contemporary global environmental challenges and finding effective solutions.

3. Common Material and Methods

3.1. Study Site

This study was conducted on research rice paddy fields of the Field Science Center (FSC) for Northern Biosphere, Hokkaido University (43°04'29" N, 141°20'16" E) (Figure 3.1). The mean annual air temperature and precipitation in Sapporo over the past 30 years (1991-2020) were 9.2℃ and 1146 mm, respectively. The site is in the Köppen climate classification subtype subarctic humid climate (Dfa). The soil type was grey, lowland soil. Organic rice farming fields have not used chemical fertilizers and agricultural chemicals since 2018. Conventional rice farming (CF) has been managed with chemical fertilizers, pesticides, and herbicides since 2019. Organic rice farming was managed without fertilizer or agricultural chemicals starting in 2019. Initial soil characteristics of the soil pH, Electrical Conductivity (EC), nitrate acid ion (NO_3^-), sulfate acid ion (SO_4^{2-}), ammonium ion (NH_4^+) contents, total C (TC) and total N (TN) at 0-10 cm depth in 2019 for CF and for organic rice farming (OF) are shown in Table 3.1.The method used to determine soil pH, EC, NO_3^-, SO_4^{2-}, and NH_4^+ are described later in the **Section 3.6.3**. TC and TN were determined by elemental analyzer (vario MAX CN Macro, Elementar, Frankfurt, Germany).

Table 3.1. Initial soil characteristics in conventional rice farming (CF) and organic rice farming (OF) site.

	Soil pH	EC	NO_3^-	SO_4^{2-}	NH_4^+	TC	TN
		mS m^{-1}	mg N kg^{-1}	mg S kg^{-1}	mg N kg^{-1}	%	%
CF	6.00	10.6	1.79	42.3	0.54	2.88	0.23
OF	6.11	6.51	0.32	22.3	0.21	2.84	0.21

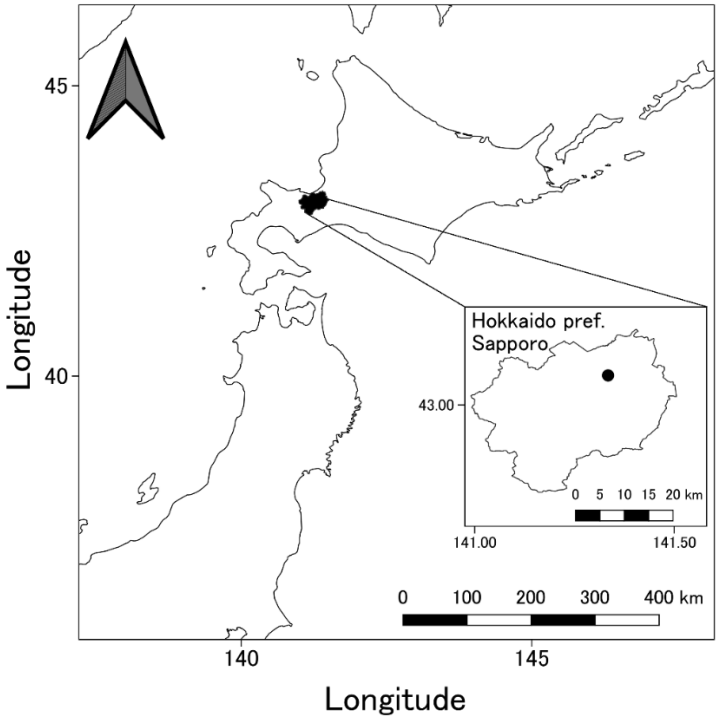


Figure 3.1. Location of the study site in Sapporo, Hokkaido, Japan.

3.2. Experimental Design and Field Management

The organic rice farming field (1000 m^2) was randomly divided into three treatments with no inter-tillage weeding (T0), two times of inter-tillage weeding (T2), and five times of inter-tillage weeding (T5) in three replications (8.33 × 13.3 m $plot^{-1}$) (Figure 3.2a). CF field (500 m^2) was established in three replications (8.33 m × 20 m $plot^{-1}$ in 2019 to 2022; 8.33 m × 10 m $plot^{-1}$ in 2023) (Figure 3.2b). However, since CF was in different locations, it was used for reference and not for analysis of the between treatments.

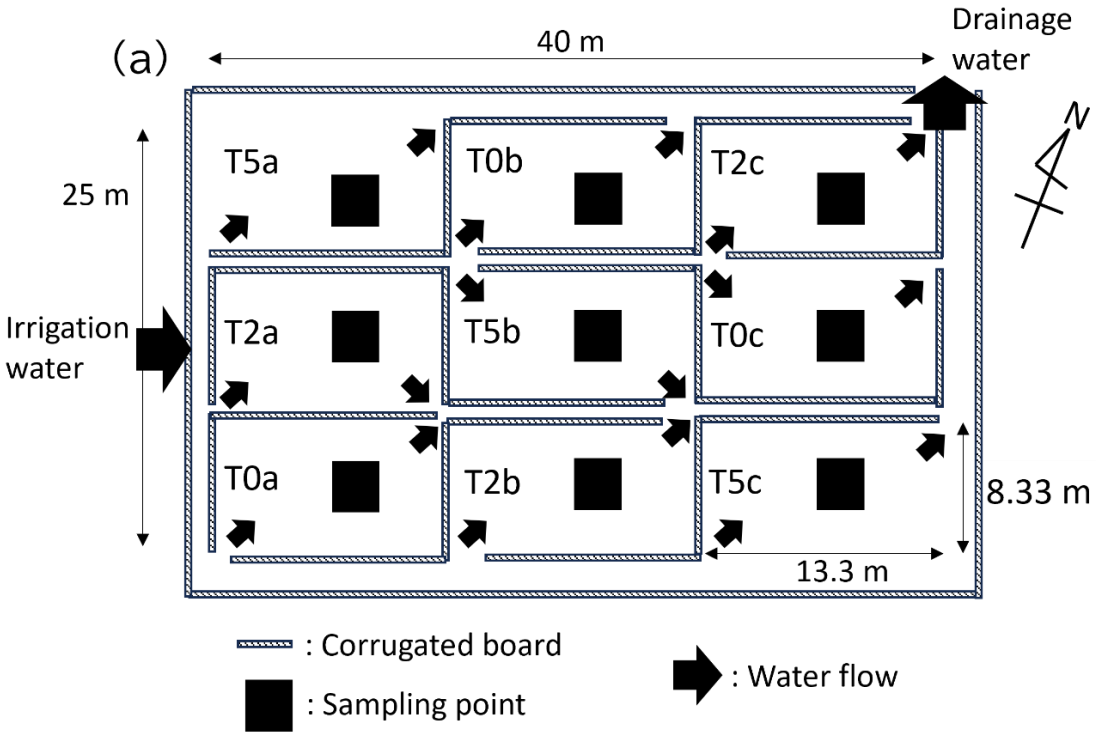


Figure 3.2. Layout of the paddy field with organic rice farming without fertilizer and agricultural chemicals which divided 3 plots by inter-tillage weeding times (a) and conventional rice farming (CF) plots (b). The lowercase alphabet means repetition.

The details of field management for 2019 to 2023 are shown in Table 3.2 to Table 3.6. At CF, the chemical fertilizer N, P, and K were applied as basal fertilizer. The amount of its applications in each year are shown in Table 3.7. Calcium silicates were applied as supplementary fertilizer at 27 kg SiO_2 ha^{-1} in 2020 and 2021. However, in 2022 and 2023, they were applied as 360 kg SiO_2 ha^{-1} basal fertilizer, respectively. In addition, herbicides and pesticides were applied several times between June and August of each year. Over five years periods, rice transplantation was conducted in late May in all treatments after soil plowing. Thirty-four-day-old greenhouse-grown *Oryza sativa* 'Nanatsuboshi' seedlings (three seeds per cell) were transplanted in late May after plowing at a density of 24 hills m^{-2}. The seeds used in the CF were disinfested with chemical agents, while those used in organic rice farming were disinfected with vinegar. Harvesting was conducted in late September or early October.

From 2019 to 2023, shredded rice straw was returned to the soil surface in all treatments after harvest. However, in 2021 and 2022, residues (rice straw, stubble, and roots) were incorporated into the soil through tillage after its application, and an additional tillage was conducted in May before the next year's transplanting. In contrast, in 2019, 2020, and 2023, the residues were left in the rice paddy fields during the winter fallow season (from October to May) after harvest. From November to April, the residues were covered with deep snow in below freezing temperatures. Tillage was then conducted in May before transplanting to incorporate the residues into the soil.

Waterlogging was maintained from mid-May to late July, followed by mid-season drainage from mid-July to early August over five years periods. After that, intermittent drainage was conducted until the complete drainage. In 2019 only, mid-season drainage and intermittent drainage were not conducted (Table 3.8).

Table 3.2 Schedule of field management in 2019.

Month/Day	CF	T0	T2	T5

4/10~18	Preparation for seeding			
4/18	Seeding			
5/13	Fertilization			
5/17	Tillage & Irrigation			
5/20	Soil plowing	Soil plowing (surface)	Soil plowing (surface)	Soil plowing (surface)
5/23	Transplantation			
	Pesticide			
5/27			Inter-tillage weeding 1	Inter-tillage weeding 1
6/5				Inter-tillage weeding 2
6/14				Inter-tillage weeding 3
6/25				Inter-tillage weeding 4
7/3			Inter-tillage weeding 2	Inter-tillage weeding 5
7/24	Pesticide			
8/9	Pesticide			
8/20	Complete Drainage			
10/2	Harvest & Spraying rice straw			

Note: Treatments CF, T0, T2 and T5 are conventional rice farming, and organic rice farming with no inter-tillage weeding, two time of inter-tillage weeding, and five time of inter-tillage weeding without fertilizer and agricultural chemical.

Table 3.3. Schedule of field management in 2020.

Month/Day	CF	T0	T2	T5
4/13-22	Preparation for seeding			
4/23	Seeding			
5/14		Leveling	Leveling	Leveling
5/18	Fertilization and Tillage			
5/20		Tillage	Tillage	Tillage
	Irrigation			
5/22	Soil plowing			
5/29	Transplantation			
6/2			Inter-tillage weeding 1	Inter-tillage weeding 1
6/11	Herbicide			
6/12				Inter-tillage weeding 2

6/24				Inter-tillage weeding 3
6/25-30	Pesticide			
7/1				Inter-tillage weeding 4
7/6	Fertilization			
7/10			Inter-tillage weeding 2	Inter-tillage weeding 5
7/17	Pesticide			
8/4	Pesticide			
8/26		Complete drainage		
10/8		Harvest		
10/21		Spraying rice straw		

Note: Treatments CF, T0, T2 and T5 are conventional rice farming, and organic rice farming with no inter-tillage weeding, two time of inter-tillage weeding, and five time of inter-tillage weeding without fertilizer and agricultural chemical.

Table 3.4. Schedule of field management in 2021.

Month/Day	CF	T0	T2	T5
4/13-22		Preparation for seeding		
4/23		Seeding		
4/28		Tillage	Tillage	Tillage
4/29		Leveling	Leveling	Leveling
5/12		Soil compaction	Soil compaction	Soil compaction
5/13	Fertilization			
5/14	Tillage			
5/16		Tillage (surface)	Tillage (surface)	Tillage (surface)
5/18		Irrigation		
5/21		Soil plowing		
5/27		Transplantation		
6/5			Inter-tillage weeding 1	Inter-tillage weeding 1
6/16				Inter-tillage weeding 2
6/23				Inter-tillage weeding 3
6/28	Herbicide			
6/30	Fertilization			

7/1				Inter-tillage weeding 4
7/8	Pesticide			
7/9			Inter-tillage weeding 2	Inter-tillage weeding 5
7/19	Herbicide			
7/29	Pesticide			
8/27		Complete drainage		
9/27		Harvest		
9/28		Spraying rice straw		
11/6		Tillage		

Note: Treatments CF, T0, T2 and T5 are conventional rice farming, and organic rice farming with no inter-tillage weeding, two time of inter-tillage weeding, and five time of inter-tillage weeding without fertilizer and agricultural chemical.

Table 3.5. Schedule of field management in 2022.

Month/Day	CF	T0	T2	T5
4/12-21		Preparation for seeding		
4/22		Seeding		
5/10	Fertilization			
5/11		Tillage	Tillage	Tillage
5/13	Tillage			
5/19		Irrigation		
5/22	Soil plowing	Soil plowing (surface)	Soil plowing (surface)	Soil plowing (surface)
5/26		Transplantation		
6/6			Inter-tillage weeding 1	Inter-tillage weeding 1
6/16				Inter-tillage weeding 2
6/23				Inter-tillage weeding 3
6/30				Inter-tillage weeding 4
7/4	Herbicide			
7/8			Inter-tillage weeding 2	Inter-tillage weeding 5
7/19	Herbicide			

8/10	Herbicide	
8/26	Complete drainage	
9/29	Harvest	
9/30	Spraying rice straw	
10/28	Tillage	

Note: Treatments CF, T0, T2 and T5 are conventional rice farming, and organic rice farming with no inter-tillage weeding, two time of inter-tillage weeding, and five time of inter-tillage weeding without fertilizer and agricultural chemical.

Table 3.6. Schedule of field management in 2023.

Month/Day	CF	T0	T2	T5
4/11~18	Preparation for seeding			
4/19	Seeding			
5/10	Fertilization & Tillage	Tillage	Tillage	Tillage
5/16	Irrigation			
5/19	Soil plowing	Soil plowing	Soil plowing	Soil plowing
5/23	Transplantation			
6/6	Herbicide		Inter-tillage weeding 1	Inter-tillage weeding 1
6/13				Inter-tillage weeding 2
6/20				Inter-tillage weeding 3
6/22	Herbicide			
6/27				Inter-tillage weeding 4
6/28	Pesticide			
7/4			Inter-tillage weeding 2	Inter-tillage weeding 5
7/7	Herbicide			
7/12	Herbicide			
8/16	Complete drainage			
9/21	Harvest & Spraying rice straw			
9/30	Harvest & Spraying rice straw			

10/18	Calcium cyanamide	

Note: Treatments CF, T0, T2 and T5 are conventional rice farming, and organic rice farming with no inter-tillage weeding, two time of inter-tillage weeding, and five time of inter-tillage weeding without fertilizer and agricultural chemical.

Table 3.7. The amount of chemical fertilizer applied in CF in each year.

	2019	2020	2021	2022	2023
N (kg N ha^{-1})	98	90	80	85	85
P (kg P_2O_5 ha^{-1})	98	119	39	80	80
K (kg K_2O ha^{-1})	72	39.6	40	40	40

Table 3.8. Water management for each year.

	2019	2020		2021	2022	2023
	CF T0/T2/T5	CF	T0/T2/T5	CF T0/T2/T5	CF T0/T2/T5	CF T0/T2/T5
Irrigation	5/17	5/20	5/20	5/18	5/19	5/16
Mid-season drainage	NA	7/12-19	7/28-8/1	7/29-8/2	7/23-27	7/21-28
Intermittent irrigation	NA	7/20-8/25	8/2-25	8/3-26	7/28-8/25	7/29-8/15
Complete drainage	8/20	8/26	8/26	8/27	8/26	8/16

Note: Treatments CF, T0, T2 and T5 are conventional rice farming, and organic rice farming with zero tillage, two tillage, and five tillage without fertilizer and agricultural chemical. NA means no implementation.

3.3. Multiple Inter-tillage Weeding (MIW) Practice

The number of MIW was determined to be 0, 2, and 5 times based on the statement that 4 to 8 times or more did not make a significant difference in rice yield (Kasubuchi et al., 2019). MIW was practiced five times at T5, about once every 7-10 days, twice at T2, on the first and final day of the period. The tools used for MIW are shown in Figure 3.3. The MIW periods were from May 27 to July 3 in 2019, June 2 to July 10 in 2020, June 5 to July 9 in 2021, June 6 to July 8 in 2022, and June 6 to July 4 in 2023, respectively.



Figure 3.3. The devices of multiple inter-tillage weeding (MIW) for weeding between the rows in 2019-2021 (a), 2022-2023 (b) and for weeding between rice plants (c).

3.4. Measuring Greenhouse Gas Fluxes by Static Closed Chamber Method

Because the static closed chamber method is logistically feasible, the experimental system is low cost, and it is easy to implement in the field scale (Minamikawa et al. 2015), we employed this method to estimate GHG emissions.

3.4.1. Gas sampling

RH, CO_2 (sum of gross primary production (GPP) and ecosystem respiration (RE)), CH_4, and N_2O fluxes from the rice paddy fields were measured using a static closed chamber method (Toma et al., 2016). During the rice-growing season, we used a combination of transparent acrylic chambers (30 cm × 60 cm × 80 cm maximum) for CO_2 (GPP+RE), CH_4, and N_2O fluxes measurements (Figure 3.4a). In 2019, 2020, 2021, transparent acrylic chamber A (30 cm × 60 cm × 80 cm) was placed on a metal chamber base. After that, A was processed to make acrylic chamber B with L-shaped angle (30 cm × 60 cm × 40 cm) and acrylic chamber base C (30 cm × 60 cm × 40 cm). In 2022 and 2023, only chamber B was used when the rice plants were small in height, and chamber B was placed on chamber C after the rice plants had grown to a certain extent. The acrylic chamber contained four rice plants at the time of measurement. Then, fan for mixing air (San Ace 80 9S0812F4011, SANYO DENKI, Osaka, Japan), pressure control bag, gas sampling port, and thermometer (PC-9215II, SATO, Tokyo, Japan) were installed to the acrylic chamber.

We used stainless-steel chambers (20 × 25 cm) for RH measurements during the rice-growing season. The stainless-steel chamber was placed on the area (0.125 m^2) where the boards were inserted to a depth of 20 cm in the inter-row space to prevent rice plant and weed's root invasions (Figure 3.4b). The lid of the stainless-steel chamber was installed with a pressure control bag, gas sampling port, and thermometer. In the fallow season, stainless-steel chambers were used for RH, CH_4, and N_2O fluxes measurements (Figure 3.4c).

Gas samples in the chamber headspace were taken at 0, 6 minutes after closing chambers and injected into a 500 mL tedlar bag by a 25 mL gas tight syringe for CO_2 (GPP+RE) and RH measurements. The CO_2 flux was calculated at two points of 0 and 6 minutes based on the theoretical consideration that the increase in the CO_2 concentration in the chamber loses linearity after about 8 minutes (Nakano et al., 2004). Gas samples in the chamber headspace were taken at 0, 15 and 30 minutes after closing chambers and 20 mL were injected into an evacuated glass vial of 10 mL by a 25 mL gas tight syringe for CH_4 and N_2O analysis.

Gas sampling was conducted between 9:00 and 14:00. It was taken at 7 to 10 day intervals during the MIW period, 14 day intervals between after MIW and harvest, and 30 days intervals during fallow season.

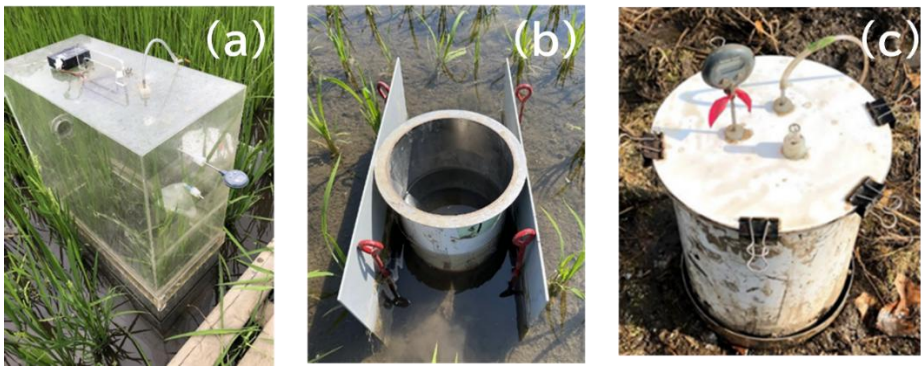


Figure 3.4. The devices of CO_2 (GPP (sum of gross primary production) + RE (ecosystem respiration)), CH_4, and N_2O fluxes sampling during the rice-growing season (a), RH (heterotrophic respiration) flux sampling during flooding period (b) and CH_4, N_2O and RH fluxes sampling during the fallow season (c).

3.4.2. Analysis of Gas concentrations

CO_2 (GPP+RE) and RH concentration were determined using an infrared CO_2 analyzer (Model ZEP9GC11; FUJI ELECTRIC, Tokyo, Japan). Before analysis, zero-point calibration was performed using nitrogen (N_2) and span calibration using 1860 ppmv CO_2. CO_2 concentration was calculated by multiplying the output value of the infrared CO_2 analyzer by 20.

In 2019 and 2020, CH_4 concentrations were determined using gas chromatography with a flame ionization detector (FID) (GC-8A and GC-14B, SHIMADZU, Kyoto, Japan). High purity N_2 was used as the carrier gas. N_2O concentrations were determined using gas chromatography with an electron capture detector (GC-2014, SHIMADZU, Kyoto, Japan). PR gas (Ar+5%CH_4) was used as the carrier gas.

In 2021, 2022, and 2023, a gas chromatography (GC-14B and GC-2014) with two detectors was used to simultaneously measure CH_4 and N_2O concentrations, and flow path was changed by a valve to allow each detector to measure the components separated by the column. Filtered N_2 to remove carbides, O_2, and moisture was used as the carrier gas, and high-concentration CH_4 was used as the make-up gas for ECD detection.

Calibration curves were prepared for CH_4 at four standard gas points (1.98, 4.79, 9.94 and 994 ppmv) and for N_2O at four standard gas points (0.3, 0.6, 1.5, 6, and 30 ppmv). The detection limits for FID and ECD were approximately 0.75 and 0.019 ppmv, respectively.

3.4.3. Calculation for Gas Fluxes

GHG fluxes from the rice paddy fields were calculated using the following liner regression equation (Toma et al., 2011):

$$F = \rho \times (V/A) \times (dC/dt) \times 273/(273 + T) \times \alpha \quad (1)$$

where, F is the total gas flux (mg C or N m^{-2} h^{-1}), ρ is the density of each gas under standard conditions (CO_2 = 1.997×10^6 mg m^{-3}, CH_4 = 0.717×10^6 mg m^{-3}, N_2O = 1.978×10^6 mg m^{-3}), V is the volume of the chamber (m^3), A is the surface area of the chamber (m^2), dC/dt is the rate of change in gas concentration in the head space of the chamber during the sampling time (10^{-6} m^3 m^{-3} h^{-1}), T is the air temperature inside the chamber (℃), and α is the ratio of molar mass of carbon to the molecular weight of CO_2 (12/44) and CH_4 (12/16), or of nitrogen to N_2O (28/44).

3.4.4. Calculation for Cumulative Gas Emissions

The cumulative GHG emissions were calculated from equation (2) using liner interpolation and trapezoidal method, using the fluxes obtained for each sampling date in each plot. The cumulative RH, CO_2 (GPP+RE), CH_4, and N_2O emissions were converted to kg C or kg N ha^{-1}.

In general, RH and CO_2 (GPP+RE) fluxes are highly dependent on temperature (Shimizu et al., 2009), which may lead to underestimation of nighttime RH and CO_2 (GPP+RE) emissions at the calculation of cumulative emission by trapezoidal method. Therefore, a method is often employed in which soil temperature is continuously measured, and a relationship between soil temperature and RH and CO_2 (GPP+RE) fluxes is used to more accurately estimate nighttime values (Shimizu et al., 2015). However, in this study, the method was not applied. Therefore, in this study, measured RH and CO_2 (GPP+RE) fluxes data was directly used for analysis.

$$Q = 1/2 \sum[(d_{i+1} - d_i) \times (F_{i+1} + F_i) \times 24 \times 10^{-5}] \quad (2)$$

where Q is the cumulative gas emission (kg C or N ha^{-1}), d_i is the measurement date, F_i is the gas flux on any measurement date.

3.5. Measuring Gas Concentrations in Paddy Field Water and Soil Air

To understand GHG dynamics in soil and paddy field water, GHG concentrations were determined using various methods described below.

3.5.1. Sampling for Soil Air and Dissolved Gas in Paddy Field Water

In 2020 to 2023, CH_4 and N_2O concentrations in the soil air were measured using a compact buried tubing soil-gas monitoring system (Kato et al., 2013) (Figure 3.5a). The centers of the gas-exchange parts were buried at 5 and 10 cm depth between rows. Soil air sampling tubes were installed one week prior to the sampling date to allow time for gas exchange. Each soil air sample (5 mL) was placed in an evacuated glass vial (10 mL) containing 10 mL of pure N_2. The CH_4 and N_2O concentrations were determined using the gas chromatography.

In 2023, the equipment used for measuring gas concentrations in soil air gas was improved to reduce variability among treatments. Specifically, a new dilution gas port was added to the existing equipment, enabling N_2 based dilution and pressure adjustment directly in the field (Figure 3.5b). In the improved equipment, 50 mL gas tight syringes were attached to both the gas sampling port and the dilution gas port. First, N_2 equivalent to the volume of the gas exchange tube (approximately 47 mL) was introduced through the dilution gas port, displacing the gas into the syringe attached to the gas sampling port (Figure 3.5c). This step was performed to maintain atmospheric pressure within the gas exchange tube and to prevent negative pressure during sampling, which could lead to inconsistent gas collection or contamination by ambient air. The displaced gas was then pushed back into the system, and this back-and-forth process was repeated twice to ensure gas homogenization. After homogenization, 20 mL of gas was sampled using a 20 mL gas tight syringe and pressurized into a 10 mL vacuum vial.

Gas sampling was conducted at 7-10 days interval during the MIW period, 14 day interval between after MIW and harvest, and 30 day intervals during fallow season.

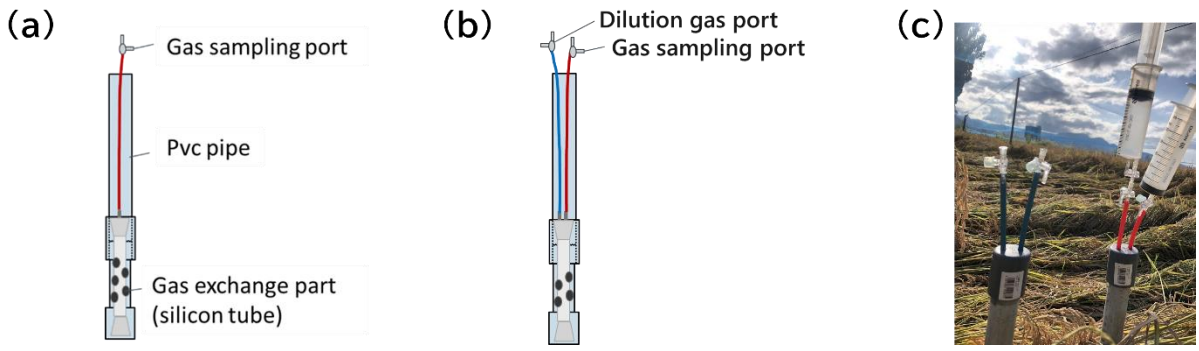


Figure 3.5. The equipment for measuring soil air gas. Scheme of existing equipment (a), improved equipment (b), and state of sampling (c).

In 2022 to 2023, dissolved CH_4 and N_2O concentrations in the paddy field water were investigated during the flooding period. This sampling was conducted at 7-10 days interval during the MIW period, 14 day interval between after MIW and harvest. In each plot, 30 mL paddy field water and 30 mL air were collected using a 60 mL gas tight syringe and shaken for 3 min. Each gas sample (20 mL) from the headspace of the syringe was placed in an evacuated glass vial (10 mL) (Morishita & Hatano, 1999). The CH_4 and N_2O concentrations were determined using the gas chromatography.

3.5.2. Calculation for Dissolved Gas Concentration in Paddy Field Water

Dissolved CH_4 and N_2O concentrations in the paddy field water were calculated using the following equations (Hu et al., 2018; Yang et al., 2020):

$$C_{water} = [(C_H - C_A) \times V_H + \beta \times C_H \times V_w]/V_w \times \alpha \quad (3)$$

where C_{water} is the dissolve CH_4 and N_2O concentrations in the paddy field water (mg C or N L^{-1}), C_H is the CH_4 and N_2O concentrations in the headspace of the syringe (mg C or N L^{-1}), C_A is the CH_4 and N_2O concentrations in air (mg C or N L^{-1}), V_H is the volume of headspace

in the syringe (= 0.03 L), β is the absorption coefficient of Bunsen (for CH_4) or Oswalt (for N_2O) (Kimochi et al., 2014), V_w is the volume of water in the syringe (0.03 L).

3.6. Environmental Factors

3.6.1. Ancillary measurements

Daily air temperature and precipitation were obtained from the close Automated Meteorological Data Acquisition System (AMeDAS) station of the Japan Meteorological Agency which are located about 2.5 km from the study site.

Soil temperature at depth of 3 cm and 10 cm and water temperature in paddy field water in each treatments was measured using a thermometer (CT-414WR, CUSTOM, Tokyo, Japan). It was taken at 7 to 10 day intervals during the MIW period, 14 day intervals between after MIW and harvest, and 30 day intervals during fallow season.

Water temperature and water depth were automatically measured approximately every 15 minutes using a water temperature and water depth sensor (FARMO, Tochigi, Japan). One sensor was installed in the center of the field in each of the CF and organic rice farming fields.

3.6.2. Soil Sampling and Soil Solution Extraction

Soil samples at 0-3 cm depth were collected from each treatment in two replicates using an auger (DIK-102A; Daiki Rika Kogyo, Saitama, Japan) at 7-10 days interval during the MIW period, 14 day interval between after MIW and harvest, and 30 day intervals during fallow season. Water and KCl extracts were obtained using deionized water (50 mL) for the soil sample 10 g and 2 M KCl (50 mL) for the soil sample 5 g.

In 2021 to 2023, the ferrous iron (Fe^{2+}) concentration was measured at 5 cm depth. Soil samples were collected in two replicates from each plot using a gas-tight syringe (20 mL) with the tip cut off. After collecting 5 g of the soil sample from the center of the syringe (approximately 5 cm depth), 50 mL of acetic acid buffer (pH 3.0) was quickly added, and the

extracted samples were obtained by shaking for 5 min and filtering. Soil sampling for Fe^{2+} measurements were conducted during the rice-growing season.

3.6.3. Analysis of Soil Physicochemical Properties

The NH_4^+ content of the KCl extract was determined by indophenol blue method using a UV-VIS Spectrophotometer (UV-1280, SHIMADZU, Kyoto, Japan) .

The soil pH of the water extract was measured using a pH meter (F-22, Horiba, Kyoto, Japan). The EC was measured using an EC meter (CM-30V, DKK-TOA Co., Tokyo, Japan). The NO_3^- and SO_4^{2-} contents of the water extracts were measured by ion chromatography (DIONEX ICS-1100, Thermo Fisher Scientific, MA, USA). And the organic carbon content of the water extracts (WEOC) was measured by TOC analyzer (TOC-L CSN, SHIMADZU, Kyoto, Japan) in 2022 and 2023. Air-dried soil was used for soil analysis from 2019 to 2020, and fresh soil was used from 2021 to 2023. Since air-drying and longtime preservation of soil have little effect on the profile of the soil microbial community (Wang et al., 2021), the soil physicochemical properties in 2019, 2020, 2021, 2022, and 2023 were assumed to be identical and used for comparison.

The Fe^{2+} concentration of the extracted samples was measured by *o*-phenanthroline method using a UV-VIS Spectrophotometer.

3.6.4. Analysis of Soil Physical Properties

Two 100 cm^3 core samplers (5.0 cm in inner diameter and 5.1 cm in height) were connected using vinyl tape to collect undisturbed soil samples from the 0–5 cm and 5–10 cm layers. Samples were collected from the inter-row spaces that were free from disturbance due to foot traffic or chamber installation during gas sampling. One sample per treatment plot was collected, for a total of 12 samples. Soil core sampling was conducted on the same day as gas sampling or within two days before or after. The samples were transported to the laboratory within two

hours of collection. Upon arrival, the cores were separated at the connection using a knife, and the core volume at 0–5 cm and 5–10 cm depths was measured using a core volumeter (DIK-1150, Daiki, Saitama, Japan). The fresh weight of the soil was then measured, followed by oven-drying at 105°C for more than 48 hours. After cooling to room temperature in a desiccator, the dry weight was measured. Based on these measurements, solid-phase ratio, liquid-phase ratio, air-phase ratio, porosity, and bulk density were calculated according to the method described by the Hokkaido Research Organization (2012). If immediate volume measurement was not possible, the samples were stored in a refrigerator (4°C).

3.6.5. Measurement of Soil Environmental Conditions

In 2022 to 2023, the redox potential (Eh) at 5 cm depth was measured from each treatment in three replicates using Eh meters (Model No:PRN-41, Platinum electrode:EP-201, Comparison electrode:4400, Electrode lead wire:ELW-45, FUJIWARA SIENTIFIC, Tokyo, Japan). For the Eh meter, measurements were taken after leaving them in the soil for at least 24 hours. Similarly, the hold function of the device was used, and measurements were recorded after the data stabilized. This measurements were conducted at 7 to 10 days interval during the MIW period, 14 day interval between after MIW and harvest period.

3.6.6. Plant Measurement

Four plants were randomly selected from each treatment, then plant height, tiller number, and chlorophyll content were measured as growth indicators. Chlorophyll content was measured using a chlorophyll meter (SPAD-502plus, KONICA MINOLTA, Tokyo, Japan). These measurements were conducted at 7 to 10 days interval during the MIW period, 14 day interval between after MIW and harvest period.

4. Multiple Inter-tillage Weeding Effect on Methane and Nitrous Oxide Emissions Pathways from Rice Paddy Fields

4.1. Introduction

Rice is a staple food for almost half of the global population, with demand rising due to population grows. However, nitrogen and phosphorus are critically oversaturated (Rockström et al., 2009), necessitating a shift to sustainable organic rice farming that maximizes soil nitrogen without the use of chemical fertilizers. Conventional rice farming achieves high yields but risks soil fertility degradation and higher GHG emissions. Specifically, rice paddy fields are important sources of CH_4 and nitrous oxide N_2O, which are potent GHGs that contribute to global warming. Rice paddy fields contribute 22% of the agricultural CH_4 and 11% of the agricultural N_2O emissions (Mboyerwa et al., 2022).

MIW, an organic rice farming used since the Edo period in Japan, involves shallow tilling to remove weeds and incorporate them into the soil. Kasubuchi et al (2019) reported that conducting MIW four or more times can produce high-quality rice comparable to conventional rice farming without chemical fertilizer inputs. MIW is also believed to reduce CH_4 emission by increasing soil oxygen, which enhances methanotroph activity and CH_4 oxidation under aerobic conditions (Ding et al., 2005). However, the MIW may also release CH_4 gas bubbles, which account for over 60% of CH_4 in paddy soils (Tokida et al., 2013), potentially causing rapid emission of high concentrations of CH_4. Additionally, N_2O is produced during nitrification and denitrification. Previous studies indicated that changes in redox conditions, associated with intermittent drainage, contribute to N_2O emissions from rice paddy fields (Fang et al., 2021; Liu et al., 2019). Thus, the oxygen supply from MIW may influence N_2O emissions as well.

CH_4 is released into the atmosphere through diffusion, ebullition, and rice-mediated pathways (Hosono and Nouchi, 1997). CH_4 emissions from diffusion are easily oxidized as they

spend the longest time transiting the aerobic and anaerobic soil areas (Ma et al., 2022). Whereas CH_4 emissions from ebullition are not easily oxidized due to the high CH_4 concentrations in the bubbles, which are rapidly emitted into the atmosphere (Zhu et al., 2016). Rice-mediated CH_4 emissions avoid aerobic areas but 20–90% can be oxidized in the rhizosphere or rice's aeration tissues (Ma et al., 2022). These pathways are influenced by the soil's redox environment, which can significantly affect CH_4 emissions. MIW may alter this environment, impacting CH_4 emissions. Changes in redox conditions also affect N_2O emissions, and it is known that the conversion of soil to anaerobic condition has a trade-off relationship where CH_4 emissions decrease while N_2O emissions increase. Therefore, in addition to monitoring the effect of MIW on CH_4, it is also important to monitor N_2O. However, research on MIW's effects on processes such as nitrification and denitrification are still limited. Furthermore, understanding the relationship between gas emissions from the MIW-mediated pathway and those from the rice-mediated pathway, diffusion, and ebullition is also crucial for elucidating the mechanism of GHG reduction. Thus, accurate field-scale quantification is crucial for understanding the MIW's impact on emission dynamics. Automated monitoring systems are currently being developed by Kajiura and Tokida (2021) and Tokida (2021), but there is also a need for simple, inexpensive, and accurate method for short term comparative investigation.

This study aimed to develop a simple, inexpensive, and accurate method for evaluating the impact of MIW disturbances on CH_4 and N_2O transport processes. Specifically, we improved the conventional bubble trap method (Holzapfel-Pschorn et al., 1986) by using a shallow tray with a large surface area to measure emissions from ebullition pathways. We also used a closed chamber method to measure diffusion pathways, setting a threshold for gas emissions in the stainless-steel chamber. This allowed us to separately measure emissions from the ebullition and diffusion pathways and indirectly calculate the emissions from the rice-mediated pathway. Additionally, we quantified the MIW-mediated gas emissions by using a closed chamber with the function of disturbance. By developing the method to individually quantify CH_4 and N_2O

emission pathways (rice-mediated, diffusion, ebullition, and MIW-mediated), we evaluated the impact of MIW on CH_4 and N_2O emissions through the verification of the following hypothesis: 1) MIW promotes oxygen supply, but its effects exceed CH_4 oxidation, inducing high-concentration CH_4 gas bubbles and ultimately increasing total CH_4 emissions. 2) MIW fluctuates redox potential, promoting N_2O production in paddy field water and soil, thereby increasing total N_2O emissions.

4.2. Materials and methods

4.2.1. Investigating periods

The study covered the cultivation period from May 30 to September 28 in 2022 and May 30 to September 9 in 2023. CH_4 and N_2O emission from each pathway were monitored during the MIW periods (June 10 to July 13 in 2022 ; June 9 to July 7 in 2023) to evaluate the measurement method. MIW was conducted on June 6, 16, 23, 30, and July 8 in 2022 and on June 6, 13, 20, 27, and July 4 in 2023 at T5; and June 6 and July 8 in 2022, and June 6 and July 4 in 2023 at T2.

4.2.2. Total and diffusive gas flux

Total CH_4 and N_2O fluxes were measured during the cultivation period (May-September) using transparent acrylic chambers (Figure 3.4a) by static closed-chamber method shown in **Section 3.4.1**. However, based on the planting density, the number of plants was underestimated by 7.4%. Gas sampling was conducted between 9:00 and 14:00 at 7-10 days interval during the MIW period and at 14 day interval during the rest of the period. The number of gas sampling for each treatment was 11 times $year^{-1}$ in 2022 and 13 times $year^{-1}$ in 2023.

For diffusive CH_4 and N_2O fluxes measurement, stainless-steel cylindrical chambers (20 × 25 cm) were deployed in bare plots (0.125 m^2) created in each treatment by inserting two root cuttings (50 × 40 cm, 20 cm depth) (Figure 3.4b). Weeds were manually removed a day before gas sampling to minimize interference. The chamber lids remained open for at least 30 minutes

before measurements to allow stabilization. Each chamber was equipped with a pressure control bag, gas sampling port, and thermometer.

Gas samples from the chamber headspace were taken at 0, 15, and 30 min after closing the chamber using a 25 mL gas tight syringe. Sample (20 mL) was injected into the evacuated glass vial (10 mL). CH_4 and N_2O concentrations were analyzed using the gas chromatograph shown in **Section 3.4.2**.

Total and diffusive CH_4 and N_2O fluxes were calculated using the liner regression equation (1) shown in **Section 3.4.3**.

For diffusive gas fluxes measurement, ebullitive gas flux was excluded based on the CH_4 concentration change rate dC/dt in the chamber headspace. A threshold of 0.29 ppmv min^{-1} was used to distinguish ebullition events (sudden increases) from diffusive emissions (gradual increases) (Komiya et al., 2015). Data exceeding this threshold was excluded to isolate the net diffusive flux.

4.2.3. Ebullitive gas flux

Ebullitive CH_4 and N_2O fluxes were measured using the bubble trap method, chosen for its low cost and ease of implementation at the field scale. This method captures gas bubbles that form within an inverted, water-filled funnel placed on the surface water (Holzapfel-Pschorn et al., 1986). To improve efficiency, the funnel was replaced with a shallow, transparent polypropylene tray (0.20 m × 0.31 m × 0.037 m) to increase the trapping surface area. During the MIW period (early June to early July), the tray was placed in the paddy field water between the central rows of each plot (Figure 4.1), displacing air in the trap with paddy field water to ensure bubble collection.

Bubble samples were collected through the tray's sampling port, and the trapped bubble volume was measured using a gas-tight syringe (50 mL). Each bubble sample (5 mL) was

placed in an evacuated glass vial (10 mL) containing 15 mL of pure nitrogen. Ebullition gas sampling was conducted during the MIW period.

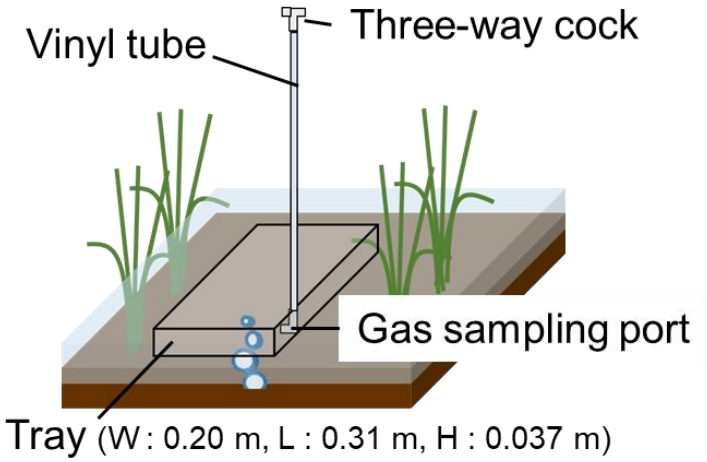


Figure 4.1. Scheme of bubble traps.

CH_4 and N_2O concentrations in the bubbles were determined by gas chromatography, and the ebullition gas fluxes were calculated using the following equation:

$$F_E = \rho \times V_{trap}/A_{trap} \times dC_{trap}/dt_{trap} \times 273/(273 + T) \times \alpha \quad (4)$$

where F_E is ebullitive gas fluxes (mg C or N m^{-2} h^{-1}), V_{trap} is the trapped bubble volume (m^3), A_{trap} is the tray surface area (0.062 m^2), C_{trap} is the gas concentration in the trapped bubbles (10^{-6} m^3 m^{-3}), t_{trap} is the trapping duration (h). T is the air temperature during the ebullition gas sampling (°C).

In 2022, gaseous CH_4 concentration was calculated from the CH_4 concentration in the trapped bubbles and the air-phase ratio. Dissolved CH_4 in pore water was estimated based on Henry's law, assuming equilibrium between the gas and liquid phases (Tokida et al., 2005). The air- and liquid- phase ratio was calculated by the method which is described in **Section 3.6.4**.

4.2.4. Rice-mediated gas flux

Rice-mediated gas fluxes (mg C or N m^{-2} h^{-1}) were calculated from the difference between the total CH_4 and N_2O flux and the diffusive and ebullitive CH_4 and N_2O fluxes. Because the total, diffusive and ebullitive gas fluxes were measured on different dates, it was necessary to match the time axes. Therefore, using the Forecast function (Microsoft Excel 2016), a regression equation was developed based on the measured values of ebullition gas flux. This equation was then used to estimate the ebullition flux on the dates when total and diffusive gas fluxes were measured, and the estimated values were used to calculate the rice-mediated gas flux.

4.2.5. Calculation for cumulative gas emission

The cumulative CH_4 and N_2O emissions from each pathway were calculated using the equation (2) shown in **Section 3.4.4**.

4.2.6. MIW-mediated gas flux

To quantify the impact of CH_4 and N_2O emissions during MIW, MIW-mediated CH_4 and N_2O fluxes were also measured using a static closed-chamber method in 2023. During the MIW period, we used transparent acrylic chambers (30 × 60 × 40 cm) with MIW function of lids to measure MIW-mediated CH_4 and N_2O fluxes (Figure 4.2). The chamber was placed stationary between the rows during the MIW period, and gas sampling was conducted in three parts: before-disturbance, immediately-after-disturbance, and after-disturbance. Between each parts, the chamber lid was opened about 30 minutes to vent the atmosphere. Gas samples (15 mL) for CH_4 and N_2O were collected at 0, 10, and 20 minutes from the chamber headspace before- and after-disturbance. For immediately-after-disturbance sampling, a 0-minute sample was taken near the chamber before closing the lid, followed by two back-and-forth disturbances, with samples collected at 10 and 30 seconds. Each gas sample (20 mL) was transferred into a 10 mL evacuated glass vial for analysis using gas chromatography. MIW gas flux measurements were conducted weekly before MIW.

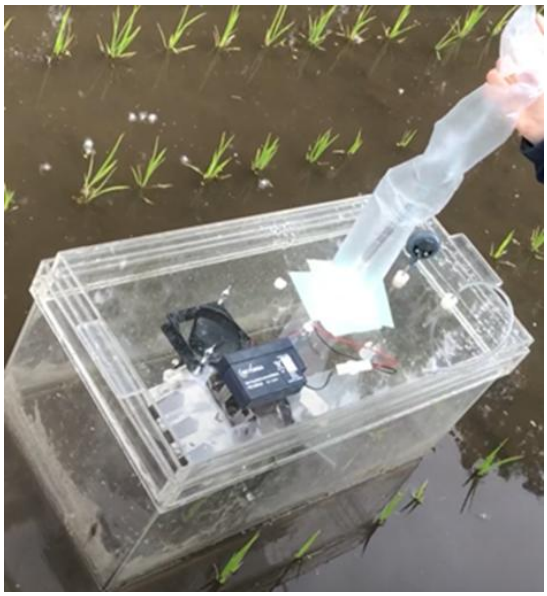


Figure 4.2. The device of multiple inter-tillage weeding (MIW)-mediated CH_4 and N_2O flux sampling.

Cumulative CH_4 and N_2O emissions from MIW-mediated were calculated using equation (5). The CH_4 or N_2O flux at three parts before-, immediately-after-, and after-disturbance was plotted on the y-axis and the end time of each gas sampling on the x-axis. Because the rapid increase in gas flux during MIW tended to converge within 1 hour, we assumed the CH_4 and N_2O emissions during MIW as converging in 1 hour, which was used in the calculations.

$$Q_{MIW} = F_{MIW} \times t_{MIW} \quad (5)$$

where Q_{MIW} is the cumulative gas emission from MIW-mediated (kg C or N ha^{-1}), F_{MIW} is the CH_4 or N_2O flux immediately-after-disturbance by MIW (kg C or N m^{-2} h^{-1}), t_{MIW} is the converging time (=1 h). The contribution ratio of Q_{MIW} to total emissions of MIW period was calculated at T2 and T5 in 2023. Q_{MIW} for 2022 was estimated using this ration and total emissions for that year.

4.2.7. Measurement of environmental factors

CH_4 and N_2O concentrations in the soil air gas at 5 and 10 cm depth were measured using a compact buried tubing soil-gas monitoring system shown in **Section 3.5.1**. Soil air gas sampling was conducted on the same day as total gas sampling. Each soil air gas sample (5 mL) was placed in an evacuated glass vial (10 mL) containing 10 mL of pure nitrogen. The CH_4 and N_2O concentrations were determined using gas chromatography.

Dissolved CH_4 and N_2O concentrations in paddy field water were measured by the method shown in **Section 3.5.1** and **3.5.2** during the flooding over the cultivation period, including the MIW period. This sampling was conducted on the same day as total gas sampling. Water samples were collected from the central depth of the surface water in each plot at 7-10 days interval during the MIW period and at 14 day interval during the rest of the period.

The average daily air temperature, precipitation and atmospheric pressure during the cultivation period of 2022 and 2023 were obtained from the AMeDAS which described in **Section 3.6.1**. Water temperature and soil temperatures at 3 cm depths in each plot were measured using a thermometer during total and diffusive gas sampling. Water depth was calculated as the difference between the height of the acrylic chamber measured during total gas sampling and its original height. These values were then compared with the readings from the water depth sensor installed at the center of each field.

Eh at 5 cm depth was measured during the cultivation period using Eh meters which describe in **Section 3.6.5**.

Rice plant height and tiller number were measured as rice growth indicators which describes in **Section 3.6.6.**

4.2.8. Statistical analysis

Differences among T0, T2 and T5 were tested using One-way ANOVA. Differences between pathways and years were tested using a two-way ANOVA for each treatment. If a significant

difference was observed, a multiple-comparison test was performed using the Tukey-HSD test. The relationship between CH_4 and N_2O fluxes and environmental factors was tested using Pearson's correlation coefficient test. For each statistical analysis, a difference or correlation was considered significant when the significance level was <5%. However, since CF was in different locations, it was used for reference and not for analysis of the between treatments. The analysis was performed using R (R Development Core Team, 2022; version 4.2.2).

4.3. Results

4.3.1. Each CH_4 flux during the MIW period

No significant differences in total CH_4 flux were observed between treatments in both years (Figures 4.3a and 4.3b). Although there were no significant differences in total CH_4 emissions, total CH_4 emissions were highest at T0 (21.2 kg C ha^{-1}) in 2022, and at T5 (16.4 kg C ha^{-1}) in 2023 at organic rice farming field. Total CH_4 emissions at T5 remained the same in both years, and the amount of the treatments tended to vary between years (Table 4.1).

Diffusive CH_4 flux ranged from -0.02 to 1.14 mg C m^{-2} h^{-1}, varying between years (Figures 4.3c and 4.3d). On 13 July 2022, T0 was significantly higher than T2 and T5, while on 7 July 2023, T2 and T5 were significantly higher than T0. Diffusive CH_4 emissions were highest at T0 (4.17 kg C ha^{-1}) in 2022 and at T2 (1.78 kg C ha^{-1}) in 2023 at organic rice farming field (Table 4.1).

Ebullitive CH_4 flux ranged from 0.0001 to 0.32 mg C m^{-2} h^{-1}, with no significant differences among treatments (Figures 4.3e and 4.3f). Ebullitive CH_4 emissions were highest at T0 and T5 (0.17 kg C ha^{-1}) in 2022 and at T2 (0.12 kg C ha^{-1}) in 2023 at organic rice farming field but showed no significant treatment differences in both year (Table 4.1).

Rice-mediated CH_4 flux ranged from 0.02 to 6.77 mg C m^{-2} h^{-1}, varying between years and were not significantly different among treatments in each year (Figures 4.3g and 4.3h). Rice-mediated CH_4 emissions were greater at T0 > T2 > T5 in 2022 but reversed in 2023 with T5 >

T2 > T0 (Table 4.1). No significant differences were found, but trends differed between the years.

MIW-mediated CH_4 flux more at T5 (disturbances every 7 days) compared to T2 (disturbances every 28 days). At T2, CH_4 flux rose from 2.64 mg C m^{-2} h^{-1} (6 June 2023) to 131 mg C m^{-2} h^{-1} (4 July 2023). At T5, CH_4 flux increased from 1.99 mg C m^{-2} h^{-1} (June 6) to 297 mg C m^{-2} h^{-1} (July 4), showing a tendency to increase with each measurement. MIW-mediated CH_4 emissions were 1.41 kg C ha^{-1} in 2022 and 1.34 kg C ha^{-1} in 2023 at T2 and 4.48 kg C ha^{-1} and 6.68 kg C ha^{-1} at T5 (Table 4.1).

4.3.2. Relationship between each CH_4 flux and environmental factors during the MIW period

Total CH_4 flux correlated positively with the water temperature at CF and T0, but not at T2 or T5 (Table 4.2). Significant correlations were also observed with soil temperature, plant height, tiller number (positive), and Eh (negative) across treatments.

Diffusive CH_4 flux correlated positively with dissolved CH_4 concentration at CF and T0, but not at T2 and T5 (Table 4.2).

Ebullitive CH_4 flux correlated positively with water and soil temperature at T5, respectively, as well as with plant height and tiller number across treatments, and negatively with Eh (Table 4.2).

Rice-mediated CH_4 flux correlated positively with water temperature at CF and T0 but not at T2 and T5 (Table 4.2). Additionally, a positive correlation with soil temperature was observed at CF, T0, and T2. Furthermore, plant height, tiller number, and Eh showed significant correlations across all treatments.

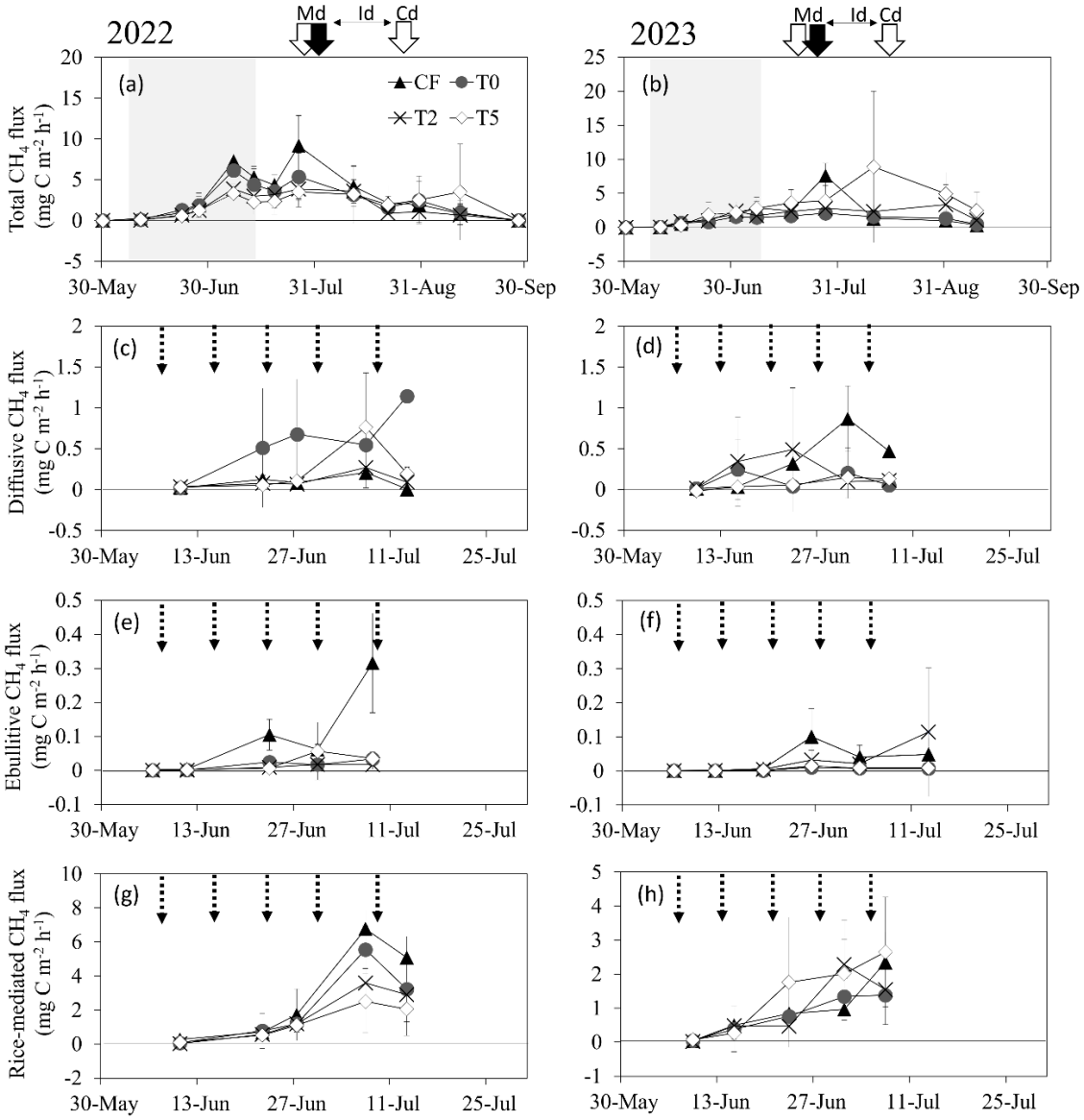


Figure 4.3. Seasonal variation in total methane (CH_4) flux in 2022 (a), 2023 (b), diffusive CH_4 flux in 2022 (c), 2023 (d), ebullitive CH_4 flux in 2022 (e), 2023 (f), rice-mediated CH_4 flux in 2022 (g), 2023 (h). Black and white arrows denote the timing of irrigation and drainage. Md indicates mid-season drainage, Id indicates intermittent drainage and Cd indicates complete drainage. Dotted arrows indicated inter-tillage weeding. Gray scale denotes the MIW period (June 10 to July 13 in 2022 and June 9 to July in 2023).

Table 4.1. Comparison of each pathways of CH_4 during multiple inter-tillage weeding (MIW) period.

		CF†		T0		T2		T5	
		CH_4 emission (Contribution ratio to total CH_4 emission)							
Year	Pathway	kg C ha^{-1}(%)							
2022	Diffusion	0.85 (4)	b‡	4.17 (20)	b	0.92 (6)	c	1.96 (13)	a
	Ebullition	1.05 (5)	b	0.17 (1)	b	0.09 (1)	c	0.17 (1)	a
	Rice-mediated	21.6 (92)	a	16.8 (80)	a	12.3 (84)	a	9.52 (61)	a
	MIW-mediated	NA§ (NA)	NA	NA (NA)	NA	1.41 (9)	c	4.48 (24)	a
	Total	23.5	NA	21.2	A	14.7	A	16.1	A
2023	Diffusion	2.48 (29)	b	0.88 (16)	b	1.78 (16)	bc	0.49 (4)	a
	Ebullition	0.25 (3)	b	0.03 (0)	b	0.12 (1)	c	0.04 (0)	a
	Rice-mediated	5.82 (68)	a	5.41 (84)	b	6.69 (71)	b	9.19 (62)	a
	MIW-mediated	NA (NA)	NA	NA (NA)	NA	1.34 (11)	c	6.68 (33)	a
	Total	8.55	NA	6.32	A	9.93	A	16.4	A
ANOVA	Pathway	***		***		***		**	
	Year	ns		**		ns		ns	
	Pathway × Year	ns		**		*		ns	

† Treatments CF, T0, T2 and T5 are conventional rice farming, and organic rice farming with no inter-tillage weeding, two time of inter-tillage weeding, and five time of inter-tillage weeding without fertilizer and agricultural chemical.

‡ Small alphabet with the same letter is not significantly different in each column and capital alphabet with the same letter is not significantly different in each line ($p < 0.05$).

§ NA means no implementation.

*** $p < 0.001$, ** $p < 0.01$, * $p < 0.05$, ns, not significant ($p > 0.05$).

Table 4.2. Peason correlation coefficient between CH_4 flux from each pathways and environmental factors during MIW period.

Pathway	Treatment	AD‡	WT	ST	WD	Plant height	Tiller number	Eh	Dis CH_4	SG5 CH_4	SG10 CH_4
		hPa	℃	℃	cm	cm	$hill^{-1}$	mv	mg C L^{-1}	ppmv	ppmv
Diffusion	CF†	0.15	-0.35	-0.21	0.54*	0.01	0.15	-0.33	0.80***	0.48	0.50
	T0	-0.30	0.46	0.64*	0.39	0.86***	0.81***	-0.85***	0.61*	-0.37	-0.38
	T2	0.40	0.48	0.35	-0.46	-0.08	0.08	-0.47	-0.06	-0.22	0.17
	T5	0.36	0.64*	0.79***	-0.39	0.70**	0.82***	-0.89***	-0.14	0.89***	-0.46
Ebullition	CF	-0.09	0.23	0.41	-0.49	0.87***	0.83***	-0.71**	0.20	-0.15	-0.26
	T0	-0.34	0.45	0.70**	0.37	0.94***	0.92***	-0.90***	0.70**	-0.34	-0.33
	T2	-0.10	-0.05	0.30	0.0003	0.69**	0.67**	-0.55*	0.48	-0.19	0.15
	T5	0.30	0.65*	0.72**	-0.39	0.61*	0.74**	-0.77**	-0.31	0.94***	-0.43
Rice-mediated	CF	0.06	0.57*	0.70**	-0.39	0.93***	0.91***	-0.77**	0.27	-0.19	-0.29
	T0	0.21	0.72**	0.93***	-0.07	0.91***	0.95***	-0.92***	0.58*	-0.44	-0.44
	T2	0.07	0.43	0.74**	-0.15	0.92***	0.94***	-0.77**	0.38	-0.44	0.08
	T5	-0.08	0.01	0.46	0.27	0.68**	0.63*	-0.65*	0.75**	0.06	-0.07
Total	CF	0.08	0.54*	0.69**	-0.35	0.94***	0.93***	-0.81***	0.35	-0.16	-0.25
	T0	0.13	0.71**	0.93***	0.01	0.94***	0.97***	-0.95***	0.61*	-0.45	-0.45
	T2	0.12	0.49	0.78***	-0.22	0.90***	0.94***	-0.83***	0.37	-0.46	0.11
	T5	-0.001	0.15	0.59*	0.16	0.76**	0.74**	-0.77**	0.64*	0.25	-0.16

† Treatments CF, T0, T2 and T5 are conventional rice farming, and organic rice farming with no inter-tillage weeding, two time of inter-tillage weeding, and five time of inter-tillage weeding without fertilizer and agricultural chemical.

‡AD represent average difference in atmospheric pressure over the days of measurement, WT represent water temperature, ST represent soil temperature at 3 cm depth, WD represent water depth, Eh represent soil redox potential at 5 cm depth, Dis CH_4 represent the dissolved CH_4 concentration in paddy field water, SG5 CH_4 and SG10 CH_4 represent CH_4 concentration in soil air gas at 5 and 10 cm depth.

*** $p < 0.001$, ** $p < 0.01$, * $p < 0.05$.

4.3.3. Comparison of CH_4 emission pathways during the MIW period

Rice-mediated CH_4 emissions were the dominant pathway (61-92%) in all treatments across both years (Table 4.1). Diffusion and ebullition were the next major contributors at CF and T0. At T5, MIW-mediated CH_4 emissions were the second-largest pathway followed and at T2, diffusion pathway or MIW-mediated, depending on the year, followed by ebullition. Diffusion contributed 4–29%, while ebullition was negligible (0–5%). MIW-mediated accounted for only 3–8% of total CH_4 emissions during cultivation, which were much higher overall. (Table 4.3).

A two-way ANOVA showed pathways significantly influenced CH_4 emissions ($p < 0.01$) (Table 4.1). At T0, year differences affected CH_4 emissions ($p < 0.01$), with interaction effects between pathway and year at T0 and T2 ($p < 0.05$).

Table 4.3. Cumulative CH_4 emissions (mean ± SD) during the cultivation period and contribution ratio of multiple inter-tillage weeding (MIW).

	CH_4 emission (Contribution ratio of MIW) kg C ha^{-1} (%)	
	2022	2023
CF[†]	85.8±20.2 (NA[‡])	49.1±9.90 (NA)
T0	68.0±29.9 (NA) a[§]	29.8±2.46 (NA) a
T2	50.9±6.19 (3) a	48.6±27.5 (3) a
T5	64.4±61.0 (8) a	97.5±81.9 (7) a

[†] Treatments CF, T0, T2 and T5 are conventional rice farming, and organic rice farming with no inter-tillage weeding, two time of inter-tillage weeding, and five time of inter-tillage weeding without fertilizer and agricultural chemical.

[‡] NA means no implementation.

[§] Value with the same letters is not significantly different in each column ($p < 0.05$).

4.3.4. Each N_2O flux during the MIW period

Total N_2O flux showed no significant differences between treatments but varied widely with time, showing both positive and negative values (Figures 4.4a and 4.4b). Total N_2O emissions were either negative or positive, showing both absorption and emission trends. The amount of treatments tended to vary between years (Table 4.4).

Diffusive N_2O flux ranged from -14.9 to 46.1 µg N m^{-2} h^{-1}, also varying between years (Figures 4.4c and 4.4d). Diffusive N_2O emissions were highest at T5 in both years, showing an increasing trend compared T0 (Table 4.4).

Ebullitive N_2O flux ranged from 0.002 to 0.43 µg N m^{-2} h^{-1}, showing no significant differences between treatments (Figures 4.4e and 4.4f). Ebullitive N_2O emissions were negligible and not significantly affected by treatments, remaining similar with or without MIW in both years (Table 4.4).

Rice-mediated N_2O flux ranged from -47.2 to 15.2 µg N m^{-2} h^{-1} and was largely negative (Figures 4.4g and 4.4h). No significant differences between treatments were found. Rice-mediated N_2O emissions followed the order T2 > T0 > T5 in 2022, and T2 > T0 > T5 in 2023, though the magnitudes differed yearly (Table 4.4).

MIW-mediated N_2O flux showed no clear pattern. At T2, it increased from 0.421 mg N m^{-2} h^{-1} (6 June 2023) to 0.705 mg N m^{-2} h^{-1} (4 July 2023). At T5, it varied from 0.092 mg N m^{-2} h^{-1} (6 June 2023) to 5.20 mg N m^{-2} h^{-1} (13 June 2023), -0.077 mg N m^{-2} h^{-1} (20 June 2023), -0.070 mg N m^{-2} h^{-1} (27 June 2023), and 0.241 mg N m^{-2} h^{-1} (4 July 2023). MIW-mediated N_2O emissions were 0.02 kg N ha^{-1} in 2022 and 0.01 kg N ha^{-1} in 2022 at T2 and 0.02 kg N ha^{-1} and 0.05 kg N ha^{-1} at T5 (Table 4.4).

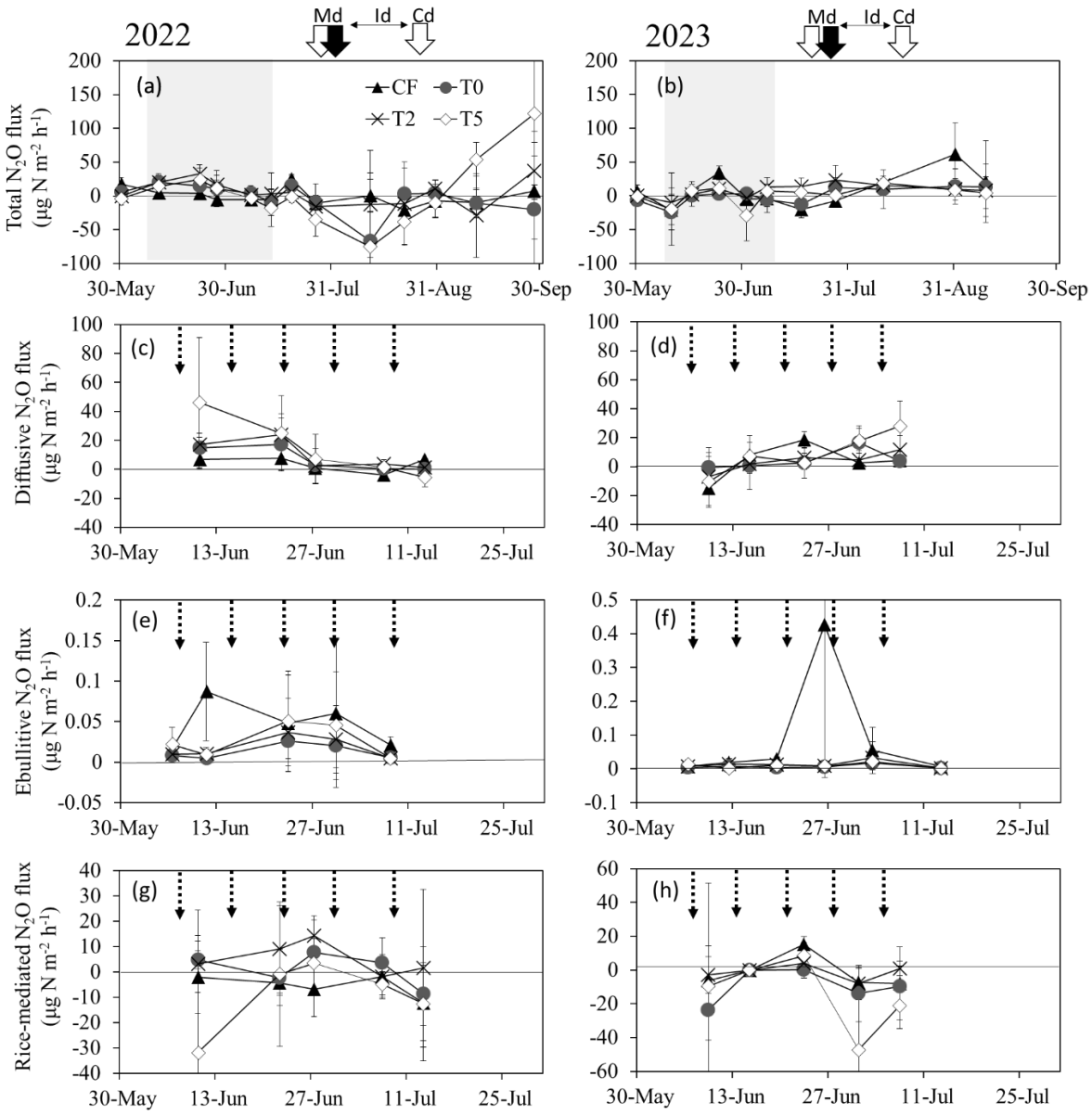


Figure 4.4. Seasonal variation in total nitrous oxide (N_2O) flux in 2022 (a), 2023 (b), diffusive N_2O flux in 2022 (c), 2023 (d), ebullitive N_2O flux in 2022 (e), 2023 (f), rice-mediated N_2O flux in 2022 (g), 2023 (h). Black and white arrows denote the timing of irrigation and drainage. Md indicates mid-season drainage, Id indicates intermittent drainage and Cd indicates complete drainage. Dotted arrows indicated inter-tillage weeding. Gray scale denotes the MIW period (June 10 to July 13 in 2022 and June 9 to July in 2023).

Table 4.4. Comparison of each pathways of N_2O during multiple inter-tillage weeding (MIW) period.

		CF†		T0		T2		T5	
		N_2O emission (Contribution ratio to total N_2O emission)							
Year	Pathway	kg N ha^{-1} (%)							
2022	Diffusion	0.03 (263)	ab‡	0.07 (79)	a	0.09 (58)	a	0.14 (164)	a
	Ebullition	0.0004 (4)	ab	0.0001 (0)	ab	0.0002 (0)	b	0.0002 (0)	ab
	Rice-mediated	-0.04 (-367)	b	0.02 (21)	ab	0.05 (31)	ab	-0.07 (-79)	b
	MIW-mediated	NA (NA)	NA	NA (NA)	NA	0.02 (11)	ab	0.02 (14)	ab
	Total	-0.01	NA	0.09	A	0.16	A	0.09	A
2023	Diffusion	0.04 (88)	a	0.04 (209)	ab	0.02 (88)	ab	0.06 (240)	ab
	Ebullition	0.0008 (2)	ab	0.0001 (0)	ab	0.0001 (0)	b	0.0001 (0)	ab
	Rice-mediated	0.01 (11)	ab	-0.05 (-310)	b	-0.01 (-28)	b	-0.09 (-365)	b
	MIW-mediated	NA (NA)	NA	NA (NA)	NA	0.01 (40)	b	0.05 (225)	ab
	Total	0.05	NA	-0.01	A	0.02	A	0.02	A
ANOVA	Pathway	***		*		*		***	
	Year	ns		ns		*		ns	
	Pathway × Year	ns		ns		ns		ns	

† Treatments CF, T0, T2 and T5 are conventional rice farming, and organic rice farming with no inter-tillage weeding, two time of inter-tillage weeding, and five time of inter-tillage weeding without fertilizer and agricultural chemical.

‡ Small alphabet with the same letter is not significantly different in each column and capital alphabet with the same letter is not significantly different in each line ($p < 0.05$)..

§ NA means no implementation.

*** $p < 0.001$, ** $p < 0.01$, * $p < 0.05$, ns, not significant ($p > 0.05$).

4.3.5. Relationship between each N_2O flux and environmental factors during the MIW period

Total N_2O flux correlated negatively with the tiller number at T2 and T5, positively with the dissolved N_2O concentration at T2, and with N_2O concentration in soil air at 10 cm depth at T0 (Table 4.5).

Diffusive N_2O flux correlated positively with dissolved N_2O concentration at T2 and T5, but not at CF and T0 (Table 4.5).

Ebullitive N_2O flux correlated negatively with atmospheric pressure differences at T0, but fewer correlations were observed with environmental factors compared to CH_4 (Table 4.5).

Rice-mediated N_2O flux correlated positively with water and soil temperatures at T0 (Table 4.5).

4.3.6. Comparison of N_2O emission pathways during the MIW period

Diffusion was the dominant N_2O pathway (58-263%) for all treatments (Table 4.4). Rice-mediated N_2O emission contributed -367-31% to total, with negative values in both years at T5. Ebullition contributed minimally (0-4%). MIW-mediated N_2O emissions accounted for 11-40% of N_2O emission at T2 and 14-225% at T5, making it the second-largest pathway after diffusion. MIW-mediated N_2O emission contributed to the total during the cultivation period was low at 4% or 5% at T2 but accounted for about 30% at T5 (Table 4.6).

A two-way ANOVA showed pathways that significantly influenced N_2O emissions ($p < 0.05$) (Table 4.4). Year differences impacted N_2O emissions at T2 ($p < 0.05$), but no interaction effects between pathway and year were observed.

Table 4.5. Peason correlation coefficient between N_2O flux from each pathways and environmental factors during MIW period.

Pathway	Treatment	AD‡ hPa	WT ℃	ST ℃	WD cm	PH cm	Tn hill^{-1}	Eh mv	Dis N_2O mg N L^{-1}	SG5 N_2O ppmv	SG10 N_2O ppmv
Diffusion	CF†	0.09	0.15	0.13	0.03	-0.08	-0.06	0.05	0.48	0.15	0.001
	T0	0.30	-0.47	-0.69**	-0.20	-0.58*	-0.63*	0.50	0.40	0.39	0.34
	T2	0.04	0.14	-0.23	0.32	-0.37	-0.49	0.34	0.76**	0.03	0.03
	T5	-0.16	0.10	-0.16	0.35	-0.28	-0.35	0.31	0.59*	-0.28	-0.16
Ebullition	CF	0.32	-0.55**	-0.50	-0.02	0.03	0.12	-0.15	-0.19	-0.29	-0.37
	T0	-0.66**	0.41	0.36	0.31	0.43	0.36	-0.37	-0.22	-0.10	-0.18
	T2	-0.51	0.39	0.19	0.47	0.20	0.08	-0.16	0.69**	-0.19	-0.25
	T5	-0.50	0.29	0.06	0.02	0.18	0.09	-0.12	0.50	-0.44	0.01
Rice-mediate	CF	0.29	-0.03	-0.04	-0.05	-0.41	-0.28	0.25	-0.01	0.22	-0.04
	T0	-0.30	0.67**	0.55*	0.18	0.06	-0.05	0.02	-0.07	0.31	0.38
	T2	-0.53	0.17	-0.09	0.15	-0.21	-0.38	0.28	0.17	0.31	0.44
	T5	-0.17	0.09	0.09	-0.13	-0.17	-0.19	0.12	-0.08	0.40	0.46
Total	CF	0.25	0.04	0.03	-0.02	-0.33	-0.23	0.20	0.21	0.23	-0.03
	T0	-0.05	0.25	-0.001	0.01	-0.34	-0.48	0.35	0.21	0.53	0.56*
	T2	-0.34	0.21	-0.20	0.30	-0.38	-0.57*	0.41	0.60*	0.24	0.32
	T5	-0.36	0.20	-0.04	0.17	-0.48	-0.57*	0.44	0.45	0.24	0.43

† Treatments CF, T0, T2 and T5 are conventional rice farming, and organic rice farming with no inter-tillage weeding, two time of inter-tillage weeding, and five time of inter-tillage weeding without fertilizer and agricultural chemical.

‡AD represent average difference in atmospheric pressure over the days of measurement, WT represent water temperature, ST represent soil temperature at 3 cm depth, WD represent water depth, PH represent rice plant height, Tn represent tiller number, Eh represent soil redox potential at 5 cm depth, Dis N_2O represent the dissolved N_2O concentration in paddy field water, SG5 N_2O and SG10 N_2O represent N_2O concentration in soil air gas at 5 and 10 cm depth.

*** $p < 0.001$, ** $p < 0.01$, * $p < 0.05$.

Table 4.6. Cumulative N_2O emissions (mean ± SD) during the cultivation period and contribution ratio of multiple inter-tillage weeding (MIW).

	N_2O emission (Contribution ratio of MIW) kg N ha^{-1} (%)	
	2022	2023
CF†	-0.06±0.40 (NA‡)	0.29±0.30 (NA)
T0	-0.17±0.23 (NA) a§	0.05±0.10 (NA) a
T2	0.08±0.60 (4) a	0.25±0.03 (5) a
T5	0.07±0.33 (33) a	0.14±0.15 (34) a

† Treatments CF, T0, T2 and T5 are conventional rice farming, and organic rice farming with no inter-tillage weeding, two time of inter-tillage weeding, and five time of inter-tillage weeding without fertilizer and agricultural chemical.

‡ NA means no implementation.

§ Value with the same letters is not significantly different in each column ($p < 0.05$).

4.3.7. Gas concentration during the MIW period

During the MIW period, dissolved CH_4 concentrations in paddy field water increased with soil and water temperatures and exceeded atmospheric equilibrium levels, indicating supersaturation across treatments (Figures 4.5a, 4.5b, 4.8c, 4.8d, 4.8e, and 4.8f). During the MIW period, they were similar in 2022 but higher at T5 and T2 compared to T0 in 2023.

During the MIW period, CH_4 concentrations at 5 cm and 10 cm depth were not significantly different among treatments in both year (Figures 4.5c, 4.5d, 4.5e and 4.5f). At 5 cm depth, the mean CH_4 concentrations for the MIW period were greater at T5 (773 ppmv) > T2 (52.1) > T0 (18.5) in 2022 but reversed in 2023 with T0 (2064) > T2 (1475) > T5 (692). At 10 cm depth were greater at T0 (38.4 ppmv) > T2 (24.2) > T5 (21.6) in 2022 and at T2 (1838) > T5 (897) > T0 (716) in 2023.

During the MIW period in 2022, gaseous CH_4 exceeded dissolved CH_4 concentrations and the gaseous CH_4 tended to increase rapidly from June 19, similar to the changes in dissolved CH_4 concentrations in the paddy field water (Figure 4.5a and Table 4.7). A significant positive correlation was found between gaseous CH_4 concentration, which was calculated from the CH_4

concentration in the trapped bubbles and the air-phase ratio. and the CH_4 concentration in soil air at 10 cm depth (Figure 4.6).

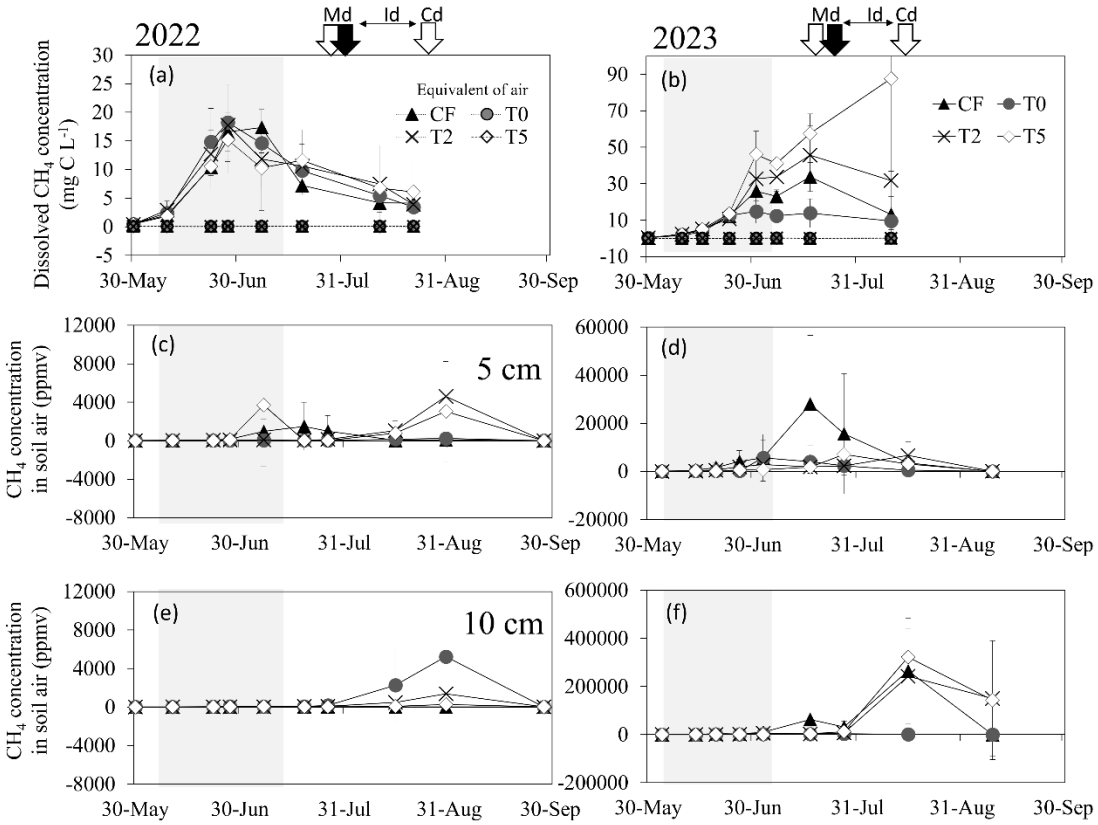


Figure 4.5. Seasonal variation in dissolved methane (CH_4) concentration in paddy field water in 2022 (a), 2023 (b), CH_4 concentration in soil air gas at 5 cm depth in 2022 (c), 2023 (d), CH_4 concentration in soil air gas at 10 cm depth in 2022 (e), 2023 (f). Black and white arrows denote the timing of irrigation and drainage. Md indicates mid-season drainage, Id indicates intermittent drainage and Cd indicates complete drainage. Gray scale denotes the MIW period (June 10 to July 13 in 2022 and June 9 to July in 2023).

Table 4.7. Concentration of gaseous and dissolved CH_4 in soil during multiple inter-tillage weeding (MIW) period in 2022.

	June 1st - June 6th		June 9th - June 11th		June 19th - June 23rd		June 23rd - June 30th		June 30th - July 8th	
	Bubble	Dissolved	Bubble	Dissolved	Bubble	Dissolved	Bubble	Dissolved	Bubble	Dissolved
	μmol L^{-1}									
CF†	289	1.58	915	5.09	23415	140	42451	223	59486	392
T0	210 a‡	1.09 a	181 a	1.10 a	14202 a	74.2 a	10093 a	55.2 a	21878 a	118 a
T2	258 a	1.35 a	286 a	1.75 a	8254 a	40.2 a	4203 a	23.8 a	19084 a	95.3 a
T5	261 a	1.35 a	1514 a	7.55 a	2529 a	14.7 a	20133 a	109 a	24016 a	141 a

† Treatments CF, T0, T2 and T5 are conventional rice farming, and organic rice farming with no inter-tillage weeding, two time of inter-tillage weeding, and five time of inter-tillage weeding without fertilizer and agricultural chemical.

‡ Value with the same letters is not significantly different in each column ($p < 0.05$).

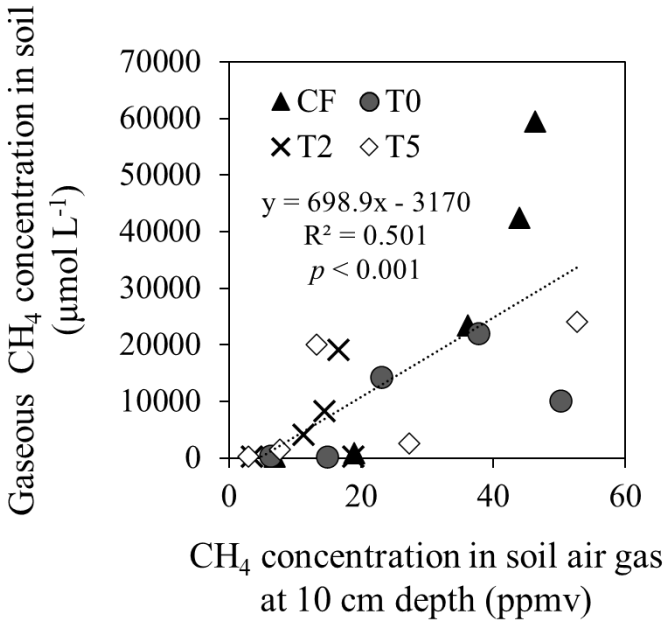


Figure 4.6. Pearson correlation between gaseous CH_4 concentrations, which was calculated from the CH_4 concentrations in the trapped bubbles and the air-phase ratio, and CH_4 concentrations in soil air gas at 10 cm depth.

During the MIW period, dissolved N_2O concentrations fluctuated above and below equilibrium, with no significant differences between treatments (Figures 4.7a and 4.7b). Mean values during the MIW period were greater at T5 (0.61 mg N L^{-1}) > T2 (0.52) > T0 (0.33) in 2022, and at T5 (0.77) > T2 (0.54) > T0 (0.44) in 2023.

During the MIW period, N_2O concentrations at 5 and 10 cm depth were not significantly different between treatments in both years (Figures 4.7c, 4.7d, 4.7e and 4.7f). At 5 cm depth, the mean N_2O concentrations for the MIW period were greater at T5 (3.94 ppmv) > T2 (2.36) > T0 (2.03) in 2022, and at T5 (2.69) > T0 (1.91) > T2 (1.46) in 2023. At 10 cm depth were greater at T5 (4.47 ppmv), T2 (2.74), and T0 (2.36) in 2022 and T5 (2.49), T0 (2.21), and T2 (1.91) in 2023.

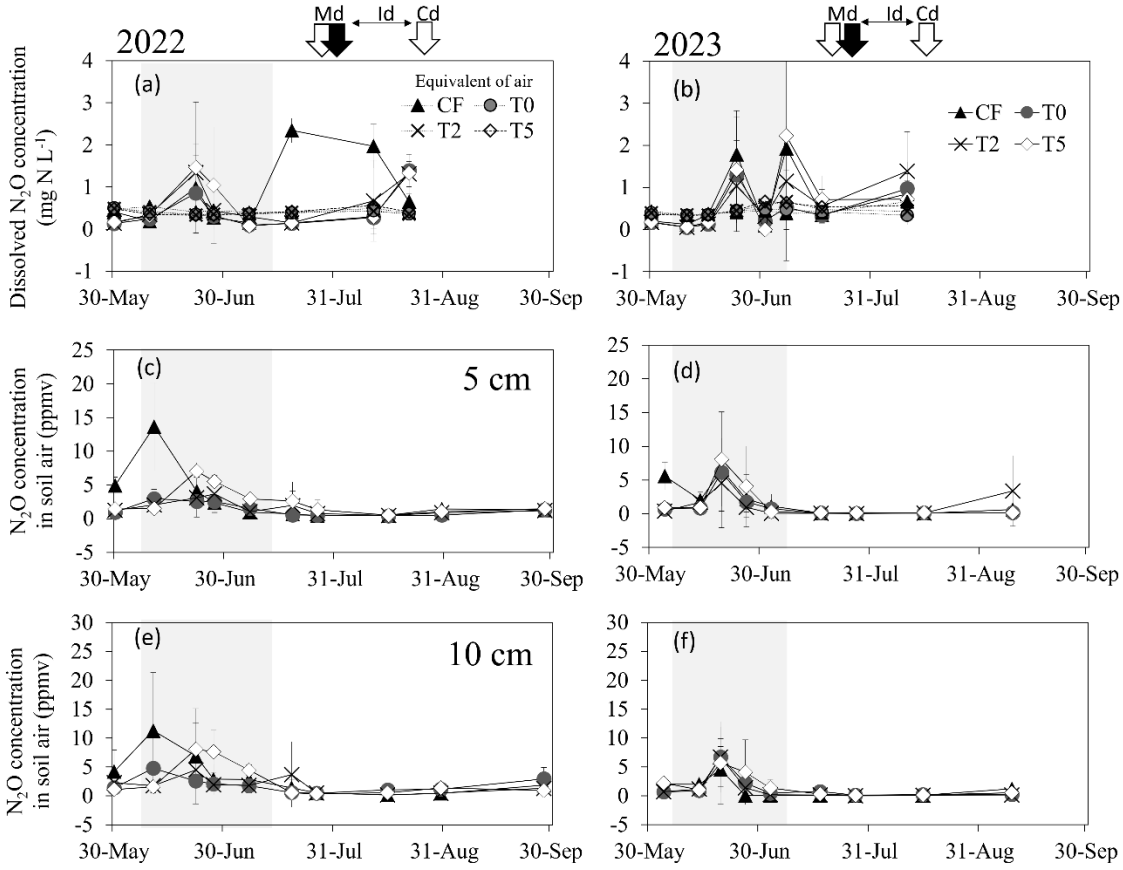


Figure 4.7. Seasonal variation in dissolved nitrous oxide (N_2O) concentration in 2022 (a), 2023 (b), N_2O concentration in soil air gas at 5 cm depth in 2022 (c), 2023 (d), N_2O concentration in soil air gas at 10 cm depth in 2022 (e), 2023 (f). Black and white arrows denote the timing of irrigation and drainage. Md indicates mid-season drainage, Id indicates intermittent drainage and Cd indicates complete drainage. Gray scale denotes the MIW period (June 10 to July 13 in 2022 and June 9 to July in 2023).

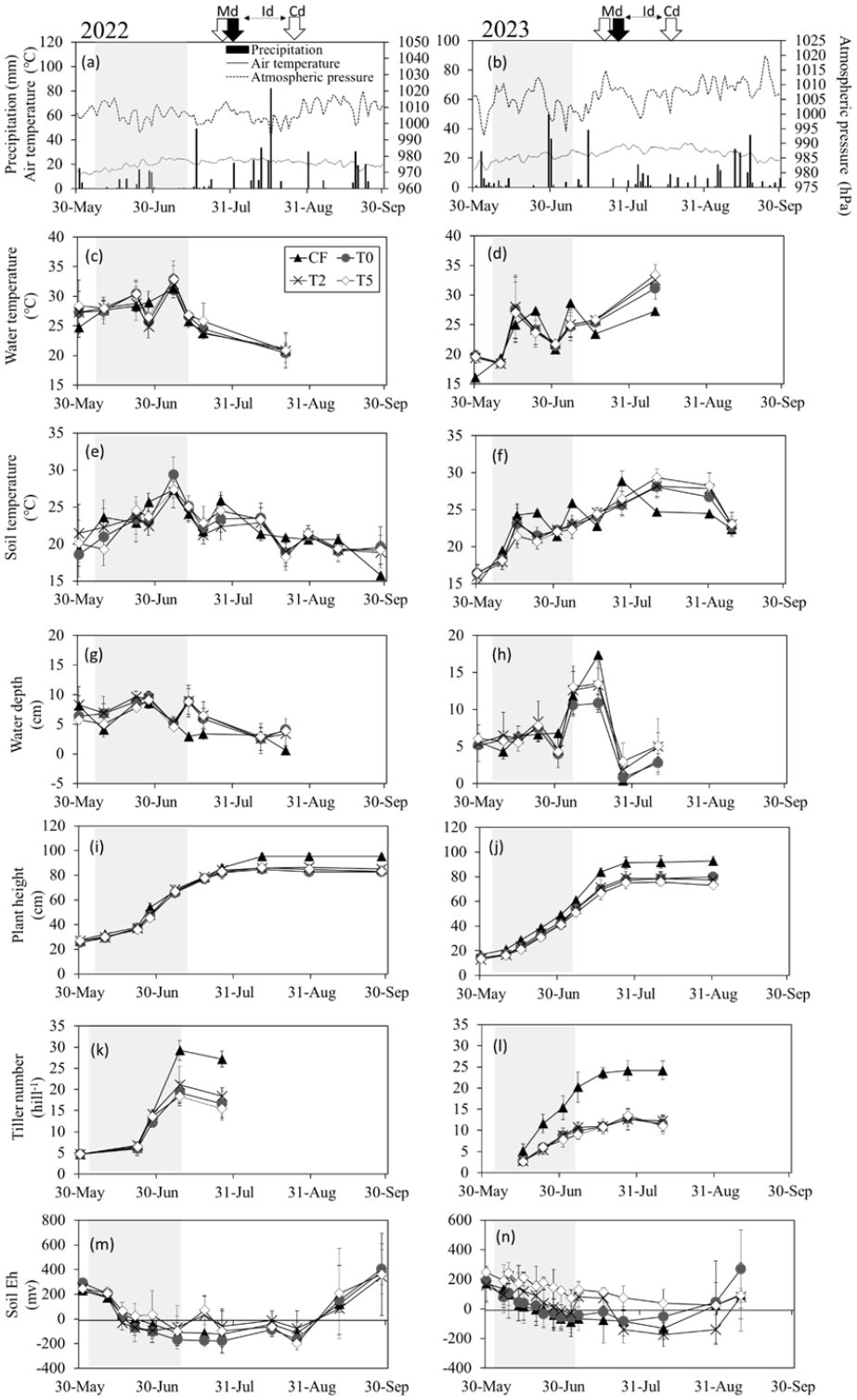


Figure 4.8. Seasonal variation in precipitation, air temperature and atmospheric pressure in 2022 (a), 2023 (b), water temperature in paddy field water in 2022 (c), 2023 (d), soil temperature at 3 cm depth in 2022 (e), 2023 (f), water depth in 2022 (g), 2023 (h), plant height in 2022 (i), 2023 (j), tiller number in 2022 (k), 2023 (l), soil Eh at 5 cm depth in 2022 (m), 2023 (n). Black and white arrows denote the timing of irrigation and drainage. Md indicates mid-season drainage, Id indicates intermittent drainage and Cd indicates complete drainage. Gray scale denotes the MIW period (June 10 to July 13 in 2022 and June 9 to July in 2023).

4.4. Discussion

4.4.1. CH_4 emission during the MIW period

In general, CH_4 emissions are primarily rice-mediated (90%), with smaller contributions from ebullition (8%) and diffusion (2%) (Butterbach-Bahl et al. 1997). Our study confirms the dominance of rice-mediated emissions (61-92%) but shows higher diffusion (4-29%) contributions compared to ebullition (3-8%) (Table 4.1).

The two-way ANOVA revealed that CH_4 emission pathways had a significant effect on total emissions, with rice-mediated CH_4 emissions playing a dominant role and influencing other pathways (Table 4.1). During the MIW period, rising soil and water temperatures reduced CH_4 solubility, leading to supersaturation and the transfer of dissolved CH_4 to the gas phase (Figures 4.5a and 4.5b). This process formed CH_4-rich soil bubbles (Table 4.7), which likely impacted the choice of emission pathways. Generally, organic-rich, shallow-water systems often show >50% ebullition (Bastviken et al., 2008; Sawakuchi et al., 2014; Yang et al., 2020; Zhu et al., 2016). However, despite high soil CH_4 levels, ebullition contributed minimally in this study. Rice-mediated CH_4 emissions occur via molecular diffusion driven by pore water-atmosphere concentration gradients (Nouchi et al., 1990) or direct transport through gas-permeable rice stems (Hosono and Nouchi, 1997). Furthermore, elevated soil temperatures increased bubble CH_4 levels, expanding root contact areas and enhancing rice-mediated uptake (Kajiura and Tokida, 2024; Nouchi et al., 1990). As a result, the abundant CH_4-rich bubbles in the soil may have been preferentially released through rice-mediated pathways rather than ebullition. Furthermore, the greater CH_4 emissions via the diffusion pathway compared to previous studies suggest that dissolved CH_4 may have competed between transport into rice roots and diffusion through floodwater, with much of it being emitted via the latter. Thus, CH_4 form (gaseous or dissolved) significantly affects emission pathways. Additionally, Kajiura et al. (2024) reported greater ebullition in 'Koshihikari' fields compared to other varieties, highlighting varietal

differences in CH_4 transport. Although this finding suggest rice varieties may influence CH_4 pathways, warranting further research.

4.4.2. MIW effects on CH_4 emission pathways

During the MIW period, CH_4 emission pathway analysis showed that at T5 (7-day disturbance interval), MIW contributed 20–30% of the total emissions, while rice-mediated emissions decreased to about 60% (Table 4.1). The MIW-mediated emissions were higher at T5 than at T2 (28 days interval). At T2, rice-mediated emissions accounted for approximately 80% of total emissions, similar to CF and T0, suggesting that bubbles accumulated over 28 days were primarily emitted through the rice pathway (Table 4.1).

Eh measurements showed temporary increase in the redox potential post-MIW, followed by declines before the next MIW, indicating a temporary oxygenation effect (Figures 4.8m and 4.8n). Oxygen supplied during sediment disturbance was likely rapidly consumed for organic matter decomposition due to increased dissolved organic matter and enhanced microbial activity, thereby accelerating soil reduction (Oliveira Junior et al., 2019). Similarly, the temporary oxygen input from MIW may have stimulated microbial activity and organic matter degradation, leading to rapid oxygen consumption and, paradoxically, an acceleration of soil reduction. Booth et al. (2021) reported that 7 days disturbance intervals align with the methanogen bubble replenishment cycles, maximizing bubble CH_4 release. Similarly, since CH_4 emissions from the MIW-mediated pathway were higher at T5 (7-day interval) than at T2 (28-day interval) (Table 4.1), the 7-day MIW interval may have promoted CH_4 production, particularly facilitating the sufficient formation of gaseous CH_4. However, no significant differences in soil CH_4 concentrations or gaseous CH_4 quantities were observed between treatments during the MIW period (Figures 4.5c, 4.5d, 4.5e and 4.5f, Table 4.7). Variability in soil air gas measurements suggests the need for more measurements within the plot and lab incubation studies to explore the link between disturbance and CH_4 production. However, the

MIW-mediated CH_4 emission were smaller compared to the total CH_4 emission over the cultivation period (Table 4.3), suggesting that this impact was low. These results contradict our hypothesis, that is oxygen supply associated with MIW promoted CH_4 production rather than oxidation. Furthermore, while MIW-induced disturbance contributed to the release of gaseous CH_4 from the soil instead of the rice-mediated pathway, its emissions did not significantly impact that total CH_4 emission.

Over the two years, the contribution ratios of each CH_4 emission pathway showed no significant variation (Table 4.1), indicating that the impact of MIW on CH_4 emission pathways did not vary annually. However, while the total CH_4 emission during the MIW period were similar in both years at T5, the total CH_4 emission during the cultivation period were 64.4 kg C ha^{-1} in 2022 and 97.5 kg C ha^{-1} in 2023. This suggests that the organic matter that has been decomposed by MIW may have been affected by external factors such as weather during the after MIW period, resulting in increased CH_4 emissions during the after MIW to harvest period (Table 4.3). In 2023, dissolved CH_4 concentration remained elevated from the end of MIW period at T5 (Figure 4.5b), indicating a more supersaturated state compared to 2022. This suggests that high concentrations of gaseous CH_4 were present in the soil, which may have been primarily emitted through the rice-mediated pathway. Additionally, water and soil temperature from the end of MIW opposite trends between 2022 and 2023 (Figures 4.8c, d, e, and f). Since total CH_4 flux showed a significant positive correlation with soil temperature (Table 4.2), MIW-induced CH_4 production appears to be temperature-dependent. Previous studies have reported that relative high temperatures (but below 32°C), microbial decomposition of crop residues is enhanced, leading to increased CH_4 emission (Chen et al., 2021). Therefore, the positive priming effect of MIW on CH_4 emission is likely temperature-dependent and may persist beyond the MIW period, highlighting the importance of monitoring CH_4 emissions throughout the cultivation period.

4.4.3. N_2O emission during the MIW period

N_2O pathway analysis revealed that diffusion was the primary emission route during the MIW period, with negligible ebullition (Table 4.4). And rice-mediated N_2O emissions fluctuated between positive and negative values, indicating that rice can both emit and absorb atmospheric N_2O. This contrasts with Yan et al. (2000), who reported that rice accounted for 87.3% of N_2O emissions under flooded conditions in pot experiments. As aquatic plants, rice can absorb or release N_2O based on the concentration gradient between the atmosphere and rhizosphere (Li et al., 2018; Senga et al., 2010). In this study, rice-mediated N_2O fluxes likely shifted according to soil N_2O concentrations. Total N_2O emissions during the MIW periods in 2022 and 2023 were significantly below the negligible threshold of 0.89-0.97 kg N ha^{-1} (Chen et al., 2021; Shang et al., 2011), indicating that the field was a minor N_2O source.

Two-way ANOVA confirmed that pathways significantly influenced N_2O emissions, with diffusion potentially affecting other pathways (Table 4.4). The absence of ebullitive N_2O emissions likely resulted from its higher solubility compared to CH_4, leading to N_2O retention in pore water (Yuan et al., 2021). Dissolved N_2O concentrations in paddy field water fluctuated around atmospheric equilibrium (Figures 4.7a and 4.7b), suggesting brief gaseous forms but predominantly dissolved forms. Dissolved N_2O likely diffused into the atmosphere, driven by pore water concentration gradients, while rice-mediated absorption partially offset diffusive emissions. When significant soil-to-atmosphere N_2O gradients exist, rice plants can act as conduits for atmospheric N_2O uptake (Li et al., 2018). This suggests that diffusion rates may have exceeded rhizosphere N_2O production, creating gradients that facilitated N_2O absorption by rice. Furthermore, nitrate availability strongly influences N_2O reduction, with lower nitrate levels promoting more complete N_2O consumption (Li et al. 2018). In nitrate-limited flooded fields, denitrification likely contributed to N_2O gradients. These combined mechanisms explain the observed N_2O dynamics in this study.

4.4.4. MIW effects on N_2O emission pathways

Comparing T0 and T5, frequent MIW did not significantly increase N_2O emissions through the diffusion pathway. However, over two years, T5 tended to have higher diffusive N_2O emissions than T0 (Table 4.4). During the MIW period, the mean of dissolved N_2O concentrations in paddy field water and soil air at 5 and 10 cm depths has the highest trend at T5. However, a pattern absents at T2, suggesting these increases were driven by frequent disturbances. Temporal changes in Eh confirmed temporally oxygenation from MIW (Figures 4.8m and 4.8n). Enhanced oxygen promotes N_2O production during denitrification, as reported in previous studies (Li et al., 2013; Morley and Baggs, 2010). MIW likely stimulated nitrification, generating NO_3^-, which acted as an electron acceptor during denitrification, thereby increasing N_2O production potential. The observed link between dissolved N_2O in paddy field water and N_2O concentration in soil air suggests rapid transport of soil-generated N_2O via porewater to paddy field water. Additionally, N_2O production in paddy field water may have been enhanced. Coupled nitrification-denitrification, favored in mixed aerobic-anaerobic environments created by suspended sediments, likely contributed to elevated N_2O emissions in water systems (Liu et al., 2013; Xia et al., 2017, 2021; Zhou et al., 2019). MIW-induced soil disturbances likely enhanced these reactions, increasing N_2O production in paddy field water.

In contrast, ebullitive N_2O emissions showed minimal differences across treatments (T0, T2, T5), indicating limited MIW effects on this pathway. However, MIW-mediated N_2O emissions accounted for 11–40% (T2) and 14–225% (T5) of total emissions, making MIW a notable source, second only to diffusion (Table 4.4). Over the cultivation period, MIW-mediated contributed over 30% of T5 emissions in both years, highlighting its importance (Table 4.6).

Rice-mediated N_2O uptake trend was consistently observed at T5 across two years. At T5, increased N_2O production during the MIW periods was accompanied by enhanced uptake via rice plants. This may be due to (1) rapid transport of N_2O through diffusion pathways, (2) fast

N_2O reduction rates, and (3) periodic N_2O release via ebullition. These factors likely steepened the N_2O gradient between soil and atmosphere, facilitating greater uptake by rice plants.

These results partially support the hypothesis that the change in the redox potential of the soil due to the oxygen supply associated with MIW promotes N_2O production in the soil, thereby increasing total N_2O emission. Specifically, oxygenation induced by MIW stimulated nitrification and denitrification, leading to increased N_2O emissions through the diffusion pathway. However, MIW-driven N_2O emissions were primarily associated with diffusion, with minimal effects on ebullition. Additionally, a portion of the N_2O generated by MIW was taken up by rice plants, suggesting a complex impact on the overall N_2O balance. These findings are crucial for understanding MIW's influence on N_2O emissions, and future research should focus on elucidating the detailed mechanisms of MIW-driven N_2O production and consumption processes.

4.4.5. Validation of quantitative methods

This study extracted net diffusive gas flux using a threshold of 0.29 ppmv min^{-1} for CH_4 concentration. Previous studies (e.g., Morishita and Hatano, 1999) reported a significant positive correlation between diffusive CH_4 flux and dissolved CH_4 concentration in lake water. Similarly, significant positive correlations were observed between diffusive CH_4 flux and dissolved CH_4 concentrations in paddy field water at CF and T0, and between diffusive N_2O flux and dissolved N_2O concentrations in paddy field water at T2 and T5 (Tables 4.2 and 4.5). These results suggest that oxygen supply associated with MIW disturbances enhanced CH_4 oxidation and N_2O production, reflecting complex MIW-driven processes. Consequently, the diffusive pathway analysis employed in this study is valuable for evaluating MIW's impact. However, the method's reliance on a CH_4-specific threshold may not accurately transition between dissolved and ebullitive N_2O states. Establishing an N_2O-specific threshold could improve accuracy.

Significant positive correlations between CH_4 concentrations in the bubble trap and soil air at 10 cm depth confirmed reproducibility in capturing soil bubble dynamics (Figure 4.6). Ebullitive CH_4 flux correlated positively with water or soil temperature, consistent with decreased gas solubility at higher temperatures (Kajiura and Tokida, 2021). Ebullitive N_2O flux quantification is complicated by potential gas re-equilibration during prolonged sampling, leading to re-dissolution. Increased sampling frequency of CH_4 and N_2O fluxes are recommended.

Some of the previous studies, e.g., Mariko et al. (1991), reported a positive correlation between CH_4 flux and tiller number. Significant positive correlations between the estimated rice-mediated CH_4 flux and plant height or tiller number across all treatments (Table 4.2) confirmed that CH_4 emissions depend on rice growth. The estimation of rice-mediated gas fluxes may be influenced by measurement errors in diffusive and ebullitive gas fluxes. Additionally, it is stated that the area covered by a chamber should be a multiple of the area (hills) occupied by one rice plant (Minamikawa et al., 2015). The area of the chamber used to measure our total gas flux is 0.180 m^2, whereas the required chamber area estimated from the planting density (24 hills m^{-2}) is 0.167 m^2. The extra area is 0.013 m^2. Thus, we calculated the contribution of CH_4 discharged from the extra area to the total CH_4 emissions. As a result, only 1 to 2% of the total CH_4 emissions were accounted for in all treatments. In this study, we considered this overestimation to have no significant impact; however, improving measurement accuracy requires further refinement of the methodology.

4.5. Conclusion

Analysis of CH_4 and N_2O emission pathways during the MIW period revealed relationships among the three main pathways. It was suggested that the presence of gaseous CH_4 may affect the ebullition and rice-mediated pathways, with the diffusion pathway contributing relatively more. High frequency (T5) MIW promoted the release of CH_4-rich bubbles and temporarily

reduced the contribution of CH_4 emissions from rice-mediated pathway. However, MIW-mediated CH_4 emissions were lower contributors (3-8%) to the total during the cultivation period.

N_2O was mainly present in the dissolved form, suggesting that it may move through the porewater via diffusion pathways. MIW at high frequency (T5) enhanced N_2O formation in paddy field water and soil, but its emission rate exceeded the rate of N_2O formation and consumption in the soil, indicating that the concentration gradient between the atmosphere and soil may be larger and enhance N_2O absorption in the rice. However, MIW-mediated N_2O emissions at medium frequency (T2) were almost the same as at no-tillage (T0). MIW-mediated N_2O emissions were the second most important emission pathway after the diffusion pathway.

5. Five-year Assessment of Multiple Inter-tillage Weeding on Greenhouse Gas Emissions, Rice Yield, and Carbon Balance in Organic Rice Farming

5.1. Introduction

Numerous studies have shown the urgency to reduce GHG emissions and increase soil carbon stock to mitigate global warming (Chen et al., 2021). However, rice paddy fields account for approximately 48% of GHG emissions from agricultural land (Qian et al., 2023), and rice paddy fields are a major source of CH_4 emission, and it has been reported that CH_4 emissions from irrigated rice paddies account for 78% of global rice-derived CH_4 emissions (Carlson et al., 2017). On the other hand, since the decomposition of organic matter is slower in flooded soil than in well-drained soil (Song et al., 2024; Witt et al., 2000), rice paddy fields play a role in stabilizing CO_2 in the soil through carbon stock. Thus, paddy fields serve as both a source of GHG emissions and a carbon sink, emphasizing the need for a comprehensive evaluation of management practices.

Therefore, we focused on the potential of MIW to supply oxygen and weeds under flooded conditions to reduce GHG emissions and promote carbon stock in the soil. MIW is conducted in a flooded state during the rice-growing season. The physical disturbance of MIW can supply oxygen, potentially improving anaerobic conditions in paddy field water and soil, thus significant mitigating CH_4 production. However, there is concern that the oxygen supply associated with MIW may not only increase N_2O emissions in the nitrification and denitrification processes due to redox state fluctuations, but also RH emissions caused by microbial respiration. MIW incorporates weeds into the soil under flooded conditions which may reduce their rate of decomposition and increase the amount of carbon remaining in the soil. However, research on MIW has not been studied to studies by Kasubuchi et al. (2019) and Zhou et al. (2023), which focus on its effects on rice yield increase and growth promotion. Few studies have investigated the impact of MIW on GHG emissions and carbon stock.

According to Wang et al. (2019), in the subtropical region of southern China, the annual cumulative RH emissions under fertilization, steel slag, biochar, and the combination of steel slag and biochar ranged from 13.0 Mg C ha^{-1} to 16.3 Mg C ha^{-1}. And regardless of the treatment, RH contributed the most to the cumulative GWP compared to CH_4 and N_2O. Naser et al. (2019) stress the importance of year-round monitoring to accurately evaluate RH, CH_4, and N_2O emissions and carbon stock in paddy fields, as field management differs significantly between the rice-growing season (flooded conditions) and the fallow season (dry conditions). MIW may have potential for affecting the physicochemical properties of paddy soil and microbial communities, and these changes may progress over the long term. In particular, the impacts on carbon stock and GHG emissions are influenced by annual weather conditions, making it difficult to capture long-term trends through short-term studies. Therefore, it is essential not only to investigate CH_4 and N_2O fluxes but also to measure RH flux derived from microbial respiration, and carbon stock over long periods and throughout the year to clarify interannual variations and long-term trends.

Various strategies have been proposed to reduce GHG emissions in rice paddy fields, such as reducing the use of organic and chemical fertilizers, cultivating rice varieties with lower CH_4 emissions, and alternate wetting and drying (Akiyama, 2024). However, Fang et al. (2021) point out that these strategies often fail to guarantee yield stability, making their economic benefits to farmers uncertain. This uncertainty may discourage farmers from adopting these practices, highlighting the need for initiatives that explicitly address both GHG reduction and increased farmer income. MIW has demonstrated yield-enhancing effects in previous studies, which could motivate farmers to adopt this method. Therefore, evaluating the stability of rice yield under MIW, along with its impact on GHG emissions and carbon stock, could lead to its establishment as a new sustainable organic farming method.

This study aims to evaluate the effects of MIW on GHG emissions, carbon balance, and yield using annual data covering both the rice-growing and fallow seasons under different

management conditions. And we construct three hypotheses: 1) Oxygen supply associated with MIW increases RH and N_2O emissions while significantly reducing CH_4 emissions and lowering GHG balance; 2) MIW increases yield and decreases GHG emission intensity per yield; and 3) The incorporation of weeds under flooded conditions enhances carbon stock. We examined these hypotheses by monitoring the effects of different frequencies of MIW over five years, referring to the rice growth, yield, soil environment, GHG balance, and carbon balance in rice paddy field.

5.2. Materials and methods

5.2.1. Study site

The study site was organic rice farming fields at the Hokkaido University FSC described in **Section 3.1**. The study period was from May 16 on 2019 to September 9 on 2023, including rice-growing season (May to September) and fallow season (September to April of next year) (Table 5.1). In winter, the study site has a long snow cover and a cold climate. However, in 2019 and 2020, the investigation was conducted only during the rice-growing season.

Table 5.1.Cumulative period and number of days from 2019 to 2023.

Year	Season	Periods			Cumulative days
2019	Rice-growing	2019/5/16	~	2019/9/15	122
2020	Rice-growing	2020/6/6	~	2020/9/29	115
2021	Fallow	2020/10/12	~	2021/5/4	204
	Rice-growing	2021/5/20	~	2021/9/11	114
2022	Fallow	2021/9/28	~	2022/4/25	209
	Rice-growing	2022/5/11	~	2022/9/28	140
2023	Fallow	2022/10/12	~	2023/5/8	208
	Rice-growing	2023/5/11	~	2023/9/9	121

5.2.2. Experimental design and field management

The organic rice farming field (1000 m^2) was randomly divided into three treatments with no inter-tillage weeding (T0), two time of inter-tillage weeding (T2), and five time of inter-tillage weeding (T5) in three replications (8.33 × 13.3 m $plot^{-1}$) (Figure 3.2a).

Field management for 2019-2023 is detailed in **Section 3.2**. MIW was conducted between early June and early July during the study period. Details on the dates of MIW are described in S**ection 3.3**.

5.2.3. Environmental factors

Daily air temperature and precipitation were obtained from the AMeDAS and soil temperature at depth of 3 cm in each treatment was measured using a thermometer describe in **Section 3.6.1**. Eh at 5 cm depth was measured using Eh meters describe in **Section 3.6.5**.

Soil samples at 0-3 cm depth were collected from each treatment in two replicates using an auger. This samples were used for analyzing soil pH, NH_4^+ content, NO_3^-, SO_4^{2-} contents, WEOC. And soil samples at 5 cm depth were collected in two replicates from each plot using a gas-tight syringe (20 mL). This samples were used for analyzing Fe^{2+} contents. They were measured by the method described in **Section 3.6.2** and **3.6.3**.

In 2021 and 2022, soil physical properties—such as solid-phase ratio, liquid-phase ratio, air-phase ratio, porosity, and bulk density—were evaluated at the 0–5 cm depth during MIW period. The detailed methods of these measurements are described in **Section 3.6.4**.It was taken at 7-10 days interval during the MIW period, 14 day interval between after MIW and harvest, and 30 days intervals during fallow season. However, Fe^{2+} contents and Eh measurements were conducted during the rice-growing season, .

5.2.4. Plant production and grain yield

Rice plant height, tiller number, and chlorophyll content were measured by the methods in **Section 3.6.6** as rice growth indicators. These measurements were conducted at 7-10 days

interval during the MIW period, 14 day interval between another period during the rice-growing season from 2020 to 2023.

Rice plant samples were collected from 30 cm depth at timing of rice transplantation and harvesting, separated by leaf and stem, grain, and root parts, and dried at 60℃ for 48 hours. After drying, the plants were weighed, and ground using a grinder (Mill TI 100; CMT, Fukushima, Japan) and their carbon content was determined. The carbon content was analyzed by the Tyurin (wet oxidation) method with $K_2Cr_2O_7$ was used in 2020 and by the elemental analyzer (vario MAX CN Macro or vario EL III, Elementar, Frankfurt, Germany) in 2019, 2021, 2022, and 2023.

Residues (rice straw, stubble, and roots), previous years' weeds and weeds during MIW at T2 and T5 were collected from a randomly selected 30 cm × 30 cm area in each treatment, respectively. The residues were collected from 30 cm depth in early May before starting waterlogging, and the previous year's weeds were collected before harvesting. The weeds during MIW were collected before each MIW practice. Similarly, the carbon content of the residue and weeds was measured. Since the carbon content of weeds sprayed after the harvesting in 2019 was not measured, the average of those sprayed in 2020-2023 was used. The carbon inputs of weeds after the harvesting at T0, T2, and T5 were assumed to be the same because the weeds were equally returned. The carbon content of the weeds during MIW was estimated for each year by multiplying the carbon content of the weeds measured during MIW in 2023 by the dry weight of the weeds during MIW in 2019, 2020, 2021, and 2022. Since weeds were completely weeded out at T2 and T5 after the MIW, these were used as the carbon input of weeds plowed in during the MIW.

To determine the yield components, 10 plant were cripped from each treatment, dried, and then measured in terms of plant height (cm), culm length (cm), number of ears (number $hill^{-1}$), and ear weight (g $hill^{-1}$). The plant closest to the average of 10 plants was selected for

measuring the number of ears per plant and the ripened grains (%). Brown rice (>1.8 mm), and the 1000-grain weight (g) and brown rice yield were also determined.

5.2.5. Greenhouse gas fluxes

RH, CO_2 (sum of gross primary production (GPP) and ecosystem respiration (RE), CO_2 (GPP+RE)), CH_4 and N_2O fluxes from the rice paddy fields were measured and calculated the method described in **Section 3.4**. Gas sampling was conducted between 9:00 and 14:00. It was taken at 7-10 days interval during the MIW period, 14 day interval between another period during the rice- growing season, and 30 days intervals during the fallow season.

However, since RH emissions during the rice-growing season were not measured in 2019 and 2021, it was estimated using the following equation (6) to (11). GPP is the sum of net primary production (NPP) and autotrophic respiration (RA), and RE is the sum of RA and RH. Therefore, $Q_{CO_2(GPP+RE)}$ could be expressed using sunlight duration (x) in equation (6). By transformation equation (7) for RA could be obtained.

$$Q_{CO_2(GPP+RE)} = -\{NPP + RA - (RA + RH)x\} \quad (6)$$

$$RA = -\left(NPP + Q_{CO_2(GPP+RE)} - xRH\right)/1 - x \quad (7)$$

The ratio of RA to GPP (β) for 2020, 2022, and 2023 was calculated using equation (8), and the average value of β (β′), was determined. Then, using the transformed equation (9), RA′ for 2019 and 2021 was calculated.

$$\beta = RA/GPP = RA/(NPP + RA) \quad (8)$$

$$RA' = \beta' NPP/(1 - \beta') \quad (9)$$

The ratio of Q_{RH} to RE (γ), for 2020, 2022, and 2023 was calculated using equation (10), and the average value (γ') was determined. Then, using the transformed equation (11), $Q_{RH}{}'$ for 2019 and 2021 was calculated.

$$\gamma = Q_{RH}/RE = Q_{RH}/(RA + Q_{RH}) \quad (10)$$

$$Q_{RH}{}' = \gamma' RA/(1 - \gamma') \quad (11)$$

In addition, the average values of RH, CH_4, and N_2O emissions during the fallow season of 2019 and 2020 were average from 2021 to 2023.

RH or CH_4 emissions per carbon input were calculated using equation (12).

$$Q/I_C = Q\ /C_{input} \times 100 \quad (12)$$

where Q/I_C is the RH or CH_4 emissions per carbon input (%). C_{input} is the carbon content of the previous year's weeds and weeds during MIW at T2 and T5, or previous year's residues (rice straw, stubble, roots) or total them (Mg C ha^{-1}).

5.2.6. Calculation of GWP, GHGB, GHGI and NECB

GWP refers to the radiative forcing potential of the two greenhouse gases converted to the carbon dioxide equivalent (CO_2-eq) based on a 100-year scale (Hu et al., 2024). Cumulative emissions of RH, CH_4 and N_2O were converted to GWP_{RH}, GWP_{CH_4}, and GWP_{N_2O}, respectively, using the CO_2 conversion coefficient (CO_2: 1, CH_4: 28, N_2O: 265) provided by IPCC (2014). GWP_{total} (Mg CO_2-eq ha^{-1}) was calculated by sum of GWP_{RH}, GWP_{CH_4} and GWP_{N_2O} as follows:

$$GWP_{RH} = Q_{RH} \times 44/12 \quad (13)$$

$$GWP_{CH_4} = Q_{CH_4} \times 16/12 \times 28 \quad (14)$$

$$GWP_{N_2O} = Q_{N_2O} \times 44/28 \times 265 \quad (15)$$

$$GWP_{total} = GWP_{RH} + GWP_{CH_4} + GWP_{N_2O} \quad (16)$$

where Q_{RH}, Q_{CH_4} and Q_{N_2O} are the annual cumulative RH, CH_4 and N_2O emissions, respectively.

GHG balance (GHGB, Mg CO_2-eq ha^{-1}) was calculated using equation (17):

$$GHGB = GWP_{total} + C_{output} - (NPP + C_{input}) \quad (17)$$

where C_{output} is defined as the carbon content of stems, shoots, and roots taken out at harvest. NPP is the rice and weed net primary production. C_{input} is the carbon content of the previous year's weeds, rice straw, stubble, roots, and weeds plowed into the soil (T2 and T5 only) by MIW. They were summed so that the uptake was negative, and the emissions were positive.

GHG intensity (GHGI, Mg CO_2-eq Mg yield $^{-1}$) was calculated by dividing GHGB by the brown rice yield.

Net ecosystem carbon balance (NECB) (Mg C ha^{-1}) was calculated using equation (18) (Naser et al., 2019):

$$NECB = (NPP + C_{input}) - (Q_{RH} + Q_{CH_4} + C_{output}) \quad (18)$$

NECB were summed so that the carbon loss was negative, and the carbon stock was positive.

In 2023, MIW-mediated CH_4 and N_2O emissions (Q_{MIW}) were measured using the method described in **Section 4.2.6**. The contribution ratio of Q_{MIW} to the cumulative CH_4 and N_2O emissions during the rice-growing season in 2023 was calculated at T2 and T5, respectively. The contribution ratio was used to estimate Q_{MIW} from 2019 to 2022 at T2 and T5, respectively, and added to the cumulative CH_4 and N_2O emissions during the rice-growing season to obtain net the cumulative gas emissions, which was used to compare the GHGB, GHGI, and NECB.

5.2.7. Statistical analysis

All statistical analysis was conducted using R ver. 4.4.2 (R Development Core Team 2024). One-way ANOVA was performed to examine the differences between treatments for the measured parameters during the experimental period. The analysis was conducted using the entire dataset from three treatments with three replications. Differences in NPP of rice plants, GHG, GWP, GHGB, GHGI and NECB between treatments and year were tested using Two-way ANOVA. When there were significant differences in the test, multiple comparison test was performed using Tukey-HSD test. The relationship between GHG emissions and soil environmental factors was tested using Pearson's correlation analysis. The relationship between each factor (RH, CH_4, N_2O, and environmental factors) was also tested using Pearson's correlation analysis. For each statistical analysis, a difference or correlation was considered significant at the significant level of 5%.

5.3. Results

5.3.1. Environmental factors

Air temperatures were highest in the summer months of July and August and lowest in the winter months of January in all five years (Figure 5.1a). Mean annual temperatures were 9.8, 10, 10.2, 10.2, and 11°C in 2019, 2020, 2021, 2022, and 2023, respectively. Annual

precipitation was 814, 905, 1089, 1154, and 966 mm for 2019, 2020, 2021, 2022, and 2023, respectively. During the study period, the air temperature was higher, and the precipitation was lower compared to the respective averages from the past 30 years (1991–2020) in Sapporo.

The soil temperature varied seasonally as the air temperature (Figure 5.1b). There were no significant differences in soil temperature among treatments throughout the study period. The variation in soil pH exhibited a similar pattern at T0, T2, and T5 throughout the study period (Figure 5.1c). The NH_4^+ content in all treatments increased as waterlogging progressed and then decreased after complete drainage throughout the study period (Figure 5.1d). The NH_4^+ content during the tillering stage (late MIW period) in 2019 at T5 was significantly higher than that at T2, but no significant differences were observed in the other years. However, the NH_4^+ content at T5 generally showed higher values compared to other treatments. The NH_4^+ content during the maximum tillering stage in 2019 was significantly higher at T2 than that at T5, but the ranking of treatments varied across the years, showing inconsistency. The NH_4^+ content during the heading stage was not significantly different among the treatments; however, the NH_4^+ content at T5 showed the highest values. The NO_3^- content peaked before irrigation and after complete drainage in all the treatments throughout the study period (Figure 5.1e).

Throughout the study period, Fe^{2+} content increased as waterlogging progressed and decreased after complete drainage in all treatments (Figure 5.1f). The SO_4^{2-} content peaked after complete drainage throughout the study period and showed an opposite trend to the NH_4^+ and Fe^{2+} contents (Figure 5.1g).

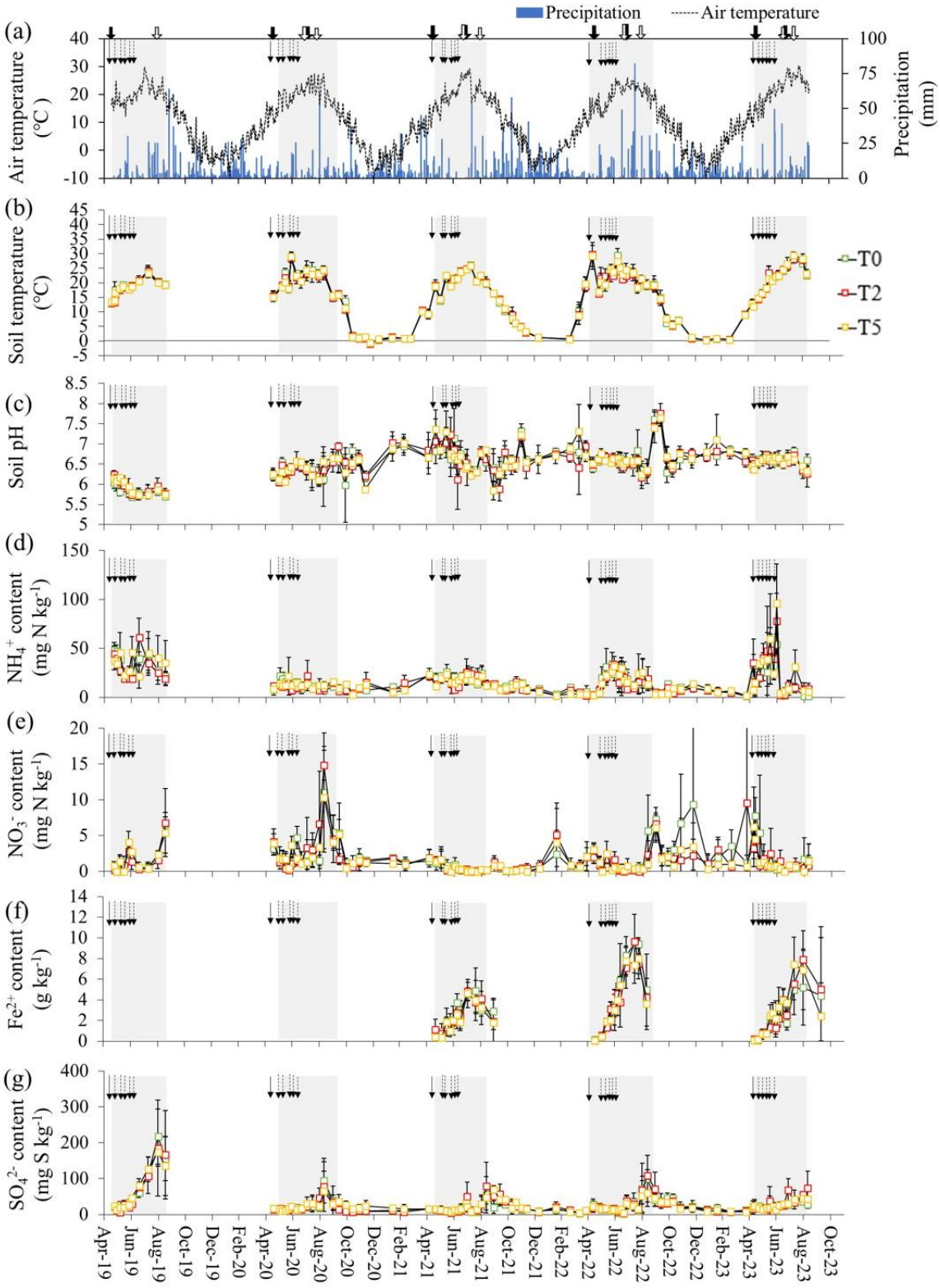


Figure 5.1. Seasonal variation of air temperature and precipitation (a), soil temperature (b), soil pH (c), NH_4^+ content (d), NO_3^- content (e), Fe^{2+} content (f) and SO_4^{2-} content (g) from 2019 to 2023. The black arrow at the top of the figure indicates irrigation and the white arrow indicates drainage. The dotted arrows indicate the timing of inter-tillage weeding. The gray scale indicates the rice-growing season; the other scales indicate the fallow season. Error bars indicate standard deviation.

Throughout the study period, Eh decreased as waterlogging progressed and increased after complete drainage (Figure 5.2a). Eh remained relatively high during the MIW period at T5, although there were no significant differences among the treatments. In 2023, Eh temporarily increased immediately after MIW and a decreasing trend was observed by the next MIW. There were no significant differences in the WEOC content among the treatments throughout the study period (Figure 5.2b).

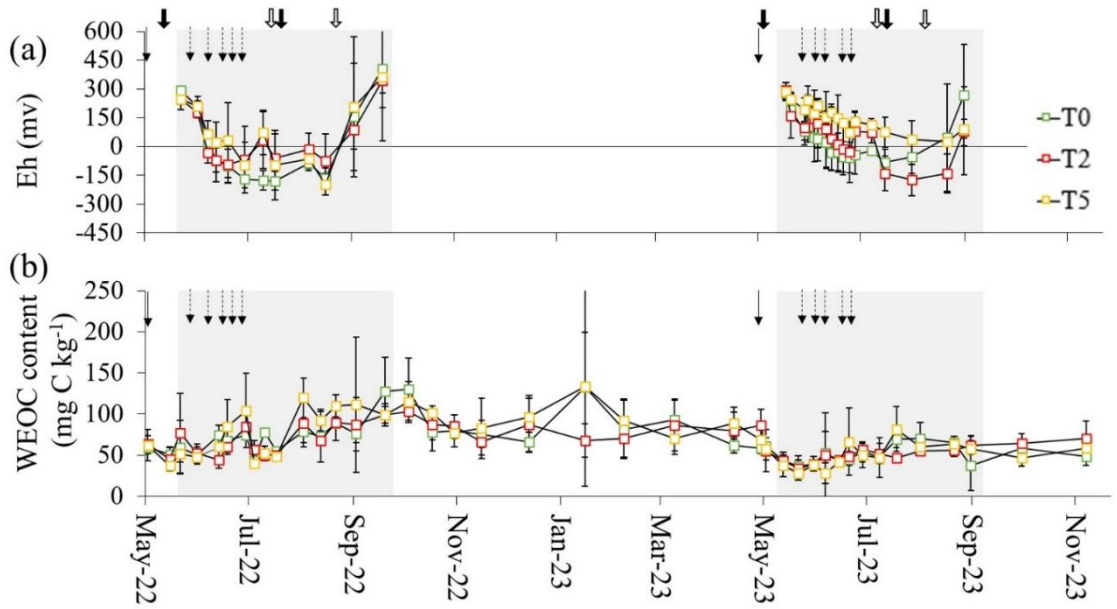


Figure 5.2. Seasonal variation of soil redux condition (Eh) (a) and water extract organic carbon content (b) from 2022 to 2023. The black arrow at the top of the figure indicates irrigation and the white arrow indicates drainage. The dotted arrows indicate the timing of inter-tillage weeding. The gray scale indicates the rice-growing season; the other scales indicate the fallow season. Error bars indicate standard deviation.

The results of soil physical properties in 2021 and 2022 are presented in Table 5.2. Although the MIW period is considered the most susceptible to disturbance, no significant differences were observed among treatments in solid-phase ratio, liquid-phase ratio, air-phase ratio, porosity, or bulk density. These findings indicate that soil disturbance caused by MIW had minimal impact on soil physical properties.

Table 5.2. Soil physicality at 0-5 cm depth (average of MIW period).

		Solid-phase ratio (%)	Liquid-phase ratio (%)	Air-phase ratio (%)	Porosity (%)	Bulk density (g cm^{-3})
2021	T0	36±2.8 a	61±2.9 a	3.7±1.9 a	64±2.8 a	0.94±0.06 a
	T2	33±3.0 a	61±2.3 a	6.0±1.8 a	67±3.0 a	0.88±0.04 a
	T5	37±1.6 a	59±2.5 a	4.5±1.1 a	63±1.6 a	0.95±0.03 a
2022	T0	32±1.0 a	60±0.4 a	7.4±1.4 a	68±1.0 a	0.85±0.02 a
	T2	33±0.8 a	59±3.7 a	7.5±3.3 a	67±0.8 a	0.88±0.02 a
	T5	32±1.4 a	60±4.1 a	7.9±3.3 a	68±1.4 a	0.85±0.04 a

Note: T0, T2 and T5 are organic rice farming with no inter-tillage weeding, two time of inter-tillage weeding, and five time of inter-tillage weeding without fertilizer and agricultural chemicals. Values represent mean ± standard deviation and value with the same letters is not significantly different in each column ($p < 0.05$).

5.3.2. Rice plants characteristics

At the maximum tillering stage in 2021, plant height was significantly higher at T5 than T2. However, there were no significant differences among T0, T2, and T5 at the other rice-growing stage of each year (Table 5.3). However, there was observed a tendency for the plant height to increase under MIW practice. There was also no significant difference in tiller number among the treatments at the rice-growing stages of each year (Table 5.3). The chlorophyll content in 2021 was significantly higher at T5 than at T2 during the tillering stage, and significantly higher at T5 than at T0 and T2 during the heading stage (Table 5.3). In other years, there were no significant differences among the treatments; however, the chlorophyll content tended to increase with the number of MIW across the growth stages.

The stems and leaves, grains, and total NPP in 2020 was significantly higher at T5 than T0, and the cumulative values over five years were also significantly higher at T5 than T0 (Table 5.4). Each year, stems and leaves, grains, and total NPP tended to increase with the number of MIW (Table 5.4). Over the five years, year and treatment differences had a significant impact on the NPP of each part and total NPP ($p < 0.05$). However, no interaction between year and treatment was observed.

Table 5.3. Rice growth indicators for each rice-growing stage.

		Plant height (cm)				Tiller number (number hill^{-1})		Chlorophyll content (SPAD)		
Stage (S)	Treatments (T)	2020	2021	2022	2023	2022	2023	2021	2022	2023
Tillering stage	T0	41.5±6.64 b	45.9±1.95 e	47.2±3.10 c	41.8±4.85 b	12.1±1.10 c	8.73±1.81 ab	31.9±1.74 ac	41.5±2.12 a	35.6±1.30 a
(Late June - Early July)	T2	40.3±7.30 b	48.0±3.16 e	48.0±4.94 c	43.2±4.31 b	14.2±0.35 bc	8.87±0.50 ab	29.3±1.16 c	41.6±1.36 a	37.0±2.54 a
	T5	41.9±2.91 b	46.3±0.69 e	45.3±2.45 c	41.1±2.20 b	13.6±0.40 bc	7.80±1.78 b	35.2±1.09 ab	41.8±1.03 a	36.8±1.22 a
Maximum Tillering stage	T0	62.8±3.09 a	62.3±1.73 cd	65.7±2.86 b	77.0±4.65 a	19.3±2.52 ab	12.7±1.62 ab	33.2±3.95 ac	41.7±1.81 a	37.3±5.79 a
(Mid - July)	T2	65.1±3.32 a	61.0±2.44 c	68.2±3.75 b	78.8±5.50 a	21.1±4.28 a	12.7±2.53 ab	32.5±1.44 ac	41.7±2.02 a	39.3±3.01 a
	T5	65.0±3.87 a	66.5±1.12 bd	66.8±3.86 b	75.1±4.80 a	18.4±2.16 ac	13.5±1.63 a	36.9±2.48 a	42.2±0.59 a	42.1±1.70 a
Heading stage	T0	69.8±2.39 a	70.1±0.82 ab	82.0±1.54 a	78.6±5.65 a	16.6±3.82 ac	11.6±1.76 ab	30.4±1.73 bc	39.2±2.56 a	36.8±8.60 a
(Late July – Early August)	T2	70.3±1.78 a	71.1±2.53 ab	84.2±1.98 a	78.5±5.27 a	18.4±1.25 ac	12.2±1.44 ab	30.5±1.35 bc	39.6±2.77 a	39.9±1.74 a
	T5	72.9±0.75 a	72.9±1.43 a	82.8±5.69 a	75.9±2.92 a	15.5±2.16 ac	11.1±2.05 ab	36.7±0.85 a	39.7±1.68 a	42.7±4.01 a

ANOVA	d.f	*F*	*p*	*F*	*p*	*F*	*p*	*F*	*p*	*F*	*p*	*F*	*p*	*F*	*p*	*F*	*p*	*F*	*p*
S	2	131	<0.001	381	<0.001	230	<0.001	177	<0.001	15.6	<0.001	15.5	<0.001	2.76	0.09	4.25	<0.05	1.90	0.178
T	2	0.503	0.613	3.99	<0.05	0.777	0.475	0.848	0.445	2.08	0.154	0.144	0.867	20.0	<0.001	0.138	0.872	2.14	0.147
S × T	4	0.201	0.934	2.72	0.062	0.158	0.957	0.070	0.990	0.316	0.864	0.327	0.856	0.712	0.594	0.016	0.999	0.296	0.877

Note: T0, T2 and T5 are organic rice farming with no inter-tillage weeding, two time of inter-tillage weeding, and five time of inter-tillage weeding without fertilizer and agricultural chemicals. Values represent mean ± standard deviation and value with the same letters is not significantly different in each column ($p < 0.05$).

Table 5.4. Net primary production (NPP) of rice plants from 2019 to 2023.

Year (Y)	Treatments (T)	Stem & leaves		Grain		Roots		Total	
		(Mg C ha^{-1})							
2019	T0	1.80 ab		1.43 cd		0.02 d		3.26 ac	
	T2	2.10 af		1.50 ad		0.02 d		3.62 ac	
	T5	2.35 a		2.09 ad		0.02 d		4.46 ab	
2020	T0	0.82 cde		0.96 d		0.16 cd		1.94 c	
	T2	1.35 bdefg		1.84 ad		0.51 ac		3.71 ac	
	T5	1.92 ag		2.73 a		0.37 ad		5.02 a	
2021	T0	0.70 e		0.99 d		0.14 cd		1.83 c	
	T2	0.91 be		1.02 bd		0.19 bcd		2.12 c	
	T5	1.06 bdeg		1.38 cd		0.29 ad		2.73 bc	
2022	T0	1.45 abde		1.93 ad		0.43 ac		3.81 ac	
	T2	1.72 abc		2.28 abc		0.51 ac		4.52 ab	
	T5	1.65 abd		2.36 ac		0.46 ac		4.47 ab	
2023	T0	0.72 e		1.28 cd		0.46 ac		2.46 bc	
	T2	0.75 de		1.49 ad		0.60 a		2.83 bc	
	T5	0.88 be		1.66 ad		0.56 ab		3.10 ac	
5 years	T0	5.49 B		6.60 B		1.22 A		13.3 B	
	T2	6.83 AB		8.14 AB		1.84 A		16.8 AB	
	T5	7.86 A		10.2 A		1.70 A		19.8 A	
ANOVA	d.f	*F*	*p*	*F*	*p*	*F*	*p*	*F*	*p*
Y	4	27.2	<0.001	7.82	<0.001	23.9	<0.001	12.1	<0.001
T	2	9.01	<0.001	10.9	<0.001	3.94	<0.05	12.8	<0.001
Y × T	8	1.24	0.31	1.60	0.17	1.03	0.44	1.74	0.13

Note: T0, T2 and T5 are organic rice farming with no inter-tillage weeding, two time of inter-tillage weeding, and five time of inter-tillage weeding without fertilizer and agricultural chemicals. Value with the same letters is not significantly different in each column (p <0.05).

Brown rice yields were not significantly different among treatments in each year or cumulative value over five years (Figure 5.3). The brown rice yields did not show significant differences among the treatments in each year, however, there was observed a tendency for the brown rice yields to increase under MIW practice (Table 5.5). Brown rice yield had a significant positive correlation with the number of MIW (r = 0.59, $p < 0.05$).

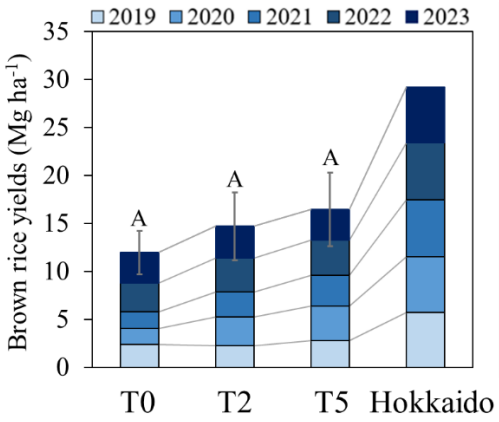


Figure 5.3. Cumulative of brown rice yields each year from 2019 to 2023. Error bars indicate standard deviation. The same letters show no significant difference in cumulative values among the treatments (p <0.05).

The number of ears did not show significant differences among the treatments in each year, however, the four-year average also indicated that T2 and T5 were significantly higher than T0 (Table 5.5). In addition, both year and treatment had a significant effect on the number of ears. For ripened grains, no significant differences were observed among the treatments in either each years or the four-year average (Table 5.5). However, the year effect was significant, and at T5 generally showed lower values compared to other treatments. Regarding the 1000-grain weight, T5 was significantly higher than T0 in 2020, but no significant differences were found among the treatments in other years (Table 5.5). The four-year average of the 1000-grain weight showed T2 and T5 were significantly higher than T0. Both year and treatment, as well as their interaction, had significant effects on the 1000-grain weight.

Table 5.5. Characteristics of yield components and brown rice yields.

Year (Y)	Treatments (T)	Number of ears (number hill^{-1})		Ripened grains (%)		1000-grain weight (g)		Yield (Mg ha^{-1})	
2019	T0	NA		NA		NA		2.40±0.30 a	
	T2	NA		NA		NA		2.27±1.10 a	
	T5	NA		NA		NA		2.82±0.51 a	
	Hokkaido	NA		NA		NA		5.71	
2020	T0	37.5±1.27 cd		95 a		18.8±1.27 d		1.68±0.46 a	
	T2	48.2±14.4 ad		95 a		21.4±1.27 bc		3.00±0.95 a	
	T5	50.7±13.2 ad		94 a		22.1±1.27 ac		3.55±1.22 a	
	Hokkaido	NA		NA		NA		5.81	
2021	T0	34.9±4.27 d		90 a		21.3±0.61 bc		1.70±0.44 a	
	T2	45.4±9.03 bd		91 a		20.9±0.78 c		2.59±1.02 a	
	T5	47.9±4.45 ad		93 a		21.5±0.60 ac		3.22±1.01 a	
	Hokkaido	NA		NA		NA		5.97	
2022	T0	47.7±9.05 ad		84 a		22.3±0.35 ac		3.04±1.05 a	
	T2	59.4±1.24 abc		86 a		21.8±0.37 ac		3.54±0.80 a	
	T5	58.1±4.85 ad		86 a		21.9±0.35 ac		3.65±0.08 a	
	Hokkaido	NA		NA		NA		5.91	
2023	T0	56.6±6.38 ad		94 a		22.8±0.99 ab		3.14±0.56 a	
	T2	70.4±10.9 a		93 a		23.2±0.71 a		3.31±0.22 a	
	T5	68.6±7.34 ab		80 a		22.2±0.28 ac		3.25±1.22 a	
	Hokkaido	NA		NA		NA		5.82	
Average of 4 year	T0	44.2±10.3 B		90 A		21.1±1.73 B		NA	
	T2	55.9±13.4 A		91 A		21.7±1.00 A		NA	
	T5	56.3±10.9 A		88 A		21.9±0.44 A		NA	
Sum of 5 year (Yield)	T0	NA		NA		NA		12.0±2.28 A	
	T2	NA		NA		NA		14.7±3.52 A	
	T5	NA		NA		NA		16.5±3.84 A	
	Hokkaido	NA		NA		NA		29.2	
ANOVA	d.f	*F*	*p*	*F*	*p*	*F*	*p*	*F*	*p*
Y	3 (4 (Yield))	13.7	<0.001	3.57	<0.05	19.3	<0.001	2.43	0.07
T	2 (2 (Yield))	8.34	<0.01	0.878	0.429	4.26	<0.05	4.68	<0.05
T × Y	6 (8 (Yield))	0.07	0.999	1.42	0.247	8.83	<0.001	0.75	0.65

Note: T0, T2 and T5 are organic rice farming with no inter-tillage weeding, two time of inter-tillage weeding, and five time of inter-tillage weeding without fertilizer and agricultural chemicals. Hokkaido is the average yield in Hokkaido. Values represent mean ± standard deviation and value with the same letters is not significantly different in each column ($p < 0.05$). NA indicates no data for the measurement.

5.3.3. RH emissions

RH flux tended to increase at mid-season drainage, intermittent drainage, and complete drainage and showed similar temporal variation across all treatments over five years (Figure 5.4a).

Correlations between RH flux and soil environmental factors were provided in Table 5.6. All treatments had significant positive correlations with RH flux and soil temperature during the fallow season ($p < 0.05$). During the fallow season, there was a significant negative correlation between RH flux and soil pH except for T5 ($p < 0.05$). There was a significant positive correlation between RH flux and SO_4^{2-} content during the rice-growing season at all treatments, except for T0 during the fallow season ($p < 0.05$).

Cumulative RH emissions during the rice-growing and fallow seasons showed positive values across all treatments over five years (Table 5.7). Cumulative RH emissions during the rice-growing season over five years were highest at T2, though there were no significant differences among the treatments. For the fallow season, there were no significant differences observed among the treatments. However, cumulative RH emissions during the fallow season were significantly affected by differences in years and treatments (Table 5.7). The contribution of RH emissions during the rice-growing season to annual values was 25–56% (average 43%) for T0, 45–77% (average 58%) for T2, 23–53% (average 38%) for T5.

There were no significant differences in RH emissions per carbon input among treatments in each column during the both seasons over five years, except for RH emissions per weeds during the fallow season (Table 5.8). RH emissions per carbon input exceeded CH_4 emissions during both seasons. Average RH emissions per weeds or residues during the rice-growing season over five years were at T0 (679% or 300%), T2 (632% or 491%) and T5 (460% or 266%). And during the fallow season, they were at T0 (700% or 410%), T2 (475% or 386%) and T5 (586% or 365%). Unlike T0 and T5, the RH emission per weeds and residues was higher during the rice-growing season than the fallow season at T2. Year differences had significant effects on

RH emissions per weeds, residues, and total (weeds + residues) during the rice-growing season, as well as on RH emissions per residues in the fallow season ($p < 0.05$). Additionally, both year and treatments differences significantly affected RH emissions per weeds during the fallow season, showing a significant interaction effect between year and treatment ($p < 0.001$). Furthermore, both year and treatments differences had a significant effect on RH emissions per total during the fallow season.

5.3.4. CH_4 emissions

CH_4 flux increased sharply due to flooding during the rice-growing season, reaching a peak in July or August. Afterward, CH_4 flux tended to decrease. During the fallow season, CH_4 flux fluctuated at very low values between consumption and emission (Figure 5.4b).

All treatments had significant positive correlations between CH_4 flux and soil temperature during the rice-growing season ($p < 0.01$, Table 5.6). There was a significant negative correlation between CH_4 flux and NO_3^- content during the rice-growing season at all treatments ($p < 0.05$). There was a significant positive correlation between CH_4 flux and Fe^{2+} content during the rice-growing season except for T0 ($p < 0.05$). There was a significant negative correlation between CH_4 flux and Eh during the rice-growing season at all treatments ($p < 0.01$).

There were no significant differences in cumulative CH_4 emissions during both seasons among the treatments over five years (Table 5.7). Cumulative CH_4 emissions during the rice-growing season and on an annual basis were significantly influenced by year, with considerable variability between years (Table 5.7). In 2019, CH_4 emissions tended to increase by 36% and 181% at T2 and T5 compared to T0, respectively. In 2020, the increases were 20% and 134%, respectively. In 2021, CH_4 emissions tended to decrease by 30% and 14%, respectively. In 2022, they decreased by 26% and 5%, respectively. In 2023, they increased by 95% at T2 and 227% at T5. Over five years, annual cumulative CH_4 emissions were highest at T5, but there were no significant differences among the treatments (Table 5.7). The contribution of cumulative CH_4

emissions during the rice-growing season to annual values was 98–100% for T0, 97–100% for T2, and 98–100% for T5.

A comparison of the proportion of CH_4 emissions derived from different carbon sources (weeds and residues) showed no significant differences among the treatments during the rice-growing season over five years (Table 5.8). However, CH_4 emissions per carbon input from weeds and residues were significantly affected between years. The CH_4 emissions per carbon input from weeds, residues, or their total (weeds + residues) during the rice-growing season averaged over five years were 29%, 15%, and 7.6% for T0; 21%, 15%, and 6.8% for T2; and 32%, 20%, and 11% for T5, respectively. Regardless of the carbon source, CH_4 emissions per carbon input tended to be slightly higher at T5.

5.3.5. N_2O emissions

N_2O flux was emitted without a specific pattern, unlike RH and CH_4 fluxes (Figure 5.4c). During the rice-growing season, N_2O flux ranged from -422 to 196 μg N m^{-2} h^{-1}, indicating low emissions and low uptake. During the fallow season, N_2O flux ranged from -29.5 to 79.6 μg N m^{-2} h^{-1}, showing lower levels compared to the rice-growing season.

There was a significant negative correlation between N_2O flux and Fe^{2+} content during the rice-growing season only at T5 ($p < 0.05$, Table 5.6). N_2O flux and Eh during the rice-growing season had a significant positive correlation only at T5 ($p < 0.01$).

Cumulative N_2O emissions during both seasons showed both emissions and absorption, with no significant differences between treatments over five years (Table 5.7). Cumulative N_2O emissions during the rice-growing season, at T0, T2, and T5, negative values were observed, indicating an absorption tendency (Table 5.7). Cumulative N_2O emissions during the fallow season were highest at T2 over five years, but again, no significant differences were found among the treatments. At T0, T2, and T5, positive values were observed, indicating an emission trend (Table 5.7). Annual N_2O emissions in the no-fertilization plots in several previous studies

ranged from 0.18 to 0.76 kg N ha^{-1} (Wang et al., 2013; Yang et al., 2015; Yao et al., 2012; Yuan et al., 2019; Zhang et al., 2010), while annual N_2O emissions in this study ranged from -1.58 to 0.60 kg N ha^{-1}. The contribution of N_2O emissions during the rice-growing season to the annual values was -179–19% (average -78%) for T0, -195–77% (average -19%) for T2, -115–83% (average 23%) for T5.

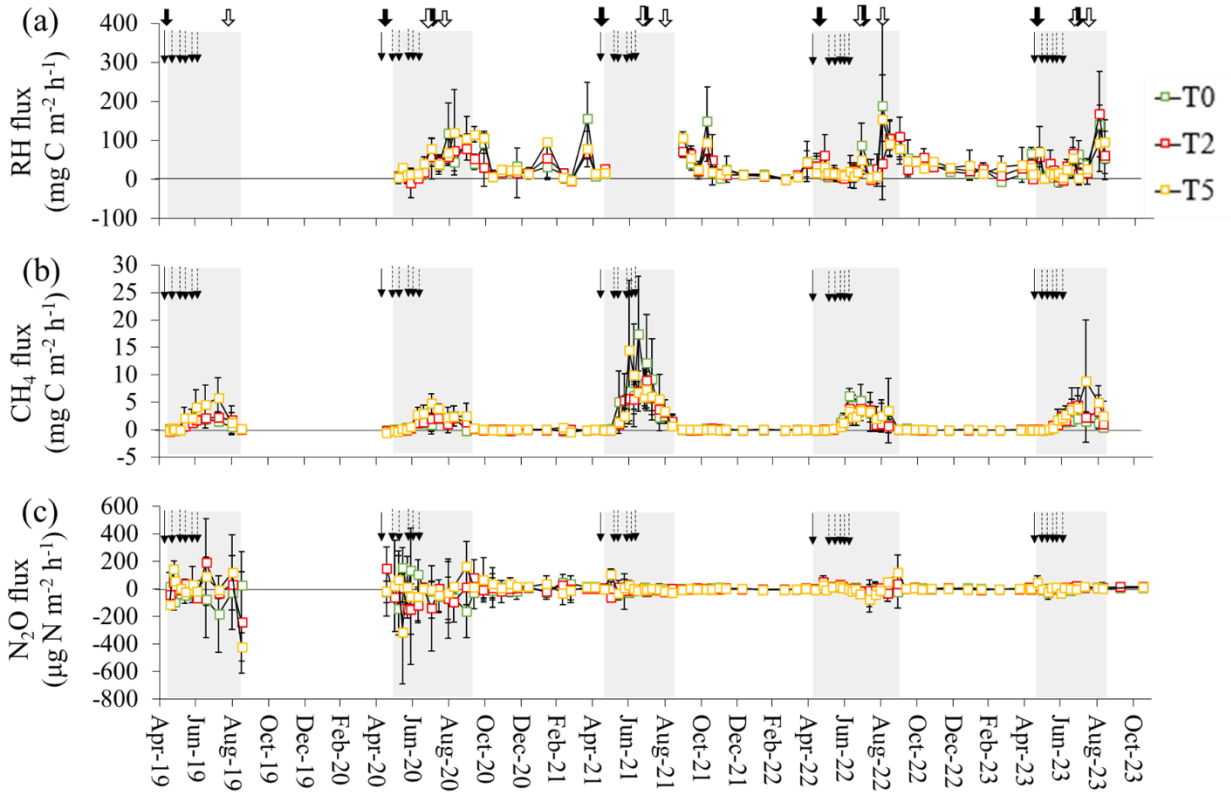


Figure 5.4. Seasonal variation of RH (heterotrophic respiration) flux (a), CH_4 flux (b) and N_2O flux (c) from 2019 to 2023. The black arrow at the top of the figure indicates irrigation and the white arrow indicates drainage. The dotted arrows indicate the timing of inter-tillage weeding. The gray scale indicates the rice-growing season; the other scales indicate the fallow season. Error bars indicate standard deviation.

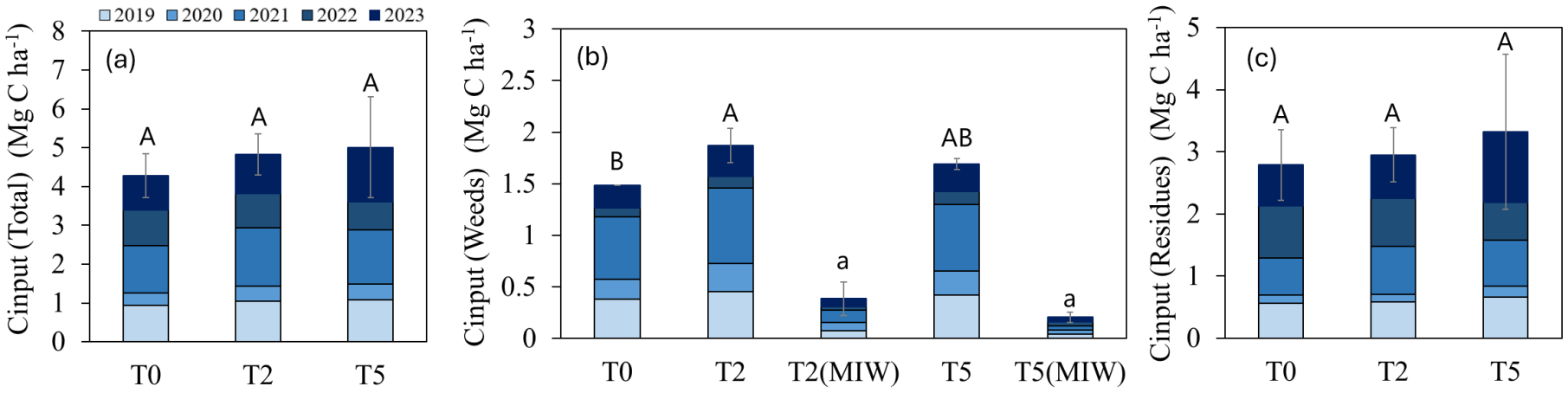


Figure 5.5. Carbon input total (a), from weeds (b), from residues (c). Error bars indicate standard deviation. The same letters are not significantly different among treatments (p <0.05).

Table 5.6. Pearson correlation coefficients for greenhouse gas (GHG) fluxes against soil environmental factors from 2019 to 2023.

	Treatment	Soil temp (°C)	Soil pH	NH_4^+ (mg N kg^{-1})	NO_3^- (mg N kg^{-1})	Fe^{2+} (g kg^{-1})	SO_4^{2-} (mg S kg^{-1})	Eh (mV)	WEOC (mg C kg^{-1})
RH flux	Rice-growing season								
	T0	0.04	-0.30	-0.56	0.36	0.46	0.75**	0.13	0.64*
	T2	-0.02	-0.28	-0.59	0.39	0.34	0.75**	0.03	0.51
	T5	-0.12	-0.46	-0.42	0.43	0.17	0.78**	0.07	0.40
	Fallow season								
	T0	0.80**	-0.77*	0.41	-0.10	-	0.45	-	-0.35
	T2	0.78*	-0.75*	0.12	-0.34	-	0.82**	-	-0.10
	T5	0.68*	-0.67	0.22	-0.01	-	0.73*	-	-0.06
CH_4 flux	Rice-growing season								
	T0	0.76**	0.04	-0.09	-0.69**	0.60	-0.41	-0.86***	0.11
	T2	0.85***	-0.27	-0.25	-0.63*	0.69*	-0.14	-0.92***	-0.05
	T5	0.77**	-0.31	-0.30	-0.63*	0.73*	0.03	-0.80**	0.52
	Fallow season								
	T0	0.44	0.00	-0.34	-0.21	-	0.13	-	0.59
	T2	-0.10	0.26	-0.28	-0.34	-	-0.14	-	0.28
	T5	-0.01	0.05	-0.03	-0.28	-	0.13	-	0.63
N_2O flux	Rice-growing season								
	T0	0.05	0.25	0.01	-0.17	-0.44	-0.51	0.02	-0.53
	T2	-0.02	-0.28	-0.59	0.39	0.34	0.75**	0.03	0.51
	T5	-0.61*	0.49	-0.07	0.18	-0.73*	-0.37	0.75**	-0.47
	Fallow season								
	T0	-0.34	-0.03	0.37	-0.19	-	0.01	-	-0.42
	T2	0.10	0.15	-0.07	-0.22	-	-0.23	-	0.19
	T5	0.00	-0.58	0.34	-0.03	-	0.05	-	-0.47

Note: * <0.05, **<0.01, ***<0.001. T0, T2 and T5 are organic rice farming with no inter-tillage weeding, two time of inter-tillage weeding, and five time of inter-tillage weeding without fertilizer and agricultural chemicals.

Table 5.7. Seasonal cumulative greenhouse gas (GHG) emissions and global warming potential (GWP_{total}) at each treatment from 2019 to 2023.

		Rice-growing season								Fallow season								Annual							
Year (Y)	Treatment (T)	RH (Mg C ha^{-1})		CH_4 (kg C ha^{-1})		N_2O (kg N ha^{-1})		GWP_{total} (Mg CO_2-eq ha^{-1})		RH (Mg C ha^{-1})		CH_4 (kg C ha^{-1})		N_2O (kg N ha^{-1})		GWP_{total} (Mg CO_2-eq ha^{-1})		RH (Mg C ha^{-1})		CH_4 (kg C ha^{-1})		N_2O (kg N ha^{-1})		GWP_{total} (Mg CO_2-eq ha^{-1})	
2019	T0	1.01	a	30.2	b	-1.63	a	4.17	a	1.45	a	0.58	a	0.05	a	5.35	a	2.46	a	30.8	b	-1.58	a	9.52	a
	T2	4.13	a	41.0	ab	0.31	a	16.8	a	1.26	a	0.57	a	0.17	a	4.69	a	5.39	a	41.5	ab	0.48	a	21.5	a
	T5	0.57	a	84.9	ab	0.07	a	5.33	a	1.59	a	1.02	a	0.16	a	5.93	a	2.16	a	86.0	ab	0.22	a	11.3	a
2020	T0	1.21	a	30.3	b	-0.02	a	5.57	a	1.45	a	0.58	a	0.05	a	5.35	a	2.65	a	30.9	b	0.03	a	10.9	a
	T2	1.02	a	36.4	ab	-1.55	a	4.47	a	1.26	a	0.57	a	0.17	a	4.69	a	2.28	a	37.0	ab	-1.38	a	9.17	a
	T5	1.56	a	71.1	ab	-1.22	a	7.91	a	1.59	a	1.02	a	0.16	a	5.93	a	3.15	a	72.1	ab	-1.07	a	13.8	a
2021	T0	0.62	a	161	a	-0.21	a	8.21	a	1.91	a	-0.47	a	-0.13	a	6.93	a	2.53	a	161	a	-0.34	a	15.1	a
	T2	2.72	a	112	ab	-0.21	a	14.1	a	1.24	a	0.33	a	0.32	a	4.69	a	3.96	a	113	ab	0.11	a	18.8	a
	T5	0.56	a	139	ab	0.27	a	7.45	a	1.89	a	2.18	a	0.34	a	7.16	a	2.46	a	141	ab	0.60	a	14.6	a
2022	T0	1.58	a	68.0	ab	-0.14	a	8.32	a	1.26	a	1.61	a	0.06	a	4.71	a	2.84	a	69.6	ab	-0.08	a	13.0	a
	T2	1.24	a	50.3	ab	0.20	a	6.57	a	1.12	a	1.34	a	0.06	a	4.17	a	2.36	a	51.7	ab	0.26	a	10.7	a
	T5	1.33	a	64.7	ab	0.13	a	7.39	a	1.20	a	1.01	a	0.03	a	4.46	a	2.53	a	65.7	ab	0.16	a	11.9	a
2023	T0	1.10	a	29.8	b	0.05	a	5.21	a	1.17	a	0.60	a	0.23	a	4.41	a	2.27	a	30.4	b	0.29	a	9.62	a
	T2	1.25	a	58.0	ab	0.31	a	6.89	a	1.41	a	0.03	a	0.13	a	5.22	a	2.66	a	58.0	ab	0.44	a	12.1	a
	T5	1.01	a	97.5	ab	0.26	a	7.43	a	1.67	a	-0.15	a	0.10	a	6.17	a	2.68	a	97.4	ab	0.36	a	13.6	a
5-year	T0	5.52	A	320	A	-1.94	A	31.5	A	7.24	A	2.90	A	0.27	A	26.8	A	12.8	A	323	A	-1.68	A	58.2	A
	T2	10.4	A	298	A	-0.95	A	48.9	A	6.28	A	2.85	A	0.85	A	23.5	A	16.7	A	301	A	-0.10	A	72.3	A
	T5	5.03	A	457	A	-0.50	A	35.5	A	7.95	A	5.08	A	0.78	A	29.7	A	13.0	A	462	A	0.28	A	65.2	A
ANOVA	d.f	*F*	*p*	*F*	*p*	*F*	*p*	*F*	*p*	*F*	*p*	*F*	*p*	*F*	*p*	*F*	*p*	*F*	*p*	*F*	*p*	*F*	*p*	*F*	*p*
Y	4	0.32	0.86	7.28	<0.001	1.46	0.24	0.63	0.64	2.93	<0.05	0.20	0.94	0.10	0.98	3.01	<0.05	0.34	0.85	7.27	<0.001	1.30	0.29	0.86	0.50
T	2	2.05	0.15	2.59	0.09	0.25	0.78	1.33	0.28	4.62	<0.05	0.13	0.88	0.28	0.76	4.65	<0.05	0.97	0.39	2.66	0.09	0.44	0.65	0.68	0.52
Y × T	8	1.08	0.41	0.73	0.67	1.03	0.43	1.02	0.44	1.07	0.41	0.19	0.99	0.23	0.98	0.95	0.49	0.83	0.59	0.70	0.69	0.94	0.50	0.82	0.59

Note: T0, T2 and T5 are organic rice farming with no inter-tillage weeding, two time of inter-tillage weeding, and five time of inter-tillage weeding without fertilizer and agricultural chemicals. RH (Heterotrophic respiration) for the rice-growing season in 2019 and 2020 were estimated, while for the fallow season the average value of 2021-2023 was used. CH_4 and N_2O emissions for the fallow season in 2019 and 2020 used the average value of 2021-2023.
Value with the same letters is not significantly different in each column (p <0.05).

Table 5.8. RH (heterotrophic respiration) or CH_4 emissions per carbon input from 2019 to 2023.

		Rice-growing season												Fallow season									
Year (Y)	Treatments (T)	RH / WeedsC		CH_4 / WeedsC		RH / ResidueC		CH_4 / ResidueC		RH / TotalCinput		CH_4 / TotalCinput		RH / WeedsC		CH_4 / WeedsC		RH / ResidueC		CH_4 / ResidueC		RH / TotalCinput		CH_4 / TotalCinput	
		(%)												(%)									
2019	T0	265	b	8	b	157	a	5	b	99	a	3	a	380	efg	0	a	270	b	0	a	157	b	0	a
	T2	879	ab	9	b	737	a	7	ab	400	a	4	a	274	bf	0	a	215	b	0	a	120	b	0	a
	T5	130	b	20	b	70	a	15	ab	43	a	8	a	376	efg	0	a	262	b	0	a	152	b	0	a
2020	T0	630	ab	16	b	880	a	22	ab	366	a	9	a	757	cd	0	a	1074	a	1	a	443	a	0	a
	T2	382	b	14	b	994	a	36	ab	271	a	10	a	468	abcd	0	a	1173	a	0	a	328	a	0	a
	T5	671	ab	31	ab	855	a	40	a	374	a	17	a	683	de	0	a	894	a	0	a	385	a	0	a
2021	T0	103	b	27	ab	79	a	32	ab	45	a	14	a	314	fg	0	a	361	b	0	a	165	b	0	a
	T2	366	b	6	b	362	a	14	ab	182	a	8	a	167	f	0	a	164	b	0	a	83	b	0	a
	T5	87	b	22	b	79	a	19	ab	41	a	10	a	293	fg	0	a	270	b	0	a	139	b	0	a
2022	T0	1900	a	82	a	214	a	10	ab	191	a	9	a	1522	a	0	a	167	b	0	a	149	b	0	a
	T2	1077	ab	44	ab	163	a	6	b	141	a	6	a	969	d	2	a	146	b	0	a	126	b	0	a
	T5	1037	ab	51	ab	227	a	11	ab	186	a	9	a	942	d	1	a	204	b	0	a	167	b	0	a
2023	T0	496	b	13	b	171	a	5	b	127	a	3	a	526	bceg	0	a	178	b	0	a	132	b	0	a
	T2	455	b	21	b	197	a	9	ab	136	a	6	a	495	cefg	0	a	231	b	0	a	155	b	0	a
	T5	375	b	37	ab	96	a	15	ab	73	a	10	a	634	dg	0	a	194	b	0	a	143	b	0	a
ANOVA	d.f	*F*	*p*	*F*	*p*	*F*	*p*	*F*	*p*	*F*	*p*	*F*	*p*	*F*	*p*	*F*	*p*	*F*	*p*	*F*	*p*	*F*	*p*	*F*	*p*
Y	4	8.20	<0.001	7.60	<0.001	9.57	<0.001	8.43	<0.001	3.58	<0.05	2.39	0.07	82.0	<0.001	2.54	0.06	58.8	<0.001	0.45	0.77	49.7	<0.001	0.43	0.79
T	2	0.94	0.40	1.33	0.28	2.31	0.12	1.17	0.32	1.16	0.33	2.49	0.10	14.4	<0.001	0.22	0.81	0.37	0.70	0.03	0.97	4.08	<0.05	0.08	0.93
Y × T	8	1.36	0.26	1.02	0.44	0.74	0.65	1,12	0.38	1.25	0.31	0.67	0.72	4.63	<0.001	0.28	0.97	1.05	0.42	0.08	1.00	1.05	0.42	0.10	1.00

Note: T0, T2 and T5 are organic rice farming with no inter-tillage weeding, two time of inter-tillage weeding, and five time of inter-tillage weeding without fertilizer and agricultural chemicals. RH emissions for the rice-growing season in 2019 and 2020 were estimated, while for the fallow season the average value of 2021-2023 was used. CH_4 emissions for the fallow season in 2019 and 2020 used the average value of 2021-2023. Weeds are the carbon content of the previous year's weeds and weeds plowed into the soil (T2 and T5 only) by MIW. Residue is the carbon content of the previous year's residues (rice straw, stubble, roots). Total means sum of residue and weed. Value with the same letters is not significantly different in each column (p <0.05).

5.3.6. Interactions among environmental factors for RH and CH_4 fluxes

In this study, we focused on the rice-growing season including the MIW period to identify which environmental factors were influenced by MIW and contributed to RH and CH_4 fluxes through correlation analysis. Figure 5.6 presents the Pearson correlation matrix of environmental factors, while Figure 5.7 illustrates factors with strong correlations (correlation coefficient ≥ 0.6).

Comparison among the treatments revealed a significant negative correlation between soil pH and SO_4^{2-}, with an increasing correlation coefficient as MIW frequency increased (Figures 5.6 and 5.7). Additionally, RH emissions showed a tendency for increased correlation with soil pH and SO_4^{2-} (Figures 5.6 and 5.7).

Notably, the relationship between CH_4 emissions and environmental factors showed an increasing number of CH_4-related factors with higher disturbance frequencies (Figure 5.7). A significant positive correlation between CH_4 emissions and Fe^{2+} was observed in all treatments, with correlation coefficients increasing with MIW frequency (Figures 5.6 and 5.7). Furthermore, significant positive correlations were found between CH_4 and soil temperature, as well as between soil temperature and Fe^{2+}, with increasing correlation coefficients in higher MIW frequency treatments (Figures 5.6 and 5.7). Also, significant positive correlations was observed between Fe^{2+} and WEOC in all treatments. A significant negative correlation between CH_4 emissions and Eh was observed in all treatments. However, the correlation coefficient was lower at T5 compared to T0 and T2 (Figures 5.6 and 5.7). Furthermore, a significant positive correlation was observed between RH and CH_4 emissions at T5 (Figures 5.6 and 5.7).

5.3.7. GWP, GHGB, GHGI and NECB

GWP during rice-growing and fallow seasons showed no significant differences among the treatments over five years (Table 5.7). Regarding GWP composition ratio during the rice-growing season, RH and CH_4 emissions were the primary contributors. RH emissions

accounted for 25–113% (average 72%) at T0, 60–85% (average 74%) at T2, -69–83% (average 41%) at T5. CH_4 emissions accounted for -7–76% (average 29%) at T0, 16–40% (average 29%) at T2, 21–166% (average 60%) at T5. The contribution of N_2O emissions was extremely lower. On the other hand, GWP during the fallow season was significantly affected by both year and treatments differences (Table 5.7). GWP composition ratio during the fallow season, RH was the primary contributor, accounting for 97–101% (average 99%) at T0, 95–99% (average 98%) at T2, 98–99% (average 99%) at T5. Throughout the year, the GWP was similar across all treatments; however, RH and CH_4 were the major contributors during the rice-growing season, while RH was the primary factor during the fallow season.

GHGB was positive value for all treatments over five years (Table 5.9). The highest GHGB values (Mg CO_2-eq ha^{-1}) were observed at T2 (17.0), T5 (11.7), T2 (13.1), T5(8.93) and T5 (8.14) in 2019, 2020, 2021, 2022, and 2023, respectively (Table 5.9). Although there were no significant differences in GHGB among the treatments over five years, T2 had the highest value, followed by T5 and T0. The contribution of GWP_{RH} to the cumulative GHGB over five years was greater than that of GWP_{CH_4} and GWP_{N_2O}. There was a significant positive correlation between GHGB and GWP_{RH} in all treatments ($p < 0.05$), and a significant positive correlation with GWP_{CH_4}, except for T2 ($p < 0.05$, Figure 5.8).

There were no significant differences in GHGI among the treatments over five years (Table 5.10). GHGI value (Mg CO_2-eq Mg^{-1} yield) was highest at T2 (24.4), followed by T0 (15.4) and T5 (13.8), although the differences among the treatments were not statistically significant.

NECB showed negative values across most treatments for all five year (Table 5.11). Over five years, there were no significant differences in NECB across treatments, but T2 (-10.3 Mg C ha^{-1}) had the lowest, followed by T5 (-7.96) and T0 (-5.42). And there was significant negative correlation between NECB and RH in all treatments ($p < 0.001$, Figure 5.9).

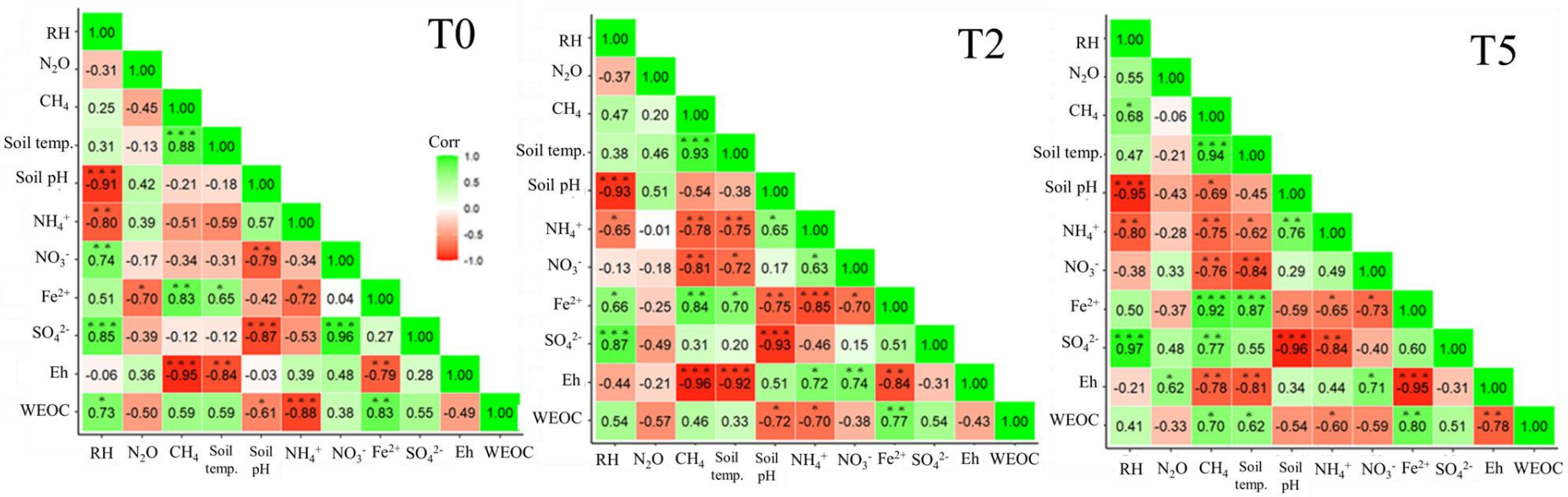


Figure 5.6. Peason correlation coefficient for GHG emissions against soil environmental factors.

* <0.05, **<0.01, ***<0.001.

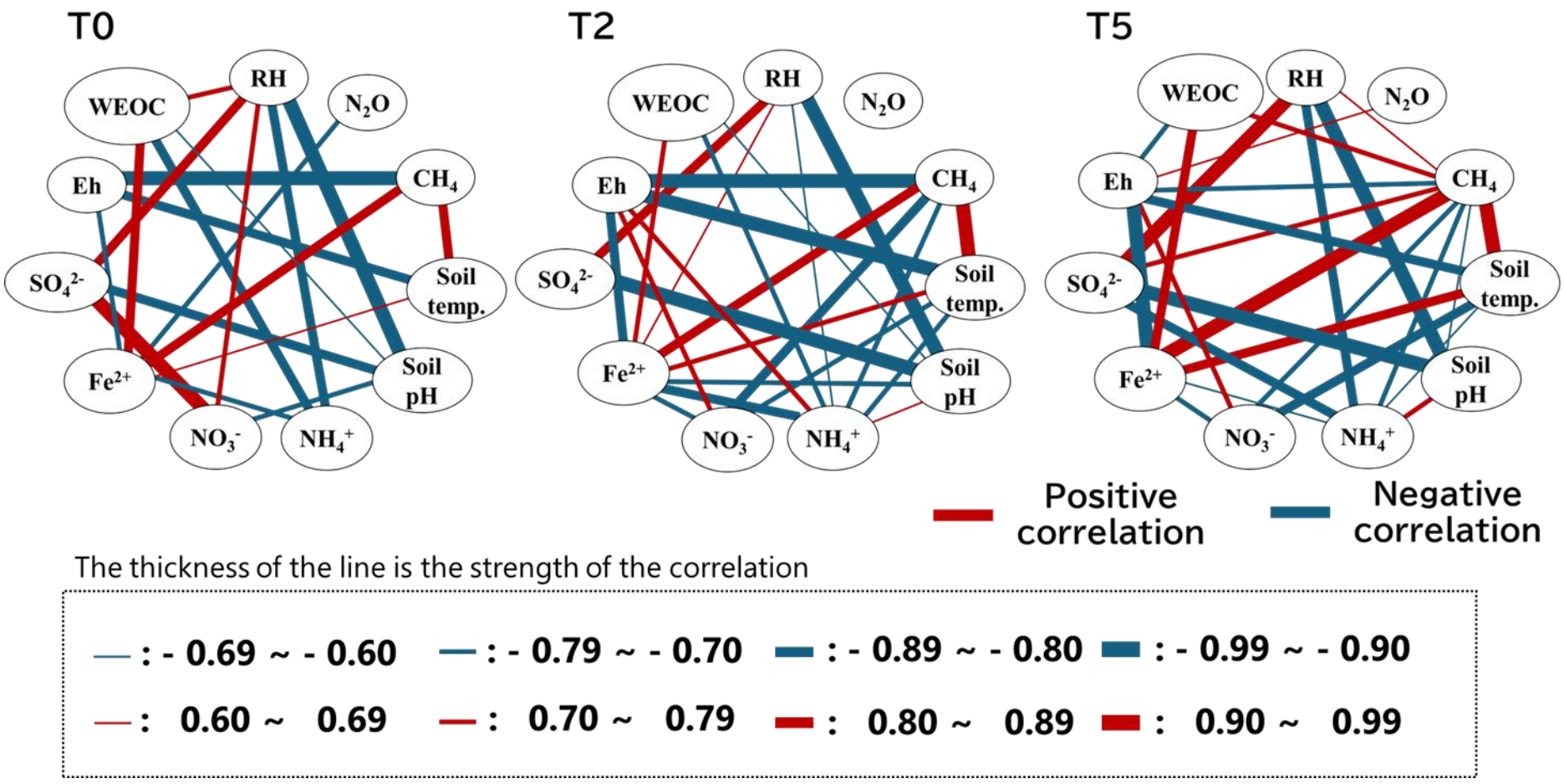


Figure 5.7. The relationship between each factor (correlation coefficient ≥ 0.6).

Table 5.9. Greenhouse gas balance (GHGB) from 2019 to 2023.

Year (Y)	Treatments (T)	GWP_{RH}			GWP_{CH_4}			GWP_{N_2O}			Coutput			NPP (Rice+weeds)			Cinput			GHGB		
		Mg CO_2-eq ha^{-1}																				
2019	T0	9.01	±5.04	a	1.15	±0.16	b	-0.66	±1.28	a	12.0	±1.16	bc	13.0	±1.40	cd	3.44	±0.42	ab	5.06	±5.01	a
	T2	19.8	±15.8	a	1.55	±1.09	ab	0.20	±0.64	a	13.3	±4.76	bc	13.9	±4.10	cd	3.84	±0.39	ab	17.0	±15.0	a
	T5	7.92	±9.11	a	3.21	±2.40	ab	0.16	±0.41	a	16.4	±2.78	ab	16.8	±2.68	bd	3.98	±0.95	ab	6.82	±10.7	a
2020	T0	9.73	±1.48	a	1.15	±0.54	b	0.01	±0.48	a	7.10	±2.46	c	10.5	±2.71	bc	1.20	±0.06	b	6.27	±2.03	a
	T2	8.34	±0.78	a	1.38	±0.38	ab	-0.58	±0.73	a	13.6	±2.32	bc	16.2	±2.82	abd	1.42	±0.28	b	5.07	±1.32	a
	T5	11.6	±3.52	a	2.69	±0.95	ab	-0.44	±0.52	a	18.4	±4.10	b	19.0	±4.05	d	1.50	±0.15	b	11.7	±3.61	a
2021	T0	9.29	1.76	a	6.01	±2.35	a	0.04	±0.50	a	6.71	±2.13	c	7.07	±2.07	c	4.42	±0.73	a	10.6	±2.76	a
	T2	14.5	±11.9	a	4.20	±1.84	ab	0.25	±0.42	a	7.76	±2.17	c	8.20	±2.02	ac	5.49	±0.07	a	13.1	±11.2	a
	T5	9.01	±6.64	a	5.27	±1.10	ab	0.23	±0.42	a	10.0	±2.86	ac	10.1	±2.80	bc	5.07	±0.58	a	9.32	±7.90	a
2022	T0	10.4	±4.26	a	2.60	±1.18	ab	-0.03	±0.07	a	14.0	±2.51	bc	16.1	±2.91	abd	3.38	±1.34	ab	7.49	±3.80	a
	T2	8.66	±0.43	a	1.93	±0.31	ab	0.11	±0.18	a	16.6	±0.74	ab	16.7	±0.63	bd	3.27	±0.32	ab	7.25	±0.39	a
	T5	9.29	±0.73	a	2.45	±2.37	ab	0.07	±0.11	a	16.4	±1.71	ab	16.6	±1.74	abd	2.70	±0.64	ab	8.93	±2.01	a
2023	T0	8.34	±0.61	a	1.14	±0.12	b	0.12	±0.02	a	9.02	±1.79	ac	14.6	±3.94	cd	3.23	±0.37	ab	0.82	±2.33	a
	T2	9.76	±2.69	a	2.17	±1.14	ab	0.18	±0.03	a	10.4	±0.90	ac	13.3	±2.97	cd	3.66	±1.17	ab	5.56	±6.53	a
	T5	9.82	±2.39	a	3.63	±3.05	ab	0.15	±0.06	a	11.4	±2.78	bc	11.7	±2.66	cd	5.12	±2.65	a	8.14	±4.73	a
5 years	T0	46.8	±9.08	A	12.0	±4.01	A	-0.51	±2.13	A	48.8	±4.80	B	61.2	±5.63	A	15.7	±2.08	A	30.2	±4.80	A
	T2	61.0	±25.9	A	11.2	±3.34	A	0.17	±0.85	A	61.6	±5.25	AB	68.4	±2.45	A	17.7	±1.96	A	48.0	±5.25	A
	T5	47.6	±21.2	A	17.3	±8.92	A	0.16	±1.07	A	72.5	±9.16	A	74.3	±8.46	A	18.4	±4.75	A	44.9	±9.16	A
ANOVA	d.f	*F*	*p*		*F*	*p*		*F*	*p*		*F*	*p*		*F*	*p*		*F*	*p*		*F*	*p*	
Y	4	0.34	0.85		7.27	<0.001		1.30	0.29		12.1	<0.001		11.1	<0.001		18.7	<0.001		1.09	0.38	
T	2	0.97	0.39		2.66	0.09		0.44	0.65		12.8	<0.001		3.28	0.05		1.36	0.27		1.22	0.31	
Y × T	8	0.83	0.59		0.70	0.69		0.94	0.50		1.74	0.13		1.81	0.11		0.96	0.48		0.92	0.51	

Note: T0, T2 and T5 are organic rice farming with no inter-tillage weeding, two time of inter-tillage weeding, and five time of inter-tillage weeding without fertilizer and agricultural chemicals. Values represent mean ± standard deviation and value with the same letters is not significantly different in each column ($p < 0.05$).

Table 5.10. Greenhouse gas intensity (GHGI) from 2019 to 2023.

Year (Y)	Treatments (T)	GHGB Mg CO_2-eq ha^{-1}			Yield Mg ha^{-1}			GHGI Mg CO_2-eq Mg^{-1} yield		
2019	T0	5.06	±5.01	a	2.40	±0.30	a	2.30	±2.34	a
	T2	17.0	±15.0	a	2.27	±1.10	a	12.7	±16.5	a
	T5	6.82	±10.7	a	2.82	±0.51	a	2.15	±3.95	a
2020	T0	6.27	±2.03	a	1.68	±0.46	a	3.74	±0.60	a
	T2	5.07	±1.32	a	3.00	±0.95	a	1.78	±0.62	a
	T5	11.7	±3.61	a	3.55	±1.22	a	3.40	±0.97	a
2021	T0	10.6	±2.76	a	1.70	±0.44	a	6.44	±2.26	a
	T2	13.1	±11.2	a	2.59	±1.02	a	6.24	±6.61	a
	T5	9.32	±7.90	a	3.22	±1.01	a	2.95	±2.73	a
2022	T0	7.49	±3.80	a	3.04	±1.05	a	2.62	±1.64	a
	T2	7.25	±0.39	a	3.54	±0.80	a	2.12	±0.45	a
	T5	8.93	±2.01	a	3.65	±0.08	a	2.44	±0.49	a
2023	T0	0.82	±2.33	a	3.14	±0.56	a	0.33	±0.72	a
	T2	5.56	±6.53	a	3.31	±0.22	a	1.64	±1.87	a
	T5	8.14	±4.73	a	3.25	±1.22	a	2.84	±2.10	a
5 years	T0	30.2	±4.80	A	12.0	±2.28	A	15.4	±6.54	A
	T2	48.0	±5.25	A	14.7	±3.52	A	24.4	±21.8	A
	T5	44.9	±9.16	A	16.5	±3.84	A	13.8	±9.17	A
ANOVA	d.f	*F*		*p*	*F*		*p*	*F*		*p*
Y	4	1.09		0.38	2.43		0.07	1.19		0.33
T	2	1.22		0.31	4.68		<0.05	0.81		0.45
Y × T	8	0.92		0.51	0.75		0.65	1.12		0.38

Note: T0, T2 and T5 are organic rice farming with no inter-tillage weeding, two time of inter-tillage weeding, and five time of inter-tillage weeding without fertilizer and agricultural chemicals. Values represent mean ± standard deviation and value with the same letters is not significantly different in each column ($p < 0.05$).

Table 5.11. Net ecosystem carbon balance (NECB) from 2019 to 2023.

Year (Y)	Treatments (T)	RH			CH_4			Coutput			NPP (Rice+weeds)			Cinput			NECB		
		Mg C ha^{-1}																	
2019	T0	2.46	±1.38	a	0.03	±0.00	b	3.26	±0.32	bc	3.54	±0.38	cd	0.94	±0.11	ab	-1.28	±1.32	a
	T2	5.39	±4.30	a	0.04	±0.03	ab	3.62	±1.30	bc	3.79	±1.12	cd	1.05	±0.11	ab	-4.21	±4.12	a
	T5	2.16	±2.48	a	0.09	±0.06	ab	4.46	±0.76	ab	4.59	±0.73	bd	1.09	±0.26	ab	-1.03	±2.50	a
2020	T0	2.65	± 0.40	a	0.03	± 0.01	b	1.94	± 0.67	c	2.87	± 0.74	bc	0.33	± 0.02	b	-1.42	±0.38	a
	T2	2.28	± 0.21	a	0.04	± 0.01	ab	3.71	± 0.63	bc	4.43	± 0.77	abd	0.39	± 0.08	b	-1.20	±0.08	a
	T5	3.15	± 0.96	a	0.07	± 0.03	ab	5.02	± 1.12	b	5.18	± 1.10	d	0.41	± 0.04	b	-2.65	±0.93	a
2021	T0	2.53	± 0.48	a	0.16	± 0.06	a	1.83	± 0.58	c	1.93	± 0.56	c	1.21	± 0.20	a	-1.39	±0.29	a
	T2	3.96	± 3.25	a	0.11	± 0.05	ab	2.12	± 0.59	c	2.24	± 0.55	ac	1.50	± 0.02	a	-2.46	±3.19	a
	T5	2.46	± 1.81	a	0.14	± 0.03	ab	2.73	± 0.78	ac	2.76	± 0.76	bc	1.38	± 0.16	a	-1.18	±1.82	a
2022	T0	2.84	±1.16	a	0.07	±0.03	ab	3.81	±0.69	bc	4.39	±0.79	abd	0.92	±0.37	ab	-1.41	±0.85	a
	T2	2.36	±0.12	a	0.05	±0.01	ab	4.52	±0.20	ab	4.57	±0.17	bd	0.89	±0.09	ab	-1.47	±0.13	a
	T5	2.53	±0.20	a	0.07	±0.06	ab	4.47	±0.47	ab	4.52	±0.48	abd	0.74	±0.17	ab	-1.81	±0.03	a
2023	T0	2.27	±0.17	a	0.03	±0.00	b	2.46	±0.49	ac	3.97	±1.08	cd	0.88	±0.10	ab	0.09	±0.61	a
	T2	2.66	±0.73	a	0.06	±0.03	ab	2.83	±0.25	ac	3.62	±0.81	cd	1.00	±0.32	ab	-0.93	±1.56	a
	T5	2.68	±0.65	a	0.10	±0.08	ab	3.10	±0.76	bc	3.20	±0.73	cd	1.40	±0.72	a	-1.29	±0.58	a
5 years	T0	12.76	±2.48	A	0.32	±0.11	A	13.3	±1.31	B	16.7	±1.53	A	4.27	±0.57	A	-5.42	±1.80	A
	T2	16.65	±7.08	A	0.30	±0.09	A	16.8	±1.43	AB	18.6	±0.67	A	4.82	±0.53	A	-10.3	±6.10	A
	T5	12.98	±5.78	A	0.46	±0.24	A	19.8	±2.50	A	20.3	±2.31	A	5.01	±1.30	A	-7.96	±5.66	A
ANOVA	d.f	*F*	*p*		*F*	*p*		*F*	*p*		*F*	*p*		*F*	*p*		*F*	*p*	
Y	4	0.34	0.85		7.27	<0.001		12.1	<0.001		11.1	<0.001		18.7	<0.001		0.89	0.48	
T	2	0.97	0.39		2.66	0.09		12.8	<0.001		3.28	0.05		1.36	0.27		1.23	0.31	
Y × T	8	0.83	0.59		0.70	0.69		1.74	0.13		1.81	0.11		0.96	0.48		0.93	0.51	

Note: T T0, T2 and T5 are organic rice farming with no inter-tillage weeding, two time of inter-tillage weeding, and five time of inter-tillage weeding without fertilizer and agricultural chemicals. Values represent mean ± standard deviation and value with the same letters is not significantly different in each column ($p < 0.05$).

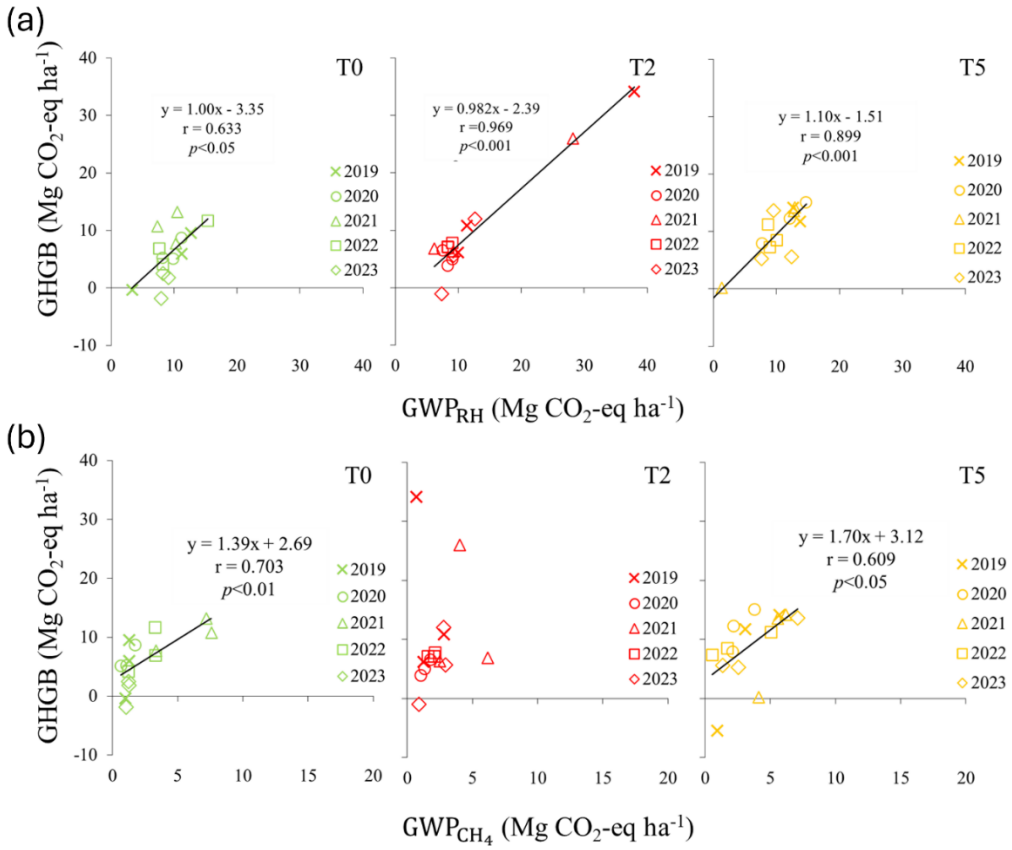


Figure 5.8. Relationship between greenhouse gas balance (GHGB) and GWP_{RH} (a) and GWP_{CH4} (b). Treatments of T0, T2 and T5 are organic rice farming paddy fields without fertilizers and agrochemicals and 0-, 2-, and 5-times inter-tillage weeding respectively.

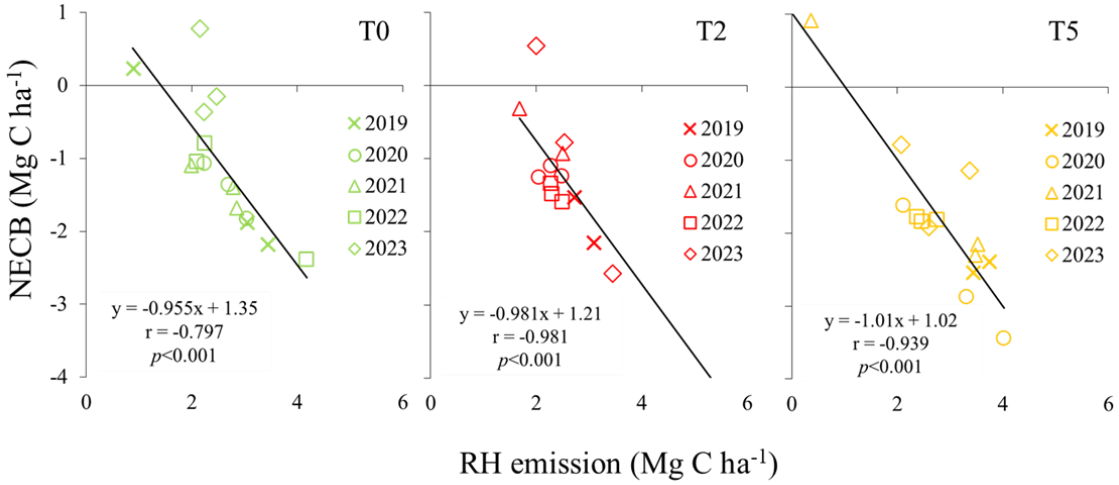


Figure 5.9. Relationship between net ecosystem carbon balance (NECB) and RH emission. Treatments of T0, T2 and T5 are organic rice farming paddy fields without fertilizers and agrochemicals and 0-, 2-, and 5-times inter-tillage weeding, respectively.

5.4. Discussion

5.4.1. Effect of MIW on GHGB

This study confirmed RH emissions throughout the year in all treatments (Table 5.7). This is similar to the report by Song et al., (2024), where 30-43% of annual CO_2-C emissions came from the rice-growing season and 57-70% from the fallow season. Contrary to our hypothesis, cumulative RH emissions did not increase significantly at T5 during the rice-growing season, with T2 showing the largest trend over the five years (Table 5.7). A significant positive correlation between RH flux and SO_4^{2-} suggests enhanced emissions under aerobic conditions (Table 5.6). At T2, larger weeds than T5 were incorporated into the soil at the final MIW (Figures 5.5 and 5.10). And at T2, RH emissions per weed and residue during the rice-growing season tended to exceed emissions during the fallow season (Table 5.8). Additionally, RH flux was highly sensitive to water management practices, showing an increasing trend across all treatments after mid-season drainage, intermittent drainage, and complete drainage (Figure 5.4). This trend was consistent with the findings of Nishimura et al. (2015), who reported a sharp pulse of CO_2 emissions following drainage. According to the few studies which have quantified net ecosystem exchange of CO_2 (NEE) from intermittently flooded paddy fields research in Japan, China and the Philippines showed significantly greater NEE than continuously flooded paddy soils, implying higher ecosystem respiration (RE) (Alberto et al., 2014; Liu et al., 2013; Miyata et al., 2000; Oliver et al., 2019). In our study site, mid-season drainage and intermittent drainage began approximately two weeks after the final MIW practice. Therefore, the increased RH emissions observed at T2 may have been triggered by a priming effect induced by weed incorporation, which was further stimulated by the timing of water management practices.

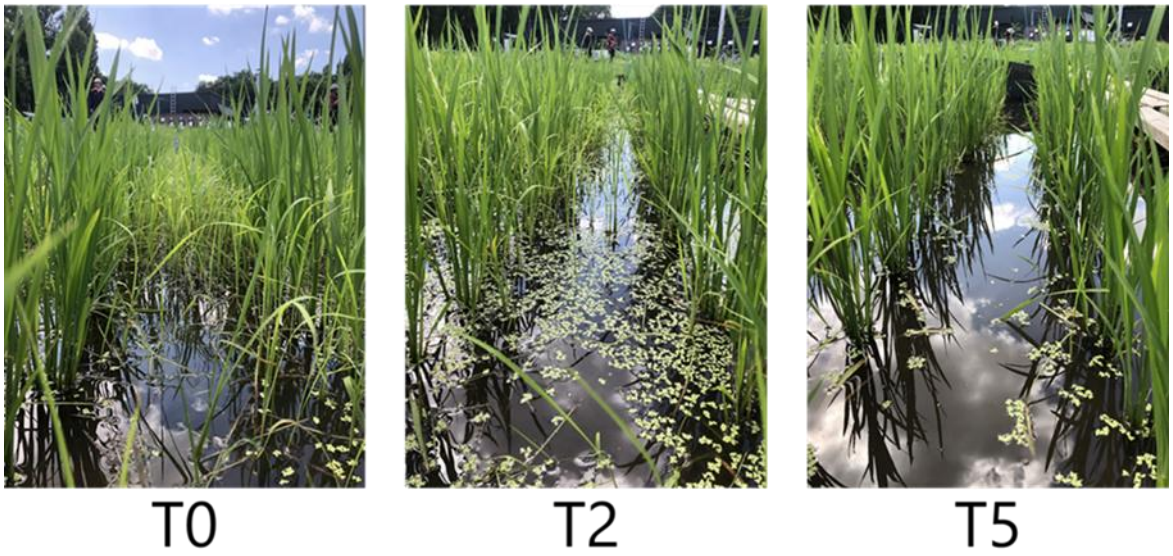


Figure 5.10. The appearance of weeds before the last multiple inter-tillage weeding (MIW). Treatments of T0, T2 and T5 are organic rice farming paddy fields without fertilizers and agrochemicals and 0-, 2-, and 5-times inter-tillage weeding, respectively.

Approximately 90% of GHG emissions during the fallow season were attributed to RH emissions (Table 5.7), indicating that RH emissions significantly contributed to the GHGB during this season. Cumulative RH emissions during the fallow season were not significantly different among the treatments, but the effects of year and treatments differences were observed (Table 5.7). Additionally, RH emissions per weed were significantly affected by year, treatment, and their interaction. RH emissions per residue were influenced by year, while RH emissions per total carbon input (weeds and residues) were affected by year and treatment (Table 5.8). These results suggest that RH emissions were influenced by annual variations in weather conditions and carbon inputs.

Furthermore, at T5, showed the highest RH emissions during the fallow season. Since weeds were uniformly returned to the field after harvest, the amount of incorporated weeds during MIW period may have also influenced RH emissions. These results are consistent with the observed significant positive correlations between RH emissions and soil temperature, pH, and SO_4^{2-} (Table 5.6), suggesting that aerobic and warm conditions promoted microbial activity and organic matter decomposition, contributing to increased RH emissions.

Contrary to our hypothesis, the application of MIW more than four times tended to increase CH_4 emissions (Table 5.7). This trend differed from the result reported by many previous studies on bioturbation and CH_4 emissions, in which increased dissolved oxygen concentrations in paddy field water and soil associated with disturbance, significantly reduced CH_4 emissions (Fang et al., 2019; Ge et al., 2023; Sheng et al., 2018; Xu et al., 2017). CH_4 emissions were promoted under anaerobic conditions, as indicated by the relationship between CH_4 flux and NO_3^-, Fe^{2+}, and Eh (Table 5.6). As shown by changes in Eh at T5, soils became aerobic immediately after MIW but shifted to anaerobic before the next MIW (Figure 5.2a). Oxygen supplied by MIW was likely used to reoxidize reduced substances, leading to further reduction and the formation of anaerobic conditions favorable for CH_4 production at T5. At T5, CH_4 emissions per carbon input from weeds, residues, and total (weeds and residues) during the rice-growing season tended to be higher than T0 and T2 (Table 5.8). It is possible that the redox potential fluctuations caused by MIW and carbon input produced a positive priming effect of CH_4. This trend is similar to previous studies indicating that in rice fields, oxygen supply associated by the disturbance of carp leads to the consumption of oxygen in the paddy field, which decreases Eh and promotes CH_4 emissions (Datta et al., 2009; Fang et al., 2019).

The continuation of MIW practice resulted in significant annual variations in CH_4 emissions, with MIW either suppressing or promoting CH_4 emissions depending on the year (Table 5.7). CH_4 emissions per carbon input from weeds and residues were significantly affected by year variability (Table 5.8), suggesting that the annual variations in cumulative CH_4 emissions may be attributed to differences in the amounts of weeds and residues incorporated into the soil each year. CH_4 emissions are influenced by soil properties and other environmental factors such as soil pH, soil bulk density, fertilization, and temperature (Chen et al., 2021). Relatively high temperatures (below 32°C) promote the decomposition of crop residues, generating large amounts of organic compounds that lead to increased CH_4 emissions (Chen et al., 2021). In this study, there was a significant positive correlation between CH_4 flux and soil temperature across

all treatments during the rice-growing season (Table 5.6), with CH_4 emissions tending to increase around 25°C. This suggests that CH_4 production by methanogens and soil temperature are closely related to the priming effect of CH_4 emissions due to MIW practice. Understanding these relationships may greatly contribute to reducing CH_4 emissions through MIW.

During the fallow season, CH_4 emissions were minimal compared to the rice-growing season, and the CH_4 emission per carbon input during the fallow season was significantly lower than that of RH emissions (Table 5.8). This suggests that most of the carbon input during the fallow season was mineralized and subsequently emitted as RH. This trend is consistent with that observed by Song et al. (2024).

The cumulative N_2O emissions during both seasons were negligible across all treatments (Table 5.7). However, the cumulative annual N_2O emissions over five years showed an absorption tendency at T0 and T2, while T5 exhibited an emission tendency. The significant relationship between N_2O flux and Fe^{2+}, and Eh during the rice-growing season at T5 indicated that N_2O emissions were promoted under aerobic conditions (Table 5.6). In soils subjected to the high-frequency MIW practice at T5, the temporal changes in Eh showed a transition from aerobic to anaerobic conditions (Figure 5.2a). Since N_2O emissions are closely related to nitrification and denitrification, they are likely affected by soil aeration and the amount of inorganic nitrogen in the substrate (Fang et al., 2021). As discussed in **Section 4.4.4**, MIW disturbances increase N_2O concentrations in both soil and paddy field water during the MIW period, which may enhance N_2O emissions. Therefore, although N_2O emissions were minimal in this field, the frequent MIW disturbances at T5 could have enhanced N_2O production, increasing the risk of emissions.

GHGB values were positive over five years at all treatments, in these fields functioned as a source of GHG emissions regardless of MIW (Table 5.9). However, over five years, the cumulative GHGB values tended to be higher at T2 and T5 compared to T0. A significant positive correlation between GHGB and GWP_{RH} or GWP_{CH_4}, suggesting RH and CH_4

emissions are key factors influencing GHGB. At T2, the timing of MIW and water management may have triggered a positive priming effect on RH emissions during the rice-growing season, increasing net GHG emissions. At T5, redox potential fluctuations due to high MIW frequency may have caused a positive priming effect of CH_4, resulting in an increase in net GHG emissions. Therefore, whether MIW is applied twice or five times, it may promote RH or CH_4 emissions, resulting in positive GHGB.

5.4.2. Effects of MIW on rice yield and GHGI

Although there were no significant differences in brown rice yield among the treatments over five years (Figure 5.3), brown rice yield had a significant positive correlation with the number of MIW ($r = 0.59$, $p < 0.05$). The relationship between the frequency of MIW and yield was consistent with the previous study by Kasubuchi et al. (2019). This confirms the yield-increasing effect of MIW in this study as well.

Nitrogen is an essential component for plant growth. Rice absorbs nitrogen in the form of NH_4^+ through its roots and uses it for growth. According to Zhou et al. (2023), five times MIW increases the concentration of NH_4^+-N in the soil or soil solution to some extent, promoting rice growth and nutrient uptake, and thus contributing to higher yields. In our study, during MIW period, there was no significant increase in NH_4^+ content at 0-3 cm depth at T2 or T5 compared to T0 (Figure 5.1d). Although no significant differences were observed among the treatments, MIW tended to increase the soil NH_4^+ contents and chlorophyll content not only in the tiller stage (late MIW period) but also in the heading stage (Table 5.3). Additionally, there were significant differences in stems and leaves, grain and total NPP, between T0 and T5 (Table 5.4). While the ripened grains decrease at T5 compared to T0 and T2, the number of ears and 1000-grain weight tended to increase (Table 5.5). The decrease in the ripened grains at T5 may be attributed to the increased number of ears, leading to nutrient competition among the grains and

an increase in immature grains. These suggests that MIW had a significant impact on rice growth.

The average brown rice yields in Hokkaido were 5.71, 5.81, 5.97, 5.91, and 5.82 Mg ha^{-1} in 2019, 2020, 2022, and 2023, respectively (Hokkaido Regional Agricultural Administration Office). However, the brown rice yield at T5 did not match average of Hokkaido in each year, which differed from the findings of Kasubuchi et al. (2019). Furthermore, the number of ears was influenced by year and treatments, ripened grains by year, and 1000-grain weight by their interaction, suggesting impacts from Hokkaido's climate and MIW frequency on yield components (Table 5.5). A previous study was conducted in Yamagata Prefecture, and this discrepancy may have been due to differences in climate and land conditions between Yamagata and Hokkaido.

We hypothesized that MIW would reduce the GHGI by increasing yield and reducing GHG emission. Although there were no significant differences in GHGI among the treatments over five years (Table 5.10), T2 showed relatively higher GHGI, followed by T0 and T5. Given that MIW increased yield at T5, it is that T0 and T2 did not produce sufficient yields to offset GHG emissions. This result is generally consistent with our hypothesis, as MIW was able to reduce GHGI by increasing yield. However, since the brown rice yield at T5 tended to be lower than at average of Hokkaido, improving the MIW practice at T5 will require further efforts should be made to increases in brown rice yields.

5.4.3. Effects of MIW on NECB

As pointed out by Song et al. (2024), assessing SOC changes accurately requires long-term experiments due to soil heterogeneity and background carbon content. Meanwhile, NECB analysis can be utilized to estimate carbon balance over a short-term if each carbon input and output is precisely examined. In this study, we adopted this approach by carefully investigating each carbon component and estimating short-term carbon balance using NECB analysis.

Over five years, there were no significant differences in NECB among the treatments, but T2 and T5 showed negative values, indicating carbon loss (Table 5.11). Previous studies on unfertilized plots reported carbon balances ranging from -1.91 to 2.78 Mg C ha^{-1} (Wu et al., 2018), whereas this study observed values between -4.21 and 0.09 Mg C ha^{-1}, suggesting a greater tendency for carbon loss compared to the previous studies. The incorporation of crop residues has two opposing effects on NECB: it increases soil carbon storage while simultaneously enhancing RH and CH_4 emissions (Naser et al., 2007). The lowest NECB at T2 is likely due to increased RH emissions caused by the timing of MIW and water management, which enhanced organic matter decomposition. The lower NECB at T5 compared to T0 is also likely due to frequent MIW, which led to fluctuations in soil redox conditions, promoting both aerobic and anaerobic organic matter decomposition and increasing CH_4 emissions.

While an increase in RH emissions was expected due to more frequent MIW at T5, the results did not support this. However, the slope of the regression between RH emissions and NECB was lowest for T5 (-1.01), followed by T2 (-0.981) and T0 (-0.955) (Figure 5.9), indicating an increase of MIW frequency may promote RH emissions and lower NECB. These suggest that NECB is highly dependent on RH emissions and these results indicate that MIW likely stimulated microbial respiration, promoting organic matter decomposition and carbon mineralization, thereby accelerating carbon loss.

5.4.4. Mechanisms of MIW Involvement in RH and CH_4 Emissions

Long-term monitoring results suggest that MIW increases RH and CH_4 emissions, particularly during the rice growing season, thereby enhancing the risk of GHG emissions. Additionally, the risk of carbon loss due to accelerated organic matter decomposition was also indicated.

Organic acids, such as acetate, butyrate, and propionate, which serve as substrates for RH and CH_4 production, have been reported to increase with straw application (Nozoe, 2000). Figure 5.11 illustrates the decomposition pathways of these organic acids into CO_2 and CH_4.

Propionate and butyrate are first decomposed into acetate, which is then converted into CH_4 by methanogens. Hori et al. (1990) reported that sulfate-reducing bacteria (SRB) utilize propionate and acetate, releasing CO_2 as a byproduct (Figure 5.11). In this study, a strong negative correlation between soil pH and SO_4^{2-} was observed with increasing MIW frequency (Figures 5.6 and 5.7). Additionally, increasing MIW frequency, RH emissions tended to correlate more with soil pH and SO_4^{2-} (Figures 5.6 and 5.7). These findings suggest that MIW-induced disturbance temporarily increased oxygen supply in the soil, promoting sulfur-oxidizing bacteria activity and leading to SO_4^{2-} formation. This SO_4^{2-} may have been utilized by SRB, facilitating the decomposition of propionate and acetate and consequently increasing CO_2 emissions (Figure 5.11).

According to Nozoe (2000), when SO_4^{2-} is sufficiently available, SRB decompose propionate and produce acetate, which is subsequently utilized by methanogens. This suggests that increased oxygen supply via MIW may have promoted SO_4^{2-} formation, thereby enhancing CH_4 production from acetate. This hypothesis aligns with the observed significant positive correlation between CH_4 emissions and SO_4^{2-} at T5 (Figures 5.6 and 5.7). The significant positive correlation between RH and CH_4 observed only at T5 suggests that RH generated during the decomposition of organic acids may have served as a substrate for CH_4 production (Figures 5.6 and 5.7).

Additionally, Nozoe (2000) reported that butyrate decomposition to acetate via iron reduction sequentially contributes to CH_4 production (Figure 5.11). The positive correlation between CH_4 emissions and Fe^{2+}, observed across all treatments, strengthened with increasing MIW frequency (Figures 5.6 and 5.7). Additionally, Fe^{2+} showed a significant positive correlation with WEOC in all treatments, suggesting a link between iron reduction and organic carbon dynamics. Furthermore, significant positive correlations were found between CH_4 and soil temperature, as well as between soil temperature and Fe^{2+}, with increasing correlation coefficients in higher MIW frequency treatments (Figures 5.6 and 5.7). These results suggest

that MIW-induced disturbances enhanced iron-reducing bacterial activity under increasing soil temperature, promoting iron oxide reduction and the associated decomposition of organic acids, thereby increasing CH_4 emissions.

The present analysis indicates that MIW particularly enhances the activity of SRB and iron-reducing bacteria, contributing to increased RH and CH_4 emissions. However, as noted in **Section 5.4.1**, RH emissions did not significantly increase at T5, the most frequent disturbance treatment, while CH_4 emissions tended to increase. Notably, the relationship between CH_4 emissions and environmental factors showed an increasing number of CH_4-related factors with higher disturbance frequencies (Figure 5.7). MIW significantly influenced redox reactions in the soil (Figure 5.2a). As indicated by the negative correlation between Eh and all treatments, however, the correlation coefficient was lower at T5 compared to T0 and T2 (Figures 5.6 and 5.7). These findings suggest that multiple microbial metabolic pathways are involved in CH_4 emissions. The oxygen supplied through regular MIW was likely consumed immediately by microorganisms rather than being used for CH_4 oxidation, contributing to the formation of an anaerobic environment favorable for methanogens.

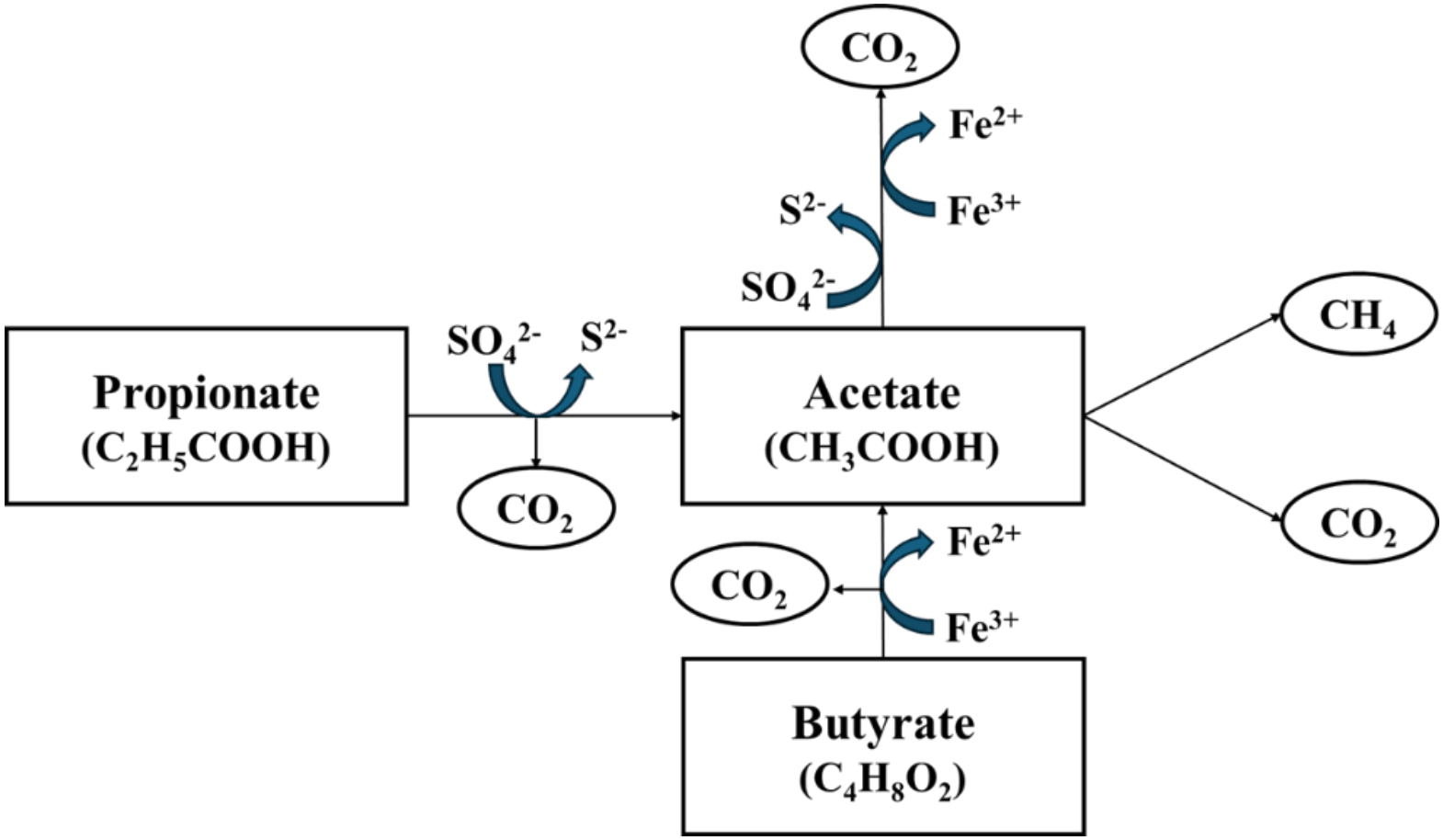


Figure 5.11. Relationship between sulfuric acid reduction, iron reduction, methane and carbon dioxide formation over organic acids (Hori et al. 1990 improve)

5.4.5. Limitation and future research

Although this study employed a comprehensive field monitoring approach over five years, results may have been influenced by external factors such as climatic conditions and soil characteristics. Therefore, the results are based on field experiments conducted in Hokkaido, Japan, and may not be directly applicable to areas with different climatic conditions and soil characteristics. Additional data collection in the field under different climatic conditions and soil characteristics is recommended to improve the generalization of these results. In addition, mesocosm experiments under controlled conditions are suggested to isolate the direct effects of MIW disturbance; similar measurements at different MIW frequencies could better elucidate the mechanisms by which MIW affects yield, GHGB, and NECB.

Our results suggest that MIW may influence microbial activity and affect GHGB and NECB. However, this study did not examine microbial community dynamics or other potential factors; future research should incorporate microbial community analysis and detailed carbon and nitrogen monitoring to better understand the mechanisms associated with MIW.

This study indirectly assessed carbon balance based on the difference between carbon inputs and emissions and did not consider direct SOC changes in the NECB. Therefore, to correctly assess SOC changes, both indirect SOC assessment, as in this method, and direct SOC assessment in terms of equivalent soil mass (ESM) should be conducted simultaneously.

5.5. Conclusion

This study was the first in the world to characterize the impact of MIW on GHG emissions, yields, and carbon balance; MIW was found to increase RH and CH_4, the major contributors to GHG emissions, increasing the risk of GHG emissions. At T2, the second larger weed input, combined with water management, caused a positive priming effect on RH, leading to increased RH emissions. At T5, frequent MIW promoted oxygen supply, which in turn increased CH_4 emissions by encouraging oxygen consumption under oxygen-deficient conditions and

facilitating the transition to an anaerobic environment. MIW was particularly associated with the activity of SRB and iron-reducing bacteria, and increased MIW frequency enhanced their activity, contributing to higher RH and CH_4 emissions. Although MIW resulted in improved rice growth and yield, yields at T5 were not as high as average yields in Hokkaido, suggesting room for further improvement. Nevertheless, the increased yields at T5 were confirmed to lead to lower GHGI, suggesting that MIW may be a sustainable organic rice farming. Increased RH emissions are strongly linked to carbon losses, indicating that MIW may increase the risk of carbon losses by increasing RH emissions.

6. General Discussion

This study examined the impact of MIW on GHG emissions in rice paddy fields from both pathway analysis and long-term monitoring perspectives.

In **Section 4**, we conducted a pathway analysis to elucidate CH_4 and N_2O emission pathways under MIW practice. The results indicated that CH_4 and N_2O emissions were affected differently by MIW. CH_4 was mainly emitted through the rice-mediated pathway, but the relatively high CH_4 emissions via the diffusion pathway, compared to previous studies, suggest that dissolved CH_4 may have competed between transport into rice roots and diffusion through floodwater, with a greater proportion being released via the latter. Furthermore, under the T5 (7-day intervals), gaseous CH_4 was released through the MIW-mediated pathway, reducing rice-mediated CH_4 emissions. This phenomenon was observed over two years, suggesting that the form of CH_4 in the soil significantly affects its emission pathways. Additionally, when comparing T5 (7-day intervals) and T2 (28-day intervals), CH_4 emissions were higher at T5, where gas release occurred more frequently, indicating that MIW influences the rate of CH_4 production and accumulation. Furthermore, the production of CH_4 from organic matter decomposed by MIW was strongly dependent on temperature, and CH_4 emissions tended to increase not only during the MIW period but also from the end of MIW period to harvest when soil temperature was high. On the other hand, N_2O was mainly emitted through the diffusion of dissolved N_2O. Nitrification and denitrification in paddy field water and soil were enhanced at T5, increasing the contribution of MIW-mediated N_2O emissions to total N_2O emissions from 4–5% at T2 to 33–34% at T5. However, since the experimental site was with or without fertilizer application, the annual N_2O emissions during the rice-growing season remained negligible. In particular, CH_4 emissions show a strong temperature dependence in the generation and accumulation of gaseous CH_4 under MIW practices, which may lead to interannual variations. Therefore, long-term monitoring of CH_4 emissions throughout the cultivation period under

MIW practices and identifying the key factors involved in CH_4 generation are crucial for achieving CH_4 emission reduction through the MIW farming method.

In **Section 5**, we evaluated the long-term effects of MIW on GHG emissions, rice yield, and carbon balance. The results indicated that MIW increased RH and CH_4 emissions during the rice-growing season, potentially raising the risk of enhancing GHG emissions. Additionally, accelerated organic matter decomposition due to MIW could increase the risk of carbon loss in the field. Although N_2O emissions at T5 showed an increasing trend, overall N_2O emissions during the rice-growing season were extremely low compared to RH and CH_4 emissions, suggesting that the study site was not a significant N_2O source. An analysis of environmental factors indicated that MIW particularly affected the activity of SRB and iron-reducing bacteria, likely contributing significantly to the degradation of organic acids, which serve as substrates for RH and CH_4 emissions. Although MIW improved rice growth and yield, the yield at T5 remained below the average yield in Hokkaido, indicating room for further improvement. However, the increased yield in T5 led to a reduction in the GHGI. This indicates that MIW farming can maintain high productivity while reducing GHG emissions, which means that it has the potential to be highly environmentally and economically sustainable.

Nevertheless, considering the increased RH and CH_4 emissions associated with MIW, the risk of carbon loss and enhancing GHG emissions, and the fact that yield did not reach conventional levels, further improvements to the current MIW farming method are necessary. Photosynthetic bacteria are able to fix more nitrogen into the soil when exposed to sunlight (Arao et al., 2015). Therefore, by performing inter-tillage weeding, the soil surface becomes more exposed to sunlight, which promotes nitrogen fixation and increases yields without the use of pesticides or fertilizers (Zhou et al., 2023). A recent study by Masuda, Chihara, and Senoo (2024) reported that dominant iron-reducing bacteria in paddy soil mainly contribute to nitrogen fixation, thereby maintaining soil nitrogen fertility. Moreover, a microcosm experiment with paddy soil amended with xylan, a major component of rice straw, demonstrated that ferrihydrite

application activated nitrogen fixation by iron-reducing nitrogen-fixing bacteria (*Geobacteraceae*) while simultaneously suppressing CH_4 production. Additionally, Nozoe (2000) suggested that acetate generated from butyrate decomposition may be utilized not only by methanogens but also by iron-reducing bacteria. Based on these findings, improving the efficiency of iron oxide utilization could be a potential strategy for CH_4 mitigation. This study suggests that MIW influences the activity of iron-reducing bacteria. Therefore, combining MIW with iron amendments (e.g., ferrihydrite) may contribute to both yield improvement and CH_4 emission reduction. Furthermore, the application of biochar or slag has been reported to increase soil pH, promoting CO_2 uptake in paddy fields and facilitating carbon sequestration as $CaCO_3$ (Wang et al., 2019). Additionally, the application of biochar produced at 525–650°C in paddy fields has been shown to slow mineralization and suppress CO_2 emissions (Wang et al., 2019).

As a future strategy, based on the field-scale data from this study and insights from previous research, it is expected that combining MIW with the application of iron amendments (e.g., slag) could enhance rice yield and suppress CH_4 emissions, although this approach differs from organic rice farming. On the other hand, our results suggest that MIW may increase the activity of iron-reducing bacteria, potentially promoting organic matter decomposition, RH and CH_4 emissions. Therefore, this combination may carry risks of soil organic carbon loss and increased GHG emissions. Hence, it will be essential to carefully consider factors such as the amount of iron amendments applied, the frequency of MIW, and the type and balance of organic materials introduced (e.g., biochar produced at high temperature), in order to move toward environmentally harmonious and sustainable agriculture.

7. Conclusion

To promote MIW practices as part of sustainable organic rice farming, we conducted a long-term study on the comprehensive effects of MIW on GHG emission pathways, GHG balance, carbon balance, and yield.

MIW influenced CH_4 and N_2O emission pathways by altering gas transport and microbial processes in paddy soils. CH_4 emissions via the rice plant pathway decreased under MIW, while emissions via surface water increased, suggesting that CH_4 accumulation and release were regulated by MIW frequency. N_2O emissions were primarily driven by dissolved N_2O diffusion, with higher emissions under frequent MIW due to enhanced nitrification and denitrification. However, overall N_2O emissions remained low in the unfertilized paddy.

At T2, carbon input and water management promoted organic matter decomposition, leading to increased RH emissions. In contrast, at T5, frequent disturbances caused significant fluctuations in soil redox potential, accelerating organic matter decomposition and increasing CH_4 emissions. However, the increased yield at T5 resulted in a lower GHGI, suggesting that MIW could enhance yield potential. Additionally, the increase in RH and CH_4 emissions during the rice-growing season indicated that MIW practices might elevate the risk of carbon loss. Therefore, optimizing water management and persistent organic matter such as biochar produced at high temperature are necessary to maximize the benefits of MIW.

Furthermore, environmental factor analysis showed that MIW-induced disturbances facilitated oxygen supply, which activated sulfate-reducing and iron-reducing bacteria involved in the decomposition of organic acids, key substrates for RH and CH_4 emissions. Given the recent recognition of iron-reducing bacteria for their nitrogen fixation potential and CH_4 reduction effects, combining iron oxide addition with MIW disturbances is expected to further enhance yield and reduce CH_4 emissions.

Summary (Japanese)

1. Introduction

二酸化炭素(CO_2)，メタン(CH_4)，亜酸化窒素(N_2O)は主要な温室効果ガス(GHG)である。水田は世界の農業由来の CH_4 排出の約 22%，N_2O 排出の 11%を占め，その削減は重要な課題である。一方で，水田は炭素貯留の大きな可能性を持ち，地球温暖化の緩和において費用対効果の高い手段の 1 つとされている。また，イネ(*Oryza sativa* L)は世界人口の約半数の主食であり，人口増加に伴い食糧需要が大幅に増加することが予想されている。したがって，収量を維持しつつ GHG 排出を削減しながら土壌への炭素貯留を促進する持続可能な稲作手法の構築が喫緊の課題である。水稲栽培中の多数回の中耕除草(MIW)法は、生育前期に 4 回以上の土壌表面の撹乱と雑草のすき込みを行うことで，無肥料・無農薬の有機栽培でありながら慣行農法に匹敵する収量が得られることがわかっている。さらに，中耕除草に伴う雑草のすき込みは炭素貯留量を向上させる可能性がある。MIW の攪乱に伴う田面水や土壌への酸素供給は CH_4 酸化菌を活性化し CH_4 排出量を大幅に削減する可能性があるが，MIW による収量，GHG 排出量，炭素貯留への影響は明らかになっていない。本研究では，MIW が GHG 排出，炭素貯留，収量に与える影響を解明し，持続可能な有機水田農法への適用可能性を評価することを目的とした。

2. Material and methods

北海道大学北方生物圏フィールド科学センターの試験水田にて調査を行った。年平均気温は 9.2℃，年降水量は 1146 mm，年間日照時間は 1718 時間である。土壌タイプは灰色低地土に分類され，品種はななつぼしを用いた。中耕除草の回数別に 0 回区(T0)，2 回/年区(T2)，5 回/年区(T5)の 3 処理区と，農薬・化学肥料を用いた慣行農法(CF)処理区をそれぞれ 3 反復で設けた。CF は圃場の位置が異なるため統計処理には用いず参照とした。

CH_4・N_2O 排出経路に対する MIW の影響を評価する方法を開発するため，2022 年 6 月 10 日から 7 月 13 日，2023 年 6 月 9 日から 7 月 7 日にかけて，拡散・気泡・イネ経路での排出量と MIW による排出の定量化方法を評価した。拡散フラックスは閾値に基づいて正味の拡散フラックスを抽出した。気泡フラックスは気泡トラップ法を用いて測定した。イネフラックスは，総フラック

スから拡散と気泡フラックスを差し引いて算出した。MIW による排出の測定には，新たに開発した攪乱機能を備えたチャンバーを用いて測定した。その他, 環境因子として地温などの気象要素, 草丈・分げつ数，酸化還元電位(Eh)，気泡態・溶存態 CH_4・N_2O 濃度を測定した。

MIW が GHG 排出・炭素収支・収量に与える影響を評価するために，MIW の回数の違いによるそれらへの影響を 2019 年 5 月から 5 年間モニタリングを実施した。GHG(RH(従属栄養性呼吸)，CH_4，N_2O)フラックス，0-3 cm 深の土壌理化学性(NO_3^-，NH_4^+，SO_4^{2-}イオン濃度など)，イネの生育(草丈，分げつ，玄米収量，純一次生産(NPP)など)，5 cm 深の酸化還元反応物質(Fe^{2+}含量，Eh)を測定した。さらに，GHG 排出への影響を GHG 収支(GHGB)，収量と GHG 排出量の関係を GHG 排出強度(GHGI)，炭素貯留への影響を炭素収支(NECB)を用いて評価した。

3. Results and discussion

気泡態 CH_4 の存在は，気泡とイネ経路に影響を与えており，溶存態 CH_4 の多くが拡散経路で排出される傾向があった。高撹乱下(T5)では，MIW 経路の CH_4 排出を促進し，イネ経路からの排出を一時的に抑制した。一方で，MIW 経路の栽培期の総 CH_4 排出量への寄与は 3-8%と小さかった。N_2O は主に溶存態で存在し，拡散経路を介して大気へ排出されていた。高撹乱下(T5)では，田面水および土壌中の N_2O 生成を促進する傾向にあり，さらに T5 における MIW 時の N_2O 排出量は栽培期の約 30%を占め，重要な排出経路であることが示唆された。

2022 年のみ MIW 区において総 GHG 排出の低下傾向が観察された。高撹乱が田面水や土壌中の N_2O 生成を促進する傾向が認められたが，総 GHG 排出への寄与は小さかった。一方，MIW による田面水の酸化は拡散経路での CH_4 排出量を抑制しただけでなく，物理的撹乱によって土壌中の気泡が破壊され，酸化された田面水中で CH_4 が消失した結果，イネ・気泡経路での CH_4 排出量も減少した。この CH_4 排出量の減少が，総 GHG 排出の低下に寄与したと考えられた

GHGB は T0<T5<T2 の順で高く，RH および CH_4 排出量と有意な正の相関を示した。T2 および T5 では GHG 排出に異なる影響を与えたが，全体として MIW は GHG 排出を促進する傾向があった。T2 では雑草のすき込みと水管理の組み合わせにより栽培期の RH 排出量が増加した。また，T5 では酸素の利用効率が高まり，酸化還元電位が大きく変動することで嫌気環境が形成され CH_4

排出量が増加していた。MIW による撹乱は微生物の活性，とくに硫酸塩還元菌および鉄還元菌を活性させ，RH および CH_4 の基質となる有機酸の分解を促進した可能性が示唆された。

MIW 回数の増加により収量が増加する傾向があった。しかし，T5 の収量は北海道の平均値に匹敵せず，気候や土壌条件の違いが影響した可能性がある。GHGI は，T5<T0<T2 の順で低く，MIW による増収効果が収量あたりの GHG 排出を低下させる傾向を示した。

NECB では T0<T5<T2 の順で炭素損失量が増加した。MIW は RH および CH_4 排出量を増加させ，炭素損失を加速させた可能性がある。また，NECB と RH は全処理区で有意な負の相関を示した。この回帰式の傾きは T5<T2<T0 であり，MIW の回数増加は RH 排出を促進し，NECB を低下させる可能性を示唆した。

4. Conclusion

MIW に起因する CH_4 排出は高濃度の気泡 CH_4 放出により総 GHG 排出増加の要因と考えられたが，実際にはほとんど寄与していなかった。さらに，総 GHG 排出が低下した 2022 年度の解析では，MIW により田面水の酸化強度が向上し CH_4 の酸化が促進することで，拡散，イネ，気泡の各経路による CH_4 排出が抑制される可能性が示された。しかしながら，MIW は RH および CH_4 排出を増加させ，総 GHG 排出の増加リスクを高める可能性がある。MIW の回数増加は CH_4 排出量が増加した一方で収量が向上したことから，MIW が増収と GHGI 低下に寄与する可能性が示唆された。また，栽培期における RH および CH_4 排出量の増加により，MIW は炭素損失のリスクを高めた。これらのことから，MIW の効果を最大限に引き出すためには，水管理の改善や難分解性有機物としてのバイオ炭の活用などの工夫が必要と考えられる。さらに，MIW に伴う酸素供給が RH や CH_4 の基質となる有機酸の分解に関与する硫酸塩還元菌および窒素固定能や CH_4 削減効果が期待されている鉄還元菌の活性に影響を与える可能性が示唆されていることから，MIW と酸化鉄の添加を組み合わせることで，さらなる収量増加と CH_4 排出削減が期待される。

Funding

This work was supported by the Japan Society for the Promotion of Science (JSPS), Grants-in-Aid for Scientific Research (KAKENHI) [grant number JP18H03963]; JST SPRING [grant number JPMJSP2119]; and Yanmar environmental sustainability support association [grant number KG0230009].

Reference

Akiyama, H. (2024). Methane and nitrous oxide emissions from agricultural fields in Japan and mitigation options: A review. *Soil Science and Plant Nutrition*, *70*(2), 79–87. https://doi.org/10.1080/00380768.2023.2298782

Alberto, M., Wassmann, R., Buresh, R., Quilty, J., Correa, T., Sandro, J., & Centeno, C. (2014). Measuring methane flux from irrigated rice fields by eddy covariance method using open-path gas analyzer. *Field Crops Research*, *160*, 12–21. https://doi.org/10.1016/j.fcr.2014.02.008

Alexandratos, N., & Bruinsma, J. (2012). *World Agriculture towards 2030/2050: The 2012 revision*.

Arao H., Kasubuchi T., & Yasuda H. (2015). *Sunlight transmittance through the surface soil and fluctuations in the total nitrogen contents at the surface of ponded paddy soi* (0). Journal of the Japanese Society of Soil Physics. https://doi.org/10.34467/jssoilphysics.131.0_23

Bastviken, D., Cole, J., Pace, M., & Van De Bogert, M. (2008). Fates of methane from different lake habitats: Connecting whole-lake budgets and CH_4 emissions. *Journal of Geophysical Research: Biogeosciences*, *113*(G2), 2007JG000608. https://doi.org/10.1029/2007JG000608

Booth, M. T., Urbanic, M., Wang, X., & Beaulieu, J. J. (2021). Bioturbation frequency alters methane emissions from reservoir sediments. *Science of The Total Environment*, *789*, 148033. https://doi.org/10.1016/j.scitotenv.2021.148033

Butterbach-Bahl, K., Papen, H., & Rennenberg, H. (1997). Impact of gas transport through rice cultivars on methane emission from rice paddy fields. *Plant, Cell & Environment*, *20*(9), 1175–1183. https://doi.org/10.1046/j.1365-3040.1997.d01-142.x

Carlson, K., Gerber, J., Mueller, N., Herrero, M., MacDonald, G., Brauman, K., Havlik, P., O'Connell, C., Johnson, J., Saatchi, S., & West, P. (2017). Greenhouse gas emissions intensity of global croplands. *Nature Climate Change*, *7*(1), 63–68. https://doi.org/10.1038/nclimate3158

Chen, Z., Zhang, H., Xue, J., Liu, S., & Chen, F. (2021). A nine-year study on the effects of tillage on net annual global warming potential in double rice-cropping systems in Southern China. *Soil and Tillage Research*, *206*, 104797. https://doi.org/10.1016/j.still.2020.104797

Conrad, R., & Rothfuss, F. (1991). Methane oxidation in the soil surface layer of a flooded rice field and the effect of ammonium. *Biology and Fertility of Soils*, *12*(1), 28–32. https://doi.org/10.1007/BF00369384

Datta, A., Nayak, D. R., Sinhababu, D. P., & Adhya, T. K. (2009). Methane and nitrous oxide emissions from an integrated rainfed rice–fish farming system of Eastern India. *Agriculture, Ecosystems & Environment*, *129*(1–3), 228–237. https://doi.org/10.1016/j.agee.2008.09.003

Ding, W., Cai, Z., & Tsuruta, H. (2005). Plant species effects on methane emissions from freshwater marshes. *Atmospheric Environment*, *39*(18), 3199–3207. https://doi.org/10.1016/j.atmosenv.2005.02.022

Fan, L., Dippold, M. A., Ge, T., Wu, J., Thiel, V., Kuzyakov, Y., & Dorodnikov, M. (2020). Anaerobic oxidation of methane in paddy soil: Role of electron acceptors and fertilization in mitigating CH4 fluxes. *Soil Biology and Biochemistry*, *141*, 107685. https://doi.org/10.1016/j.soilbio.2019.107685

Fan, L., Schneider, D., Dippold, M. A., Poehlein, A., Wu, W., Gui, H., Ge, T., Wu, J., Thiel, V., Kuzyakov, Y., & Dorodnikov, M. (2021). Active metabolic pathways of anaerobic methane oxidation in paddy soils. *Soil Biology and Biochemistry*, *156*, 108215. https://doi.org/10.1016/j.soilbio.2021.108215

Fang, K., Gao, H., Sha, Z., Dai, W., Yi, X., Chen, H., & Cao, L. (2021). Mitigating global warming potential with increase net ecosystem economic budget by integrated rice-frog farming in eastern China. *Agriculture, Ecosystems & Environment*, *308*, 107235. https://doi.org/10.1016/j.agee.2020.107235

Fang, K., Yi, X., Dai, W., Gao, H., & Cao, L. (2019). Effects of Integrated Rice-Frog Farming on Paddy Field Greenhouse Gas Emissions. *International Journal of Environmental Research and Public Health*, *16*(11), 1930. https://doi.org/10.3390/ijerph16111930

Ge, L., Sun, Y., Li, Y., Wang, L., Guo, G., Song, L., Wang, C., Wu, G., Zang, X., Cai, X., Li, S., & Li, P. (2023). Ecosystem sustainability of rice and aquatic animal co-culture systems and a synthesis of its underlying mechanisms. *Science of The Total Environment*, *880*, 163314. https://doi.org/10.1016/j.scitotenv.2023.163314

Gomiero, T. (2016). Soil Degradation, Land Scarcity and Food Security: Reviewing a Complex Challenge. *Sustainability*, *8*(3), 281. https://doi.org/10.3390/su8030281

Hokkaido Research Organization. (2012). [Soil physical properties] Dojyo buturisei (in Japanese). 42. https://www.hro.or.jp/upload/13654/3v2.pdf

Holzapfel-Pschorn, A., Conrad, R., & Seiler, W. (1986). Effects of vegetation on the emission of methane from submerged paddy soil. *Plant and Soil*, *92*(2), 223–233. https://doi.org/10.1007/BF02372636

Hori K., Inubushi K., Matsumoto S., & Wada H. (1990). Competition for Acetic Acid between Methane Formation and Sulfate Reduction in the Paddy Soil. *Japanese Society of Soil Science and Plant Nutrition*, *61*(6), 572–578. https://doi.org/10.20710/dojo.61.6_572 (in Japanese with English summary).

Hosono, T., & Nouchi, I. (1997). Effect of gas pressure in the root and stem base zone on methane transport through rice bodies. *Plant and Soil*, *195*, 65–73. https://doi.org/10.1023/A:1004214829124

Hu, B., Wang, D., Zhou, J., Meng, W., Li, C., Sun, Z., Guo, X., & Wang, Z. (2018). Greenhouse gases emission from the sewage draining rivers. *Science of The Total Environment*, *612*, 1454–1462. https://doi.org/10.1016/j.scitotenv.2017.08.055

Hu, M., Wade, A. J., Shen, W., Zhong, Z., Qiu, C., & Lin, X. (2024). Effects of different organic fertilizers on nitrous oxide and methane emissions from double-cropping rice fields. *Pedosphere*, *34*(1), 52–62. https://doi.org/10.1016/j.pedsph.2023.03.006

Intergovernmental panel on climate change (IPCC). (2014). *Synthesis Report. Contribution of Working Groups I, II and III to the Fifth Assessment Report of the Intergovernmental Panel on Climate Change [Core Writing Team, R.K. Pachauri and L.A. Meyer (eds.)].* Intergovernmental Panel on Climate Change.

Intergovernmental Panel on Climate Change (IPCC). (2023a). *Climate Change 2021 – The Physical Science Basis: Working Group I Contribution to the Sixth Assessment Report of the Intergovernmental Panel on Climate Change* (1st ed.). Cambridge University Press. https://doi.org/10.1017/9781009157896

Intergovernmental Panel on Climate Change (IPCC). (2023b). *Climate Change 2022 – Impacts, Adaptation and Vulnerability: Working Group II Contribution to the Sixth Assessment Report of the Intergovernmental Panel on Climate Change* (1st ed.). Cambridge University Press. https://doi.org/10.1017/9781009325844

Kajiura, M., Saito, T., Nishiwaki, J., & Tokida, T. (2024). *Pathway-specific emissions and dissolved CH-₄ pool in the soil across 22 rice varieties*. https://doi.org/10.21203/rs.3.rs-4746090/v1

Kajiura, M., & Tokida, T. (2021). Quantifying bubbling emission (ebullition) of methane from a rice paddy using high-time-resolution concentration data obtained during a closed-chamber measurement. *Journal of Agricultural Meteorology*, *77*(4), 245–252. https://doi.org/10.2480/agrmet.D-21-00022

Kajiura, M., & Tokida, T. (2024). Diurnal variation in methane emission from a rice paddy due to ebullition. *Journal of Environmental Quality*, *53*(2), 265–273. https://doi.org/10.1002/jeq2.20553

Kasubuchi T., Arao H., & Yasuda H. (2016). *Role of multiple intertillage weeding for the paddy cultivation described in agricultural books the Edo era* (0). Journal of the Japanese Society of Soil Physics. https://doi.org/10.34467/jssoilphysics.132.0_55 (in Japanese with English summary).

Kasubuchi T., Arao H., & Yasuda H. (2019). *Warning for modern agriculture depending on chemical fertilizers and agricultural chemicals—Significance of the multiple-intertillage-weeding method developed in Edo-era—* (0). Journal of the Japanese Society of Soil Physics. https://doi.org/10.34467/jssoilphysics.141.0_65 (in Japanese with English summary).

Kato C., Imoto H., Nishimura T., & Miyazaki T. (2013). *Invesyigation of changes in soil CO_2 concentration by using compact buried tubing soil gas monitoring system* (0). Journal of the Japanese Society of Soil Physics. https://doi.org/10.34467/jssoilphysics.124.0_25 (in Japanese with English summary).

Kimochi Y., Tanaka H., Xu K. Q., Inamori R., & Inamori Y. (2014). Evaluation of Generation and Emission Potential of N_2O and CH_4 from Water Environment using Newly Improved Quick and Effective Sampling Method of Dissolved Gas. *Japanese Journal of Water Treatment Biology*, *50*(3), 121–131. https://doi.org/10.2521/jswtb.50.121 (in Japanese with English summary).

Komiya, S., Noborio, K., Katano, K., Pakoktom, T., Siangliw, M., & Toojinda, T. (2015). Contribution of Ebullition to Methane and Carbon Dioxide Emission from Water between Plant Rows in a Tropical Rice Paddy Field. *International Scholarly Research Notices*, *2015*, 1–8. https://doi.org/10.1155/2015/623901

Kon Kam King, J., Granjou, C., Fournil, J., & Cecillon, L. (2018). Soil sciences and the French 4 per 1000 Initiative—The promises of underground carbon. *Energy Research & Social Science*, *45*, 144–152. https://doi.org/10.1016/j.erss.2018.06.024

Lal, R. (2004). Soil Carbon Sequestration Impacts on Global Climate Change and Food Security. *Science*, *304*(5677), 1623–1627. https://doi.org/10.1126/science.1097396

Le Mer, J., & Roger, P. (2001). Production, oxidation, emission and consumption of methane by soils: A review. *European Journal of Soil Biology*, *37*(1), 25–50. https://doi.org/10.1016/S1164-5563(01)01067-6

Li, X., Hu, F., & Shi, W. (2013). Plant material addition affects soil nitrous oxide production differently between aerobic and oxygen-limited conditions. *Applied Soil Ecology*, *64*, 91–98. https://doi.org/10.1016/j.apsoil.2012.10.003

Li, Y., Wang, D., Chen, Z., & Hu, H. (2018). Comprehensive effects of a sedge plant on CH_4 and N_2O emissions in an estuarine marsh. *Estuarine, Coastal and Shelf Science*, *204*, 202–211. https://doi.org/10.1016/j.ecss.2018.03.008

Liu, T., Xia, X., Liu, S., Mou, X., & Qiu, Y. (2013). Acceleration of Denitrification in Turbid Rivers Due to Denitrification Occurring on Suspended Sediment in Oxic Waters. *Environmental Science & Technology*, *47*(9), 4053–4061. https://doi.org/10.1021/es304504m

Liu, X., Zhou, T., Liu, Y., Zhang, X., Li, L., & Pan, G. (2019). Effect of mid-season drainage on CH_4 and N_2O emission and grain yield in rice ecosystem: A meta-analysis. *Agricultural Water Management*, *213*, 1028–1035. https://doi.org/10.1016/j.agwat.2018.12.025

Liu, Y., Wan, K., Tao, Y., Li, Z., Zhang, G., Li, S., & Chen, F. (2013). Carbon Dioxide Flux from Rice Paddy Soils in Central China: Effects of Intermittent Flooding and Draining Cycles. *PLoS ONE*, *8*(2), e56562. https://doi.org/10.1371/journal.pone.0056562

Ma, S., Jiang, L., Wilson, R. M., Chanton, J. P., Bridgham, S., Niu, S., Iversen, C. M., Malhotra, A., Jiang, J., Lu, X., Huang, Y., Keller, J., Xu, X., Ricciuto, D. M., Hanson, P. J., & Luo, Y. (2022). Evaluating alternative ebullition models for predicting peatland methane emission and its pathways via data–model fusion. *Biogeosciences*, *19*(8), 2245–2262. https://doi.org/10.5194/bg-19-2245-2022

Mariko, S., Harazono, Y., Owa, N., & Nouchi, I. (1991). Methane in flooded soil water and the emission through rice plants to the atmosphere. *Environmental and Experimental Botany*, *31*(3), 343–350. https://doi.org/10.1016/0098-8472(91)90059-W

Masuda, Y., Chihara, M., & Senoo, K. (2024). Ferrihydrite Addition Activated *Geobacteraceae*, the Most Abundant Iron-reducing Diazotrophs, and Suppressed Methanogenesis by Heterogeneous Methanogens in Xylan-amended Paddy Soil Microcosms. *Microbes and Environments*, *39*(3), n/a. https://doi.org/10.1264/jsme2.ME24028

Mboyerwa, P. A., Kibret, K., Mtakwa, P., & Aschalew, A. (2022). Greenhouse gas emissions in irrigated paddy rice as influenced by crop management practices and nitrogen fertilization rates in eastern Tanzania. *Frontiers in Sustainable Food Systems*, *6*, 868479. https://doi.org/10.3389/fsufs.2022.868479

Miller, B. G. (2005). Coal Energy Systems. *ELSEVIER ACADEMIC PRESS*, 116. http://dx.doi.org/10.1016/B978-0-12-497451-7.X5000-1

Minamikawa, K., Sakai, N., & Hayashi, H. (2005). The effects of ammonium sulfate application on methane emission and soil carbon content of a paddy field in Japan. *Agriculture, Ecosystems & Environment*, *107*(4), 371–379. https://doi.org/10.1016/j.agee.2004.10.027

Minamikawa, K., Tokida, T., & Sudo, S. (2015). *Guidelines for Measuring CH_4 and N_2O Emissions from Rice Paddies by Manually Operated Closed Chamber Method.pdf* (p. 76).

Ministry of Agriculture, Forestry and Fisheries. (2024). *The Situation Surrounding Organic Agriculture in Japan* (pp. 1–10). https://www.maff.go.jp/e/policies/agri/attach/pdf/index-2.pdf

Ministry of Agriculture, Forestry, and Fisheries . (2024). *MIDORI Strategy for Sustainable Food Systems*. file:///C:/Users/kenda/Downloads/midori-1.pdf

Miyata, A., Leuning, R., Denmead, O. T., Kim, J., & Harazono, Y. (2000). Carbon dioxide and methane fluxes from an intermittently flooded paddy field. *Agricultural and Forest Meteorology*, *102*(4), 287–303. https://doi.org/10.1016/S0168-1923(00)00092-7

Morishita T., & Hatano R. (1999). *Methane Emissionfrom Dam-Lake and Methane Uptake by Forest SoilSurreunding the Lake* (6). Japanese Society of Soil Science and Plant Nutrition. https://doi.org/10.20710/dojo.70.6_791

Morley, N., & Baggs, E. M. (2010). Carbon and oxygen controls on N_2O and N_2 production during nitrate reduction. *Soil Biology and Biochemistry*, *42*(10), 1864–1871. https://doi.org/10.1016/j.soilbio.2010.07.008

Nakano, T., Sawamoto, T., Morishita, T., Inoue, G., & Hatano, R. (2004). A comparison of regression methods for estimating soil–atmosphere diffusion gas fluxes by a closed-chamber technique. *Soil Biology and Biochemistry*, *36*(1), 107–113. https://doi.org/10.1016/j.soilbio.2003.07.005

Naser, H. M., Nagata, O., Sultana, S., & Hatano, R. (2019). Carbon Sequestration and Contribution of CO_2, CH_4 and N_2O Fluxes to Global Warming Potential from Paddy-Fallow Fields on Mineral Soil Beneath Peat in Central Hokkaido, Japan. *Agriculture*, *10*(1), 6. https://doi.org/10.3390/agriculture10010006

Naser, H. M., Nagata, O., Tamura, S., & Hatano, R. (2007). Methane emissions from five paddy fields with different amounts of rice straw application in central Hokkaido, Japan. *Soil Science and Plant Nutrition*, *53*(1), 95–101. https://doi.org/10.1111/j.1747-0765.2007.00105.x

Nishimura, S., Yonemura, S., Minamikawa, K., & Yagi, K. (2015). Seasonal and diurnal variations in net carbon dioxide flux throughout the year from soil in paddy field. *Journal of Geophysical Research: Biogeosciences*, *120*(1), 63–76. https://doi.org/10.1002/2014JG002746

Nouchi, I., Mariko, S., & Aoki, K. (1990). Mechanism of Methane Transport from the Rhizosphere to the Atmosphere through Rice Plants. *Plant Physiology*, *94*(1), 59–66. https://doi.org/10.1104/pp.94.1.59

Nozoe, T. (2000). *Mechanisms and Suppression of the Accumulation of Volatile Fatty Acids and the Production of Methane in Submerged Paddy Soil* (97; p. p.75-129). Bull. Tohoku Natl. Agric. Exp. Stn. https://doi.org/10.11501/3163883 (in Japanese with English summary).

Oliveira Junior, E., Temmink, R. J. M., Buhler, B. F., Souza, R. M., Resende, N., Spanings, T., Muniz, C. C., Lamers, L. P. M., & Kosten, S. (2019). Benthivorous fish bioturbation reduces methane emissions, but increases total greenhouse gas emissions. *Freshwater Biology*, *64*(1), 197–207. https://doi.org/10.1111/fwb.13209

Oliver, V., Cochrane, N., Magnusson, J., Brachi, E., Monaco, S., Volante, A., Courtois, B., Vale, G., Price, A., & Teh, Y. A. (2019). Effects of water management and cultivar on carbon dynamics, plant productivity and biomass allocation in European rice systems. *Science of The Total Environment*, *685*, 1139–1151. https://doi.org/10.1016/j.scitotenv.2019.06.110

Pan, G., Li, L., Wu, L., & Zhang, X. (2004). Storage and sequestration potential of topsoil organic carbon in China's paddy soils. *Global Change Biology*, *10*(1), 79–92. https://doi.org/10.1111/j.1365-2486.2003.00717.x

Qian, H., Zhu, X., Huang, S., Linquist, B., Kuzyakov, Y., Wassmann, R., Minamikawa, K., Martinez-Eixarch, M., Yan, X., Zhou, F., Sander, B. O., Zhang, W., Shang, Z., Zou, J., Zheng, X., Li, G., Liu, Z., Wang, S., Ding, Y., … Jiang, Y. (2023). Greenhouse gas emissions and mitigation in rice agriculture. *Nature Reviews Earth & Environment*, *4*(10), 716–732. https://doi.org/10.1038/s43017-023-00482-1

Ray, A. (2022). The darker side of agricultural intensification—Disappearance of autumn or aus rice, entry of HYVs, and implications in terms of environmental sustainability in a 'Green Revolution' state of eastern India. *World Development Sustainability*, *1*, 100028. https://doi.org/10.1016/j.wds.2022.100028

Rockström, J., Steffen, W., Noone, K., Persson, Å., Chapin, F. S., Lambin, E. F., Lenton, T. M., Scheffer, M., Folke, C., Schellnhuber, H., Nykvist, B., De Wit, C. A., Hughes, T., Van Der Leeuw, S., Rodhe, H., Sörlin, S., Snyder, P. K., Costanza, R., Svedin, U., … Foley, J. A. (2009). A safe operating space for humanity. *Nature*, *461*(7263), 472–475. https://doi.org/10.1038/461472a

Sawakuchi, H., Bastviken, D., Sawakuchi, A. O., Krusche, A. V., Ballester, M. V. R., & Richey, J. E. (2014). Methane emissions from Amazonian Rivers and their contribution to the global methane budget. *Global Change Biology*, *20*(9), 2829–2840. https://doi.org/10.1111/gcb.12646

Schütz, H., Seiler, W., & Conrad, R. (1989). Processes involved in formation and emission of methane in rice paddies. *Biogeochemistry*, *7*(1). https://doi.org/10.1007/BF00000896

Senga, Y., Hirota, M., & Nohara, S. (2010). The Transport of Nitrous Oxide via Aquatic Plant. *Bulletin of Geo-Environmental Science*, *12*, 127–132. (in Japanese)

Shang, Q., Yang, X., Gao, C., Wu, P., Liu, J., Xu, Y., Shen, Q., Zou, J., & Guo, S. (2011). Net annual global warming potential and greenhouse gas intensity in Chinese double rice-cropping systems: A 3-year field measurement in long-term fertilizer experiments: LONG-TERM FERTILIZER EFFECTS ON GWP AND GHGI. *Global Change Biology*, *17*(6), 2196–2210. https://doi.org/10.1111/j.1365-2486.2010.02374.x

Sheng, F., Cao, C., & Li, C. (2018). Integrated rice-duck farming decreases global warming potential and increases net ecosystem economic budget in central China. *Environmental Science and Pollution Research*, *25*(23), 22744–22753. https://doi.org/10.1007/s11356-018-2380-9

Shimizu, M., Limin, A., Desyatkin, A. R., Jin, T., Mano, M., Ono, K., Miyata, A., Hata, H., & Hatano, R. (2015). Effect of manure application on seasonal carbon fluxes in a temperate managed grassland in Southern Hokkaido, Japan. *CATENA*, *133*, 474–485. https://doi.org/10.1016/j.catena.2015.05.011

Shimizu, M., Marutani, S., Desyatkin, A. R., Jin, T., Hata, H., & Hatano, R. (2009). The effect of manure application on carbon dynamics and budgets in a managed grassland of Southern Hokkaido, Japan. *Agriculture, Ecosystems & Environment*, *130*(1–2), 31–40. https://doi.org/10.1016/j.agee.2008.11.013

Song, H. J., Park, S. Y., Chae, H. G., Kim, P. J., & Lee, J. G. (2024). Benefits of organic amendments on soil C stock may be offset by increased methane flux in rice paddy field. *Agriculture, Ecosystems & Environment*, *359*, 108742. https://doi.org/10.1016/j.agee.2023.108742

Stewart, W. M., Dibb, D. W., Johnston, A. E., & Smyth, T. J. (2005). The Contribution of Commercial Fertilizer Nutrients to Food Production. *Agronomy Journal*, *97*(1), 1–6. https://doi.org/10.2134/agronj2005.0001

Takai, Y. (1969, January 1). *The Mechanism of Reduction in Paddy Soil*. https://www.jircas.go.jp/en/publication/jarq/4/4/20

Tokida, T. (2021). Increasing measurement throughput of methane emission from rice paddies with a modified closed-chamber method. *Journal of Agricultural Meteorology*, *77*(2), 160–165. https://doi.org/10.2480/agrmet.D-20-00029

Tokida, T., Cheng, W., Adachi, M., Matsunami, T., Nakamura, H., Okada, M., & Hasegawa, T. (2013). The contribution of entrapped gas bubbles to the soil methane pool and their role in methane emission from rice paddy soil in free-air [CO_2] enrichment and soil warming experiments. *Plant and Soil*, *364*(1–2), 131–143. https://doi.org/10.1007/s11104-012-1356-7

Tokida, T., Miyazaki, T., Mizoguchi, M., & Seki, K. (2005). *In situ* accumulation of methane bubbles in a natural wetland soil. *European Journal of Soil Science*, *56*(3), 389–396. https://doi.org/10.1111/j.1365-2389.2004.00674.x

Toma, Y., Fernández, F. G., Sato, S., Izumi, M., Hatano, R., Yamada, T., Nishiwaki, A., Bollero, G., & Stewart, J. R. (2011). Carbon budget and methane and nitrous oxide emissions over the growing season in a Miscanthus sinensis grassland in Tomakomai, Hokkaido, Japan: C BUDGET IN M. SINENSIS GRASSLAND IN JAPAN. *GCB Bioenergy*, *3*(2), 116–134. https://doi.org/10.1111/j.1757-1707.2010.01070.x

Toma, Y., Oomori, S., Maruyama, A., Ueno, H., & Nagata, O. (2016). Effect of the number of tillages in fallow season and fertilizer type on greenhouse gas emission from a rice (*Oryza sativa* L.) paddy field in Ehime, southwestern Japan. *Soil Science and Plant Nutrition*, *62*(1), 69–79. https://doi.org/10.1080/00380768.2015.1109999

Wang, C., Wang, W., Sardans, J., Singla, A., Zeng, C., Lai, D. Y. F., & Peñuelas, J. (2019). Effects of steel slag and biochar amendments on CO_2, CH_4, and N_2O flux, and rice productivity in a subtropical Chinese paddy field. *Environmental Geochemistry and Health*, *41*(3), 1419–1431. https://doi.org/10.1007/s10653-018-0224-7

Wang, F., Che, R., Deng, Y., Wu, Y., Tang, L., Xu, Z., Wang, W., Liu, H., & Cui, X. (2021). Air-drying and long time preservation of soil do not significantly impact microbial community composition and structure. *Soil Biology and Biochemistry*, *157*, 108238. https://doi.org/10.1016/j.soilbio.2021.108238

Wang, J., Chen, Z., Ma, Y., Sun, L., Xiong, Z., Huang, Q., & Sheng, Q. (2013). Methane and nitrous oxide emissions as affected by organic–inorganic mixed fertilizer from a rice paddy in southeast China. *Journal of Soils and Sediments*, *13*(8), 1408–1417. https://doi.org/10.1007/s11368-013-0731-1

Wang, L., Lu, P., Feng, S., Hamel, C., Sun, D., Siddique, K., & Gan, G. Y. (2024). Strategies to improve soil health by optimizing the plant–soil–microbe–anthropogenic activity nexus. *Agriculture, Ecosystems & Environment*, *359*, 108750. https://doi.org/10.1016/j.agee.2023.108750

Wang, Y., Hu, Z., Shang, D., Xue, Y., Islam, A. R. M. T., & Chen, S. (2020). Effects of warming and elevated O_3 concentrations on N_2O emission and soil nitrification and denitrification rates in a wheat-soybean rotation cropland. *Environmental Pollution*, *257*, 113556. https://doi.org/10.1016/j.envpol.2019.113556

Witt, C., Cassman, K. G., Olk, D. C., Biker, U., Liboon, S. P., & Samson, M. I. (2000). Crop rotation and residue management effects on carbon sequestration, nitrogen cycling and productivity of irrigated rice systems. *Plant and Soil*, *225*, 263–278. https://doi.org/10.1023/A:1026594118145

Wu, X., Wang, W., Xie, X., Yin, C., Hou, H., Yan, W., & Wang, G. (2018). Net global warming potential and greenhouse gas intensity as affected by different water management strategies in Chinese double rice-cropping systems. *Scientific Reports*, *8*(1), 779. https://doi.org/10.1038/s41598-017-19110-2

Xia, X., Jia, Z., Liu, T., Zhang, S., & Zhang, L. (2017). Coupled Nitrification-Denitrification Caused by Suspended Sediment (SPS) in Rivers: Importance of SPS Size and Composition. *Environmental Science & Technology*, *51*(1), 212–221. https://doi.org/10.1021/acs.est.6b03886

Xia, X., Zhang, L., Wang, G., Wang, J., Zhang, L., Zhang, S., & Li, Z. (2021). Nitrogen loss from a turbid river network based on N_2 and N_2O fluxes: Importance of suspended sediment. *Science of The Total Environment*, *757*, 143918. https://doi.org/10.1016/j.scitotenv.2020.143918

Xu, G., Liu, X., Wang, Q., Yu, X., & Hang, Y. (2017). Integrated rice-duck farming mitigates the global warming potential in rice season. *Science of The Total Environment*, *575*, 58–66. https://doi.org/10.1016/j.scitotenv.2016.09.233

Yan, X., Shi, S., Du, L., & Xing, G. (2000). Pathways of N_2O emission from rice paddy soil. *Soil Biology*.

Yang, B., Xiong, Z., Wang, J., Xu, X., Huang, Q., & Shen, Q. (2015). Mitigating net global warming potential and greenhouse gas intensities by substituting chemical nitrogen fertilizers with organic fertilization strategies in rice–wheat annual rotation systems in China: A 3-year field experiment. *Ecological Engineering*, *81*, 289–297. https://doi.org/10.1016/j.ecoleng.2015.04.071

Yang, P., Zhang, Y., Yang, H., Guo, Q., Lai, D. Y. F., Zhao, G., Li, L., & Tong, C. (2020). Ebullition was a major pathway of methane emissions from the aquaculture ponds in southeast China. *Water Research*, *184*, 116176. https://doi.org/10.1016/j.watres.2020.116176

Yao, Z., Zheng, X., Dong, H., Wang, R., Mei, B., & Zhu, J. (2012). A 3-year record of N_2O and CH_4 emissions from a sandy loam paddy during rice seasons as affected by different nitrogen application rates. *Agriculture, Ecosystems & Environment*, *152*, 1–9. https://doi.org/10.1016/j.agee.2012.02.004

Yu, K., Chen, G., & Patrick, W. H. (2004). Reduction of global warming potential contribution from a rice field by irrigation, organic matter, and fertilizer management. *Global Biogeochemical Cycles*, *18*(3), 2004GB002251. https://doi.org/10.1029/2004GB002251

Yuan, J., Liu, D., Xiang, J., He, T., Kang, H., & Ding, W. (2021). Methane and nitrous oxide have separated production zones and distinct emission pathways in freshwater aquaculture ponds. *Water Research*, *190*, 116739. https://doi.org/10.1016/j.watres.2020.116739

Yuan, Y., Dai, X., & Wang, H. (2019). Fertilization effects on CH_4, N_2O and CO_2 fluxes from a subtropical double rice cropping system. *Plant, Soil and Environment*, *65*(4), 189–197. https://doi.org/10.17221/453/2018-PSE

Zhang, A., Cui, L., Pan, G., Li, L., Hussain, Q., Zhang, X., Zheng, J., & Crowley, D. (2010). Effect of biochar amendment on yield and methane and nitrous oxide emissions from a rice paddy from Tai Lake plain, China. *Agriculture, Ecosystems & Environment*, *139*(4), 469–475. https://doi.org/10.1016/j.agee.2010.09.003

Zhou, Y., Xu, X., Han, R., Li, L., Feng, Y., Yeerken, S., Song, K., & Wang, Q. (2019). Suspended particles potentially enhance nitrous oxide (N_2O) emissions in the oxic estuarine waters of eutrophic lakes: Field and experimental evidence. *Environmental Pollution*, *252*, 1225–1234. https://doi.org/10.1016/j.envpol.2019.06.076

Zhou, Z., Ishiguro, M., Kashiwagi, J., Araki, H., Zhou, P., & Soluttanavong, V. (2023). Effect of inter-tillage weeding on rice yield, rice growth, and nutrient dynamics without agrochemical and fertilizer application: Results of a three-year study. *Soil and Tillage Research*, *232*, 105766. https://doi.org/10.1016/j.still.2023.105766

Zhu, D., Wu, Y., Chen, H., He, Y., & Wu, N. (2016). Intense methane ebullition from open water area of a shallow peatland lake on the eastern Tibetan Plateau. *Science of The Total Environment*, *542*, 57–64. https://doi.org/10.1016/j.scitotenv.2015.10.087